

Sources and chemistry of secondary organic
aerosols formed from carbonyl compounds

Neha Sareen

Submitted in partial fulfillment of the
requirements for the degree of Doctor of
Philosophy
in the Graduate School of Arts and Sciences

COLUMBIA UNIVERSITY

2012

© 2012

Neha Sareen

All rights reserved

ABSTRACT

Sources and chemistry of secondary organic aerosols formed from carbonyl compounds

Neha Sareen

Atmospheric aerosols serve an important role in climate and air quality. However, there are still significant gaps in our scientific understanding of their impacts on climate. One of the greatest factors contributing to uncertainties in our estimations of these impacts can be attributed to the gap in the sources and formation pathways of secondary organic aerosols (SOAs). Carbonyl compounds, in particular, glyoxal and methylglyoxal, are two oxidation products of both anthropogenic and biogenic volatile organic compounds (VOCs) in the atmosphere. Field and modeling studies have indicated that these two compounds can serve as potentially important precursors to SOAs, and alter the physical and chemical properties of the aerosols. The mechanisms and atmospheric significance of these processes pose important questions which need to be addressed. Here, we report experiments targeted to study the following topics: 1) the chemical kinetics of methylglyoxal uptake to aqueous aerosols, and the subsequent formation of SOA material; 2) the oxidative aging of SOA material formed by methylglyoxal; 3) the impact of methylglyoxal on the cloud condensation nuclei (CCN) activity of the aerosol. These studies were conducted using either aerosols generated from bulk solutions of the organic and ammonium sulfate or by exposing the gas-phase organic to pure ammonium sulfate seed aerosols. A number of techniques were utilized including: a custom-built Aerosol Chemical Ionization Mass Spectrometer (Aerosol-CIMS), UV-Vis

spectrophotometer, pendant drop tensiometry (PDT), continuous flow stream-wise thermal gradient CCN counter (CFSTGC), aerosol flow tube reactors, and an aerosol chamber.

We found that the uptake of methylglyoxal to aerosols is a potentially significant source of light-absorbing SOA in the atmosphere. Additionally, the presence of methylglyoxal leads to surface tension depression with important implications for aerosol CCN activity. The aqueous-phase reaction products of glyoxal and methylglyoxal when NH_4^+ is present include species featuring unsaturated C=C bonds such as aldol condensation products and imidazoles. Upon oxidation by O_3 and OH, these particles show an increase in light absorption, accompanied by the formation of smaller, more volatile organic acids. Aerosol chamber studies conducted where pure ammonium sulfate particles were exposed to gas-phase methylglyoxal and/or acetaldehyde show significant enhancements in CCN activity, which can increase cloud droplet number concentrations by up to 20%. The results of this work will provide for a more accurate representation of gas-aerosol interactions and cloud formation in climate and atmospheric chemistry models.

Table of Contents

Table of Contents.....	i
List of Tables.....	v
List of Figures.....	vii
List of Schemes.....	x
Acknowledgements.....	xi
Dedication.....	xiii
Chapter 1: Introduction.....	1
1.1. Motivation.....	1
1.2. Aerosols.....	3
1.2.1. Organic Aerosols.....	3
1.2.2. Secondary Organic Aerosols.....	5
1.2.3. Impact of SOAs on Aerosol Chemical and Physical Properties.....	6
1.2.3.1. SOAs and Direct Effect.....	7
1.2.3.2. SOAs and Indirect Effect.....	7
1.2.4. The Importance of Carbonyl Compounds and Aerosol Heterogeneous Chemistry.....	8
1.3. Goals of this Research.....	11
1.4. Thesis Outline.....	12
Chapter 2: Secondary Organic Material Formed by Methylglyoxal in Aqueous Aerosol Mimics.....	17

2.1	Introduction.....	17
2.2	Methods.....	20
2.2.1	Bulk Solution Properties.....	20
2.2.2	UV-Vis Spectrophotometry.....	21
2.2.3	Surface Tension Measurements.....	21
2.2.4	Aerosol-CIMS.....	22
2.2.5	DFT Calculations.....	27
2.3	Results and Discussion.....	28
2.3.1	UV-Vis Absorption.....	28
2.3.1.1	Experimental Results.....	28
2.3.1.2	DFT Calculations.....	32
2.3.2	Surface Tension.....	35
2.3.3	Aerosol-CIMS.....	38
2.3.3.1	Negative Ion Detection with I ⁻	38
2.3.3.1.1	DFT Calculations.....	41
2.3.3.1.2	Volatile Species.....	43
2.3.3.1.3	(Hemi)acetals and Aldol Condensation Products.....	43
2.3.3.1.4	Sulfur-Containing Species.....	44
2.3.3.2	Positive Ion Detection Using H ₃ O ⁺ (H ₂ O) _n	46
2.3.3.2.1	(Hemi)acetals and Aldol Condensation Products.....	50
2.3.3.2.2	Sulfur-Containing Species.....	51

2.3.3.2.3	High-Molecular-Weight Species.....	51
2.3.3.3	Role of NaCl from Aerosol-CIMS data.....	52
2.3.4	Mechanism.....	53
2.3.5	Kinetics.....	54
2.4	Conclusions and Atmospheric Implication.....	56
Chapter 3: Oxidative Aging of Light-Absorbing Secondary Organic Aerosol Material Formed by Methylglyoxal and Glyoxal.....63		
3.1	Introduction.....	63
3.2	Methods.....	65
3.2.1	Aerosol Generation.....	65
3.2.2	Gas-Phase Reactants.....	65
3.2.3	Flow Reactors.....	66
3.2.4	Aerosol-CIMS Detection of Products.....	68
3.2.5	Particle Collection and UV-Vis Spectrophotometry.....	69
3.2.6	Heterogeneous Reaction Kinetics.....	69
3.3	Results and Discussion.....	71
3.3.1	Ozonolysis Products for SOAs from (NH ₄) ₂ SO ₄ and methylglyoxal.....	71
3.3.2	Kinetics of Ozonolysis.....	76
3.3.3	Changes in UV-Vis Absorption with Ozonolysis.....	78
3.3.4	Photolysis, OH Oxidation Products and Kinetics of SOAs from (NH ₄) ₂ SO ₄ and methylglyoxal.....	80
3.3.5	Volatilization.....	84

3.4	Conclusions and Atmospheric Implications.....	84
Chapter 4: Surfactants from the Gas-Phase Promote Cloud Droplet Formation.....		87
4.1	Introduction.....	87
4.2	Methods.....	89
4.3	Calculations.....	92
4.3.1	Cloud Droplet Number (CDN) Calculations.....	92
4.3.2	Kinetics of Methylglyoxal Hydration and Oligomerization.....	93
4.3.3	Inorganic:Organic Ratio.....	94
4.3.4	Köhler Theory Analysis (KTA)	94
4.3.5	Surface Tension of the Particle Based on Henry’s Law.....	95
4.3.6	Concentration of Methylglyoxal at the Moment of Activation....	97
4.3.7	Calibration of Supersaturation in the CCN Counter.....	97
4.4	Results and Discussion.....	98
4.5	Conclusions.....	116
Chapter 5: Conclusions and Future Directions.....		117
References.....		121

List of Tables

Table 2.1.	Proposed reaction products and predictions for the energy of the gas phase HOMO-LUMO transition and the wavelength of UV-Vis absorption.....	32
Table 2.2.	Proposed peak assignments for Aerosol-CIMS mass spectra with I ⁻ as the reagent ion.....	40
Table 2.3.	Proposed reaction products and predictions for the free energy change...	41
Table 2.4.	Proposed peak assignments for Aerosol-CIMS mass spectra with H ₃ O ⁺ (H ₂ O) _n as the reagent ion.....	47
Table 3.1.	Table adapted from Sareen et al. (2010) showing proposed peak assignments for Aerosol-CIMS mass spectra with I ⁻ as the reagent ion for solutions containing methylglyoxal and (NH ₄) ₂ SO ₄	72
Table 3.2.	Compounds formed upon the ozonolysis, photolysis, and/or OH oxidation of the SOA products of (NH ₄) ₂ SO ₄ and methylglyoxal.....	75
Table 3.3.	Kinetic parameters for the ozonolysis of the SOA products of (NH ₄) ₂ SO ₄ and methylglyoxal.....	77
Table 3.4.	Relative increase in absorption after oxidation.....	79
Table 3.5.	Photolysis rate constants for the SOA products of (NH ₄) ₂ SO ₄ and methylglyoxal for our experimental setup.....	81
Table 3.6.	Kinetic parameters for the oxidation of the SOA products of (NH ₄) ₂ SO ₄ and methylglyoxal by OH.....	84

Table 4.1.	Exponents of the power log fits for the SS vs dry diameter graphs for the various chamber experiments.....	108
Table 4.2.	Hygroscopicity parameter, κ , values for the different chamber and flowtube experiments for methylglyoxal and acetaldehyde	109

List of Figures

Figure 1.1.	The major factors that affect the radiative forcing of climate.....	2
Figure 1.2.	Aerosol Mass Spectrometer (AMS) data for various locations in the Northern Hemisphere.....	4
Figure 2.1.	Schematic of Aerosol-CIMS setup.....	23
Figure 2.2.	UV-Vis spectra of aqueous solutions containing 3.1M (NH ₄) ₂ SO ₄ and methylglyoxal.....	29
Figure 2.3.	Absorbance at 282 nm of aqueous solutions.....	31
Figure 2.4.	Results of pendant drop tensiometry measurements of aqueous mixtures as a function of initial methylglyoxal concentration.....	36
Figure 2.5.	Negative-ion mass spectrum of aerosolized aqueous solutions initially containing methylglyoxal alone or with NaCl or (NH ₄) ₂ SO ₄	39
Figure 2.6.	Detail of a 0.5 amu-resolution negative ion mass spectrum of aerosolized methylglyoxal/(NH ₄) ₂ SO ₄ solution.....	45
Figure 2.7.	Positive ion mass spectrum of aerosolized aqueous solutions initially containing methylglyoxal alone or with NaCl or (NH ₄) ₂ SO ₄	47
Figure 2.8.	Detail of a positive ion mass spectrum of an aerosolized methylglyoxal/(NH ₄) ₂ SO ₄ solution.....	52
Figure 3.1.	Schematic for O ₃ setup.....	67
Figure 3.2.	Schematic for OH setup.....	68
Figure 3.3.	Spectrum showing the difference between (NH ₄) ₂ SO ₄ and methylglyoxal particles exposed to 0.2 ppm of O ₃ and not being exposed to O ₃	73

Figure 3.4.	Loss of the peak at 271.5 amu as a function of reaction time in the presence of O ₃	76
Figure 3.5.	Average k' values for the peak at 271.5 amu over varying ozone concentrations.....	77
Figure 3.6.	UV-Vis spectra of (NH ₄) ₂ SO ₄ and a) glyoxal SOA particles exposed to 0.2 ppm of O ₃ b) methylglyoxal SOA particles exposed to 0.2 ppm of O ₃	78
Figure 3.7.	Spectrum showing the difference between (NH ₄) ₂ SO ₄ and methylglyoxal particles exposed to 9.5 x 10 ⁶ molecules cm ⁻³ of OH and not being exposed to OH.....	83
Figure 4.1.	Schematic of the experimental setup for the aerosol chamber.....	90
Figure 4.2.	Cloud condensation nuclei (CCN) activity data for humidified (NH ₄) ₂ SO ₄ aerosols exposed to gas-phase methylglyoxal or acetaldehyde in a 3.5 m ³ Teflon reaction chamber.....	99
Figure 4.3.	Cloud condensation nuclei (CCN) activity data for each individual experiment.....	100
Figure 4.4.	Change in CCN concentration when surfactant effects are included for marine aerosols.....	104
Figure 4.5.	Change in CCN concentration when surfactant effects are included for continental aerosols.....	105
Figure 4.6.	Cloud droplet number concentrations computed using a droplet activation parameterization.....	107
Figure 4.7.	SMPS data showing the number size distribution of particles over time.....	112

Figure 4.8.	CFSTGC data of the extracted filter samples.....	114
Figure 4.9.	CFSTGC data from organics in solution compared to the $(\text{NH}_4)_2\text{SO}_4$ control.....	115

List of Schemes

Scheme 2.1. Proposed reaction pathways for methylglyoxal.....	19
Scheme 3.1. Ozonolysis of the product at 271.5 amu leads to the formation of (a) formic acid and CO ₂ and/or (b) acetic acid and CO ₂	74
Scheme 3.2. Photooxidation mechanism for methylglyoxal in air.....	81

Acknowledgements

This work and the completion of my thesis has been made possible through the invaluable contribution of a number of people. I cherish my relationships with all of you and thank you for inspiring me.

I would especially like to express my deepest gratitude to my advisor, Dr. Faye McNeill, for her constant guidance and motivation. It has been an honor to be her first Ph.D. student. She has continually and convincingly conveyed a spirit of adventure and excellence in regard to research. I will forever treasure the time I have spent with her and her contagious love for science. She will be my mentor and role model throughout my life. Thanks, Prof. and Sid, for always looking out for me. No words can express the knowledge and maturity I have gained under your guidance.

I would like to thank my thesis committee, Dr. West, Dr. Banta, Dr. Venkatasubramanian, and Dr. Park for giving their time and expertise towards the completion of my thesis.

I am thankful to my lab mates, particularly, Allie, Samar, Coty, Sophie, Min, Joe, DooWon, Dhruv, for sharing their vast knowledge and for being an important part of my life. Every one of you is very special to me. I will miss our food expeditions, dessert sushi, dimsum, and particularly our cake tastings.

I would like to thank my undergraduate advisor, Dr. Lynden Archer for motivating me to pursue chemical engineering. I am also thankful to Dr. Edward Coleman, my mentor at Kraft during my summer internship for encouraging me to pursue a Ph.D.

I would like to thank our collaborators Dr. Athanasios Nenes and Terry Lathem for teaching me about clouds. I want to express my gratitude towards Walter Kahn, Kevin Kuchta at Extrel, and Noah at TechAir.

I would like to thank all my family members, especially my *masis* for their endless support and love. My grandparents, for always believing in me as a scientist and as their granddaughter. My parents, Tejinder and Sunita Sareen for always holding me in high esteem and loving me. Papa, for teaching me the value of patience, and ma for persistence. Tani, you are the best sister ever for bringing Amit and Sachi to my life. You are the reason for who I am today. To all my friends through the years, particularly, Mansi, Aboli, Mahwish, Ritika, Karnika, Riti, Rohan, and Navi for all the amazing moments we have shared and will share. To Neves, for continuously challenging me, showing me a whole new world with your kindness and undefeatable smile. *You're just too good to be true.*

For every single step you have taken, you have inspired me to keep moving forward.

For every smile of yours, you have added thousands to my journey.

This page intentionally left blank

CHAPTER 1. Introduction

Atmospheric aerosol particles can have a substantial impact on climate. There are a variety of uncertainties associated with them owing to their variable composition and the multiphase reactions that can occur within them. Previously, atmospheric chemistry focused primarily on chemical processes that can happen in the gas-phase. In the past decade increasing importance has been given to aqueous heterogeneous chemistry in aerosols leading to a growing number of studies that have focused on understanding its impacts on climate.

1.1 Motivation

Experimental, modeling, and field studies have all shown that atmospheric aerosols are ubiquitous in the atmosphere and are important for the climate and chemistry of the atmosphere besides having an impact on air quality, affecting human health and visibility. (IPCC, 2007; Rudich, 2003; Rudich et al., 2007) Aerosols have two main effects on climate: the direct effect and the indirect effect. The direct effect involves their ability to absorb and scatter incoming solar radiation, which can have a net warming or a net cooling effect, respectively. An increasing concentration of particles in the atmosphere provides additional surface area to absorb and scatter light, thereby affecting the Earth's radiation balance. Furthermore, depending on the composition of the aerosol, they might either absorb or scatter radiation. For instance, black carbon, which is formed via combustion, absorbs radiation, having a net warming effect, whereas sulfate aerosols have a net cooling effect. In addition, aerosols can also affect cloud properties such as

their lifetime, albedo, optical and radiative properties. This is termed the aerosol indirect effect. (IPCC, 2007) The Intergovernmental Panel on Climate Change has recognized that the level of scientific understanding of the effect of aerosols on the radiative forcing of climate is low, as can be seen in Figure 1.1. Besides aerosols, they highlight a variety of different factors that influence radiative forcing such as greenhouse gases and ozone, but it should be noted that the uncertainty related to the indirect effect of aerosols is the largest. Hence, there is a need to enhance our fundamental understanding of the influence of aerosols on Earth’s climate and the chemical composition of the atmosphere.

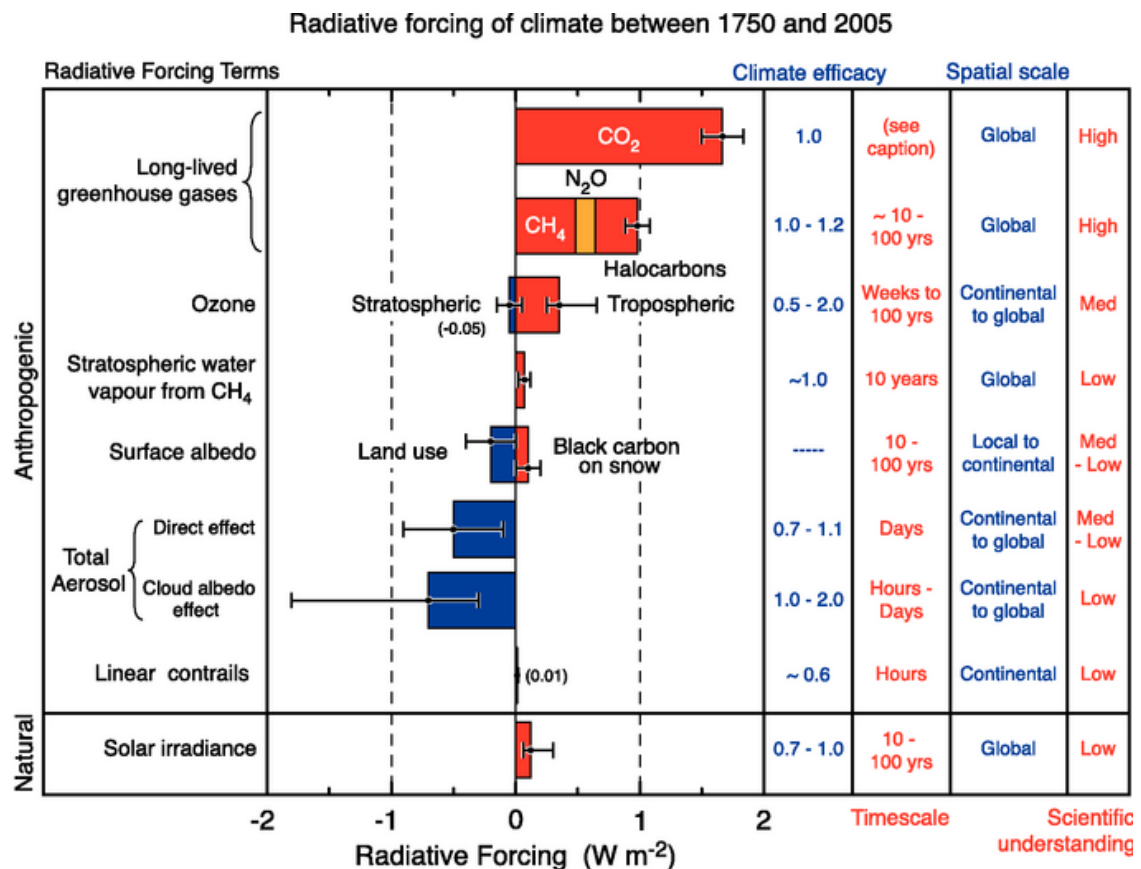


Figure 1.1. The major factors that affect the radiative forcing of climate. Figure adapted from the 2007 IPCC report. (IPCC, 2007)

1.2 Aerosols

Aerosol particles range in size from ~ 2 nm to 20 μ m. They can last for up to a week in the atmosphere. Their heterogeneous chemistry in the troposphere has been shown to play a critical role in climate and gas-phase atmospheric chemistry. (Liao and Seinfeld, 2005; Ravishankara, 1997; Jacob, 2000) Due to the uncertainty involved with tropospheric aerosol composition and morphologies, the heterogeneous interactions in the troposphere are not well-classified, thereby limiting our understanding of the atmospheric chemistry, making it an important area for future research.

1.2.1 Organic Aerosols

Tropospheric aerosol particles are typically comprised of inorganic and organic matter. A major uncertainty associated with studying them is their highly variable composition; the organic mass in particles can range anywhere from 10 to 90%. (Kanakidou et al., 2005) This organic aerosol (OA) material can influence various chemical and physical properties of the aerosol such as the heterogeneous reactivity of aerosol particles, (Brown et al., 2006; Folkers et al., 2003; McNeill et al., 2006; Thornton and Abbatt, 2005) their ability to act as cloud condensation nuclei (CCN), (Abbatt et al., 2005; Köhler, 1936; Rudich et al., 2007) and their radiative properties. (Tabazadeh, 2005; Kent et al., 1983) For instance, organic matter can form a film on the surface of the particle and then influence its reactivity and/or uptake by various gases in the atmosphere including ozone (O_3), hydroxyl radical (OH), and N_2O_5 . (Anttila et al., 2006; Brown et al., 2006; McNeill et al., 2006; McNeill et al., 2007; Park et al., 2007; Thornton and

Abbatt, 2005) Additionally, the presence of organic matter can suppress the surface tension of the aerosol and affect its ability to form a cloud droplet. (McNeill et al., 2012)

Figure 1.2 shows a map by Zhang et al., where they compiled particle composition data measured using an Aerosol Mass Spectrometer (AMS) from field campaigns at various urban and rural locations in the Northern hemisphere. (Zhang et al., 2007a) Each color in the pie chart represents a different component of the aerosol composition, including nitrate, sulfate, ammonium, and organics. As can be seen from the figure, a majority of these sites contain over 50% of organic mass, which reiterates the importance of organic matter in aerosols.

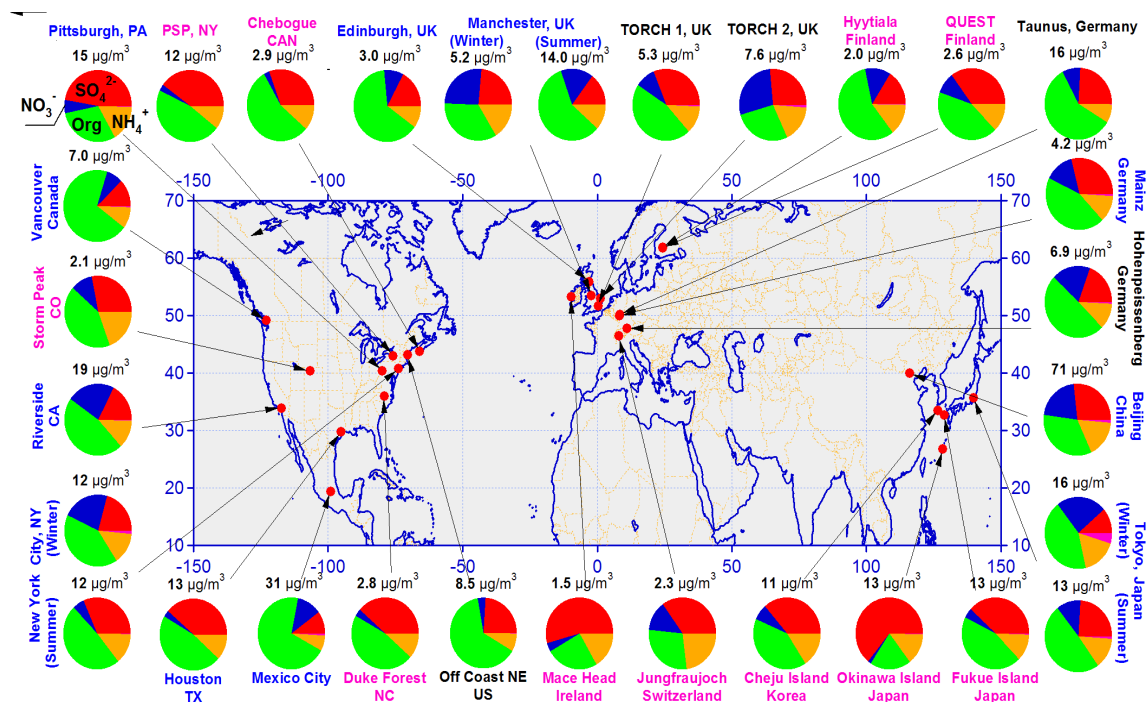


Figure 1.2. Aerosol Mass Spectrometer (AMS) data for various locations in the Northern Hemisphere adapted from Zhang et al. (Zhang et al., 2007a) Colors for the study labels indicate the type of sampling location: urban areas (blue), <100 miles downwind of major cities (black), and rural/remote areas >100 miles downwind (pink). Pie charts show the

average mass concentration and chemical composition: organics (green), sulfate (red), nitrate (blue), and ammonium (orange).

In the past decades, field measurements have identified numerous organic species in particles in the atmosphere, although their impact on atmospheric chemistry has still not been completely understood. (Jacobson et al., 2000; McMurry, 2000; Saxena and Hildemann, 1996) In the following sections, an overview will be provided on the role of OAs in tropospheric chemistry, and the increasing interest in understanding their sources and sinks. (Rudich et al., 2007)

1.2.2 Secondary Organic Aerosols

Organic aerosols can be either primary or secondary in nature. Primary organic aerosols (POA) refer to particles that are directly emitted into the atmosphere. They have both biogenic and anthropogenic sources, which include bubble bursting in marine environments, industrial emissions, and combustion amongst others. (Kanakidou et al., 2005) Secondary organic aerosols (SOA) are not directly emitted, but are formed as a result of chemical reactions in the atmosphere.

One way in which the organic content of aerosol may increase is by the oxidation of volatile organic compounds (VOCs) in the atmosphere, which can lead to the formation of less volatile products that can condense onto existing aerosols. (Seinfeld and Pankow, 2003) Heterogeneous reactions of gas-phase organic compounds on aqueous aerosols or cloud droplets can also form OA. (Carlton et al., 2006; Jang and Kamens,

2001; Kroll et al., 2005; Sareen et al., 2010; Schwier et al., 2010; Shapiro et al., 2009; Tan et al., 2010) These two classes of processes that lead to an increase in the organic content of aerosols are considered to be the two important sources of SOAs in the atmosphere. (Fuzzi et al., 2006) SOA formation can have important consequences for the physical and chemical properties of the seed aerosol. It is also essential to remember that SOAs are formed via interactions of VOCs with inorganic aerosols; they are not directly emitted into the atmosphere, hence reducing emissions is not necessarily effective in reducing their impacts on climate. There is a need to understand the different formation mechanisms and reaction pathways for SOAs. The formation of SOA material is still a major source of uncertainty in atmospheric chemistry models. An improved understanding of SOA formation pathways can help reduce the uncertainty in the aerosol forcing of climate and will allow for a more accurate representation of these processes in atmospheric chemistry and climate models, thereby enhancing their prognostic capabilities.

1.2.3 Impact of SOAs on Aerosol Chemical and Physical Properties

In addition to our lack of understanding of the formation pathways of SOA, it is unclear how they contribute to the aerosol direct and indirect effect. SOAs can alter the optical properties of the seed particles, hence the direct effect. They can also affect the ability of a particle to nucleate and grow into a cloud droplet, i.e. the CCN activity of the seed aerosol, and hence the indirect effect.

1.2.3.1 SOAs and Direct Effect

It has been hypothesized that SOAs can be a source of atmospheric brown carbon. Brown carbon includes non-soot, light-absorbing carbonaceous aerosols that have been identified in air affected by pollution or the burning of biomass or biofuel. (Alexander et al., 2008; Andreae and Gelencsér, 2006; Bank and Castillo, 1987; Havers et al., 1998; Pósfai et al., 2004) Compared to black carbon (soot, formed from incomplete combustion of fossil fuels and biomass), brown carbon does not absorb at wavelengths of ~550 nm and higher, thereby not having a major impact on aerosol absorption in these ranges. (Kirchstetter et al., 2004) But, brown carbon does absorb strongly at the lower UV wavelengths which can alter tropospheric photochemistry, reducing ozone levels. (Jacobson, 1999, 2002) Because of the lack of understanding of the formation mechanisms and physical properties of brown carbon, they are not well-represented in atmospheric chemistry and climate models; consequently their role in heating or cooling of the atmosphere can not be accurately known.

1.2.3.2 SOAs and Indirect Effect

SOA formed from the condensation of gas-phase semivolatile oxidation products has been shown to form thin (~10nm) multilayer coatings around aqueous inorganic seed aerosols. (Anttila et al., 2007) This phenomenon of film formation could also play a role in the generation of SOA from the heterogeneous uptake of VOCs. SOA species are likely to be surface-active as they will contain oxygenated, polar functional groups, thereby making possible the formation of a film on aqueous aerosols. (Asa-Awuku et al.,

2010; Sareen et al., 2010; Schwier et al., 2010) This organic film formation has the potential of inhibiting the transfer of gas phase species to and from the aerosol surface layer; hence affecting the particle's heterogeneous reactivity and its CCN ability.

Numerous experimental (Corrigan and Novakov, 1999; Cruz and Pandis, 1997, 1998; Ekström et al., 2009; Henning et al., 2005; Prenni et al., 2001; Raymond and Pandis, 2002, 2003) and field studies (Liu et al., 1996; Facchini et al., 1999) have shown that the presence of surfactants in aerosols can impact the CCN activity of the aerosol. Köhler theory describes cloud droplet activation and growth from soluble particles as an equilibrium process. (Köhler, 1936) The ability of a particle to act as a CCN is dependent on its surface tension and typically Köhler Theory is used to describe how it activates at a given supersaturation. The Köhler equation takes into account two competing effects: the Raoult, or solute effect, which tends to decrease the equilibrium vapor pressure of water over the growing droplet, and the Kelvin or curvature effect, which serves to increase the equilibrium vapor pressure. Surface films affect the surface tension of the aerosol, which comes into play in the Kelvin effect here. Surface films can affect cloud formation by retarding the growth of CCN and driving up cloud supersaturation, hence proving to be an important factor in the aerosol-cloud-climate problem. (Feingold and Chuang, 2002)

1.2.4 The Importance of Carbonyl Compounds and Aerosol Heterogeneous Chemistry

Carbonyl compounds are prevalent in the atmosphere in the gas-phase and can have adverse health effects. (Possanzini et al., 1996) They are important for atmospheric

chemistry in the troposphere primarily due to their role as stable intermediate products of photooxidation reactions of organics. Industrial and vehicular exhausts are the primary sources of carbonyls in the atmosphere. Photochemical reactions of other VOCs are a secondary source. Recent work has focused on understanding the mechanisms of how carbonyl compounds like glyoxal, methylglyoxal, acetaldehyde, formaldehyde, can be potential SOA precursors and how they can impact the properties of the seed aerosol. (Grosjean et al., 2002; Sin et al., 2001; De Haan et al., 2009a; Galloway et al., 2009; Li et al., 2011; Nozière et al., 2009b; Sareen et al., 2010; Schwier et al., 2010; Shapiro et al., 2009)

Recent field measurements have shown the presence of significantly more SOA than has been predicted by state-of-art atmospheric chemistry models, which means that there is a need to identify other SOA precursors or mechanisms, as highlighted in the previous section. (Heald et al., 2005; Volkamer et al., 2007) Studies suggest that a significant source of this unaccounted-for OA might be the heterogeneous uptake of glyoxal by aerosols, followed by particle-phase chemical processing to yield low-vapor-pressure organics. (Volkamer et al., 2007) Glyoxal is a first-generation gas-phase oxidation product of various biogenic and anthropogenic VOCs. (Baker et al., 2005; Tuazon et al., 2005) It has recently been observed that the glyoxal concentrations in Mexico City were significantly lower than those predicted by models. These studies concluded that this missing sink of glyoxal resulted from irreversible heterogeneous uptake to aqueous inorganic aerosol. (Volkamer et al., 2007) Hence, it was hypothesized that there is a link between the missing glyoxal sink and missing SOA source observed in Mexico City; particularly that glyoxal is taken up by existing particles to form SOAs,

making it a potential SOA precursor. Even though the exact mechanisms of this process were unknown, adding an uptake coefficient for glyoxal to aerosols into the model helped bridge the gap between the measured and predicted SOA in Mexico City.

As a result of these observations, there has been an increased focus in recent years on understanding the role of glyoxal as an SOA precursor. Various techniques have since been used to study the different chemical and physical properties of SOAs resulting from glyoxal. It has been observed that glyoxal forms light-absorbing compounds and that they can react in the aqueous phase to form organic acids, oligomers, organo-sulfates, nitrogen containing compounds. (Galloway et al., 2009; Nozière et al., 2009b; Shapiro et al., 2009) Various mechanisms have been identified that lead to the formation of these compounds, including photochemical oxidation, acid-catalyzed reactions, and self-oligomerization. (De Haan et al., 2009a; De Haan et al., 2009b; Galloway et al., 2009; Kroll et al., 2005; Liggio et al., 2005; Shapiro et al., 2009; Lim et al., 2010)

Another dicarbonyl compound that has been proposed to be a potential SOA precursor is methylglyoxal. It has an additional methyl group, which can lead to potentially more interesting chemistry as compared to glyoxal. Both compounds coexist in the atmosphere as they are first-generation oxidation products of similar biogenic and anthropogenic VOCs. (Baker et al., 2005; Tuazon et al., 2005; Tuazon et al., 1984; Tuazon et al., 1986; Volkamer et al., 2005; Volkamer et al., 2001) Aerosol chamber studies have shown negligible particle growth when methylglyoxal is exposed to inorganic seed aerosols, contrary to what was observed for glyoxal. (Kroll et al., 2005) It has also been suggested that oligomers formed from methylglyoxal can explain the presence of polymeric material observed in SOA reaction chamber studies. (Kalberer et

al., 2004) Compared to glyoxal less is known about the effect of methylglyoxal in atmospheric chemistry and formation of SOAs.

1.3 Goals of this Research

The main goal of this research has been to explore the role of carbonyl compounds in the atmosphere, with a focus on methylglyoxal as a potential SOA precursor and its impacts on aerosol physical and chemical properties. Using our understanding of the chemistry of the atmosphere and various analytical tools, we will address the following science questions:

1. Can the interactions of methylglyoxal with inorganic aqueous aerosols be an atmospherically relevant pathway for SOA formation with important implications for properties of the seed aerosol?
2. What is the lifetime of aerosols formed from methylglyoxal and ammonium sulfate in an oxidizing environment and how does oxidation impact light-absorption of these aerosols?
3. Can the presence of carbonyls like methylglyoxal and acetaldehyde affect the CCN activity of aerosols?

1.4 Thesis Outline

The main goal of my research has been to assess the hypothesis that **methylglyoxal can be a potential SOA precursor, and that it can affect the optical properties and CCN activity of the seed aerosol.**

In chapter 2, the focus lies on analyzing the optical properties and the surface tension of bulk solutions containing methylglyoxal and ammonium sulfate and determining the composition and reaction pathways of these aerosol mimics. Various tools are used to evaluate this goal. We will use bulk solutions that mimic atmospheric aerosols as a proxy to study the chemistry and various properties of aerosols formed from methylglyoxal and ammonium sulfate. These bulk solutions provide us with a first order estimate of how the presence of methylglyoxal can impact aqueous aerosol chemistry. It helps us to narrow the scope of future studies which can be conducted at even more atmospherically relevant conditions in aerosol chambers and flow tube reactors.

An Aerosol Chemical Ionization Mass Spectrometer (Aerosol-CIMS) is used to determine the composition of these aerosol mimics. Knowing the products of this reaction, allows us to outline the different reaction pathways and mechanisms that can occur in the presence of methylglyoxal in the atmosphere. Chemical ionization is a relatively soft ionization technique, which is essential for our studies as we focus on organics and require the least amount of fragmentation of our particles.

To study how these aerosols can impact the direct effect on climate, we use UV-Vis spectrophotometry. Time, pH, and concentration dependent studies can provide

insight into the kinetics of the reactions with methylglyoxal. We will explore the possibility of these aerosols to be a source of “brown carbon”.

Lastly, we will evaluate the impact of the presence of methylglyoxal on the indirect effect of climate, i.e. if it influences the ability of a particle to form a cloud droplet. To this effect, we will study the surface tension properties of the bulk mixtures containing methylglyoxal and ammonium sulfate using pendant drop tensiometry (PDT). Organic material in the atmosphere can be surface-active comprising of both hydrophilic and hydrophobic moieties. In an aerosol particle, these can partition to the gas-liquid interface and form a film that can lower the surface tension of the aerosol. (Sareen et al., 2010; Schwier et al., 2010) This has important implications for the heterogeneous reactivity of the aerosol towards gases like N_2O_5 , ozone, and, OH in the atmosphere, for ice nucleation, and for the cloud forming potential of the particle. Numerous experimental (Corrigan and Novakov, 1999; Cruz and Pandis, 1997, 1998; Ekström et al., 2009; Henning et al., 2005; Prenni et al., 2001; Raymond and Pandis, 2002, 2003) and field studies (Liu et al., 1996; Facchini et al., 1999) have shown that the presence of surfactants in aerosols can impact the ability of an aerosol to nucleate and grow into a cloud droplet, also known as cloud condensation nucleus (CCN) activity. Hence, if the presence of methylglyoxal affects the surface tension of the aerosol, it can have important implications for CCN activity.

We show that methylglyoxal forms light-absorbing secondary organic material in aqueous ammonium sulfate and ammonium nitrate solutions mimicking tropospheric aerosol particles. Aqueous solutions of methylglyoxal, with and without inorganic salts, exhibit significant surface tension depression. Evidence of aldol condensation products

and oligomeric species up to 759 amu was found using Aerosol-CIMS. These observations add to the growing body of evidence that dicarbonyl compounds may form secondary organic material in the aerosol aqueous phase, and that secondary organic aerosol formation via heterogeneous processes may affect seed aerosol properties.

In chapter 3, we will study the effect of oxidation by ozone and OH on the secondary organic material formed from methylglyoxal and ammonium sulfate. If the atmospheric lifetimes of this SOA material are sufficiently long, they may affect aerosol optical properties and could potentially be used as tracer species for methylglyoxal SOA formation chemistry. The atmosphere is a huge reservoir of oxidants such as ozone, OH, and NO_3 . In such an environment, the formation of SOAs that have methylglyoxal as a precursor will be competed with their degradation via the above-mentioned oxidants. Upon oxidation, the optical and CCN properties of the SOAs can also be altered. In order to study the lifetimes of these compounds, the aerosol mimics of methylglyoxal and ammonium sulfate will be exposed to the oxidant of choice in a flow tube reactor coupled to the Aerosol-CIMS. Reaction rates and other kinetic parameters can be attained by changing the reaction times in the reactor. UV-Visible absorption of particles will be compared before and after oxidation. Oxidation mechanisms, products, and atmospheric lifetimes will be discussed.

Chapter 4 explores the ability of secondary organic surface-active material in the atmosphere to affect the CCN activity of the seed aerosol, and thereby the indirect effect on climate as highlighted previously. If methylglyoxal is found to be surface-active in aerosols, it can consequently influence the CCN activity of the seed aerosols. As

mentioned previously, the equilibrium growth and activation of an aqueous particle is described by Köhler Theory:

$$S = \frac{A}{D_p} - \frac{B}{D_p^3} \quad (1.1)$$

with

$$A = \frac{4M_w\sigma}{RT\rho_w} \text{ and } B = \frac{6n_sM_w}{\pi\rho_w}$$

where S is the equilibrium water vapor supersaturation, D_p is the diameter of the aqueous droplet, M_w is the molecular weight of water and ρ_w is its density, R is the gas constant, T is temperature, σ is surface tension, and n_s is the number of moles of solute.

The ‘A’ term which accounts for the surface tension of the particle is called the Kelvin effect, and it describes the enhancement of vapor pressure due to the curvature of the droplet. The ‘B’ term or the Raoult effect accounts for the changes in vapor pressure due to solute concentration. According to the assumptions of Köhler theory, when the ambient water saturation ratios exceed S , the particles spontaneously activate and grow to form cloud droplets.

Here, an aerosol chamber will be used to study how gas-phase methylglyoxal and/or acetaldehyde interact with inorganic seed aerosols and alter their CCN potential. Compared to a flow tube reactor, an aerosol chamber allows for longer residence times to be tested that can be more atmospherically relevant. A continuous flow stream-wise thermal gradient CCN counter (CFSTGC) is coupled to the chamber to study the CCN activity of the aerosols. This instrument comprises of a vertical column with wetted walls. These wet walls and a temperature gradient through the column forms the water

vapor needed to produce the various supersaturations. Under these supersaturation conditions, a particle can activate to form droplets, which are measured by an optical particle counter. Scanning Mobility CCN Analysis (SMCA) (Moore et al., 2010) is used to obtain fast measurements of size-resolved CCN activity of the aerosol particles.

Significant enhancements in CCN activity, up to 15% reduction in critical dry diameter for activation, are observed over a timescale of hours. This reduction in critical diameter enhances the apparent particle hygroscopicity up to 65%, which can lead to a significant increase in cloud droplet number concentrations by up to 20%. This is the first time that the presence of relatively insoluble VOCs has been shown to enhance aerosol CCN activity.

Finally, chapter 5 summarizes the main conclusions of the work and scope for future work.

CHAPTER 2. Secondary organic material formed by methylglyoxal in aqueous aerosol mimics

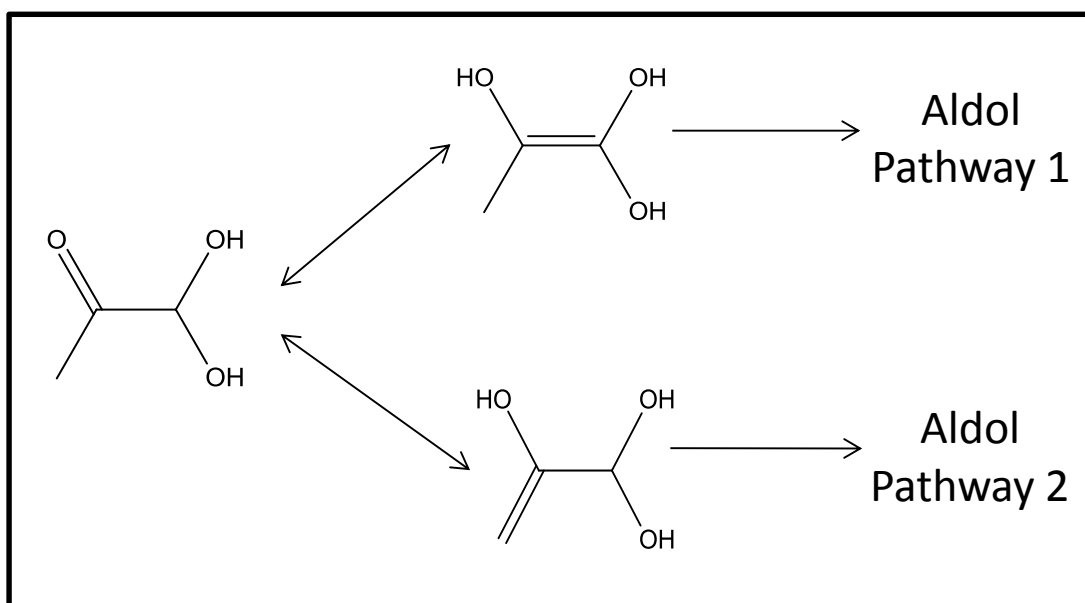
2.1 Introduction

Laboratory and field studies suggest that carbonyl-containing volatile organic compounds, when absorbed by aqueous aerosol particles or cloud droplets, participate in aqueous-phase chemistry to form low-volatility secondary organic material (SOA). (Altieri et al., 2008; Carlton et al., 2008; De Haan et al., 2009a; El Haddad et al., 2009; Fu et al., 2009; Galloway et al., 2009; Jang et al., 2002; Kroll et al., 2005; Liggio et al., 2005; Loeffler et al., 2006; Nozière et al., 2009b, a; Shapiro et al., 2009; Volkamer et al., 2007; Zhao et al., 2006; Gao et al., 2006; Volkamer et al., 2006; Volkamer et al., 2009) There is evidence that SOA formation may affect properties of the seed aerosol such as CCN activity (Cruz and Pandis, 1997; Engelhart et al., 2008a; King et al., 2009; Michaud et al., 2009; Duplissy et al., 2008; Huff Hartz et al., 2005; King et al., 2007), optical properties (Casale et al., 2007; De Haan et al., 2009a; Nozière et al., 2007, 2009b; Nozière and Esteve, 2007; Shapiro et al., 2009), and heterogeneous reactivity towards gases such as N_2O_5 (Anttila et al., 2006; Folkers et al., 2003). A variety of potentially surface-active SOA products have been proposed, including organic acids, organosulfates, nitrogen-containing organics, aldol condensation products, and highly oxygenated oligomeric material. In an aqueous aerosol particle, surface-active products may partition to the gas-particle interface, lowering the surface tension (and thus the critical supersaturation required for cloud droplet activation) and acting as a barrier to

mass transport between the gas and aqueous phases. Light-absorbing SOA products which could increase the absorption index of the seed aerosol have also been identified in laboratory studies. Aldehydes have been reported to undergo aldol condensation in aqueous aerosol mimics to form π -conjugated species. (Casale et al., 2007; Nozière et al., 2007; Nozière and Esteve, 2007) We recently reported the formation of light-absorbing, oligomeric molecules in aqueous aerosol mimics containing glyoxal and ammonium salts. (Shapiro et al., 2009) De Haan et al. (2009a,b) observed browning upon the reaction of glyoxal with amino acids in aerosol and cloud droplet mimics. (De Haan et al., 2009a; De Haan et al., 2009b; Nozière et al., 2009a)

Methylglyoxal ($C_3H_4O_2$) is an atmospheric oxidation product of many anthropogenic and biogenic volatile organic compounds. (Grosjean et al., 1993; Smith et al., 1999; Tuazon et al., 1986) There is mixed evidence in the literature regarding the potential of methylglyoxal to be a direct precursor for heterogeneous SOA formation in aqueous aerosols. Methylglyoxal becomes hydrated and forms acetal and hemiacetal oligomers in aqueous solution. (Kalberer et al., 2004; Krizner et al., 2009; Loeffler et al., 2006; Nemet et al., 2004; Paulsen et al., 2005; Zhao et al., 2006) Kalberer et al. (2004) suggested that methylglyoxal acetal oligomers could explain their observation of polymeric material in secondary organic aerosols formed in a reaction chamber by the photooxidation of 1,3,5-trimethylbenzene. Barsanti and Pankow (2005) and Krizner et al. (2009) predicted that aldol condensation should be favorable for methylglyoxal in aerosols. (Barsanti and Pankow, 2005; Krizner et al., 2009) Singly hydrated methylglyoxal has been reported to be the dominant monomeric species in aqueous methylglyoxal systems. (Nemet et al., 2004) Singly hydrated methylglyoxal may

participate in self-aldol condensation via two possible pathways initiating with enol formation with the C=C double bond forming from either terminal carbon, as shown in Scheme 2.1. Note that we refer to the overall process of aldol addition followed by dehydration as aldol condensation. (Muller, 1994) Zhao et al. (2006) measured non-zero methylglyoxal uptake onto aqueous sulfuric acid solutions in a coated-wall flow tube reactor. However, in aerosol chamber studies Kroll et al. (2005) observed that methylglyoxal uptake to acidic ammonium sulfate seed aerosols did not lead to significant particle growth.



Scheme 2.1. Proposed reaction pathways for methylglyoxal.

We studied the formation of light-absorbing secondary organic products in aqueous solutions containing methylglyoxal and ammonium salts. The kinetics of formation were characterized using UV-Vis spectrophotometry. We also characterized

the reaction products via atomization of diluted reaction mixtures followed by detection with chemical ionization mass spectrometry with a volatilization flow tube inlet (Aerosol-CIMS). We found evidence of aldol condensation products and high-molecular-weight oligomeric species, as well as possible sulfur-containing compounds and carbon-nitrogen species. Pendant drop tensiometry measurements show that aqueous solutions of methylglyoxal exhibit surface tension depression, and the effect is enhanced when NaCl or $(\text{NH}_4)_2\text{SO}_4$ is present. These observations add to the growing body of evidence that dicarbonyl compounds form secondary organic material in the aqueous phase, and that SOA formation via heterogeneous processes may affect seed aerosol properties.

2.2 Methods

2.2.1 Bulk Solution Preparation

Salt concentrations in atmospheric aerosols at typical relative humidities exceed bulk saturation concentrations. (Tang, 1997; Tang and Munkelwitz, 1994) In an effort to mimic atmospheric aerosol compositions to the extent possible in a bulk solution, solutions were prepared using Millipore water and high (near-saturation) concentrations of the salt of interest (3.1 M $(\text{NH}_4)_2\text{SO}_4$, 5.1 M NaCl, 1.18 M Na_2SO_4 , 8.7 M NH_4NO_3). Methylglyoxal concentrations ranged from 0–2.0 M, corresponding to ~0-25 wt% of the solute. Methylglyoxal was introduced from a 40 wt% aqueous solution (Sigma Aldrich). Mixing time was counted as time after the 40 wt% methylglyoxal solution was introduced to the aqueous salt solution. The aqueous methylglyoxal stock solution was pH = 2.0 (± 0.1) when tested with an Accumet model 20 pH/conductivity meter (Fisher Scientific), and the reaction mixtures that contained ≥ 16.2 mM methylglyoxal

were $\text{pH} = 2.0 (\pm 0.1)$, without buffering or further addition of acid. This is within the range of pH relevant to tropospheric aerosols. (Keene et al., 2004; Zhang et al., 2007b) In experiments performed to test the effect of varying pH, dilute HNO_3 was added to the reaction mixtures dropwise until the desired pH was reached.

Methylglyoxal stock solution is acidic due to the presence of a small amount of pyruvic acid impurity. Pyruvic acid is a relatively strong organic acid, with $\text{pK}_a = 2.49$. Therefore, the fact that our stock solution is $\text{pH} = 2$ corresponds to a very small (0.07% by mole) impurity of pyruvic acid in the methylglyoxal stock solution.

Solutions were prepared in 100 mL Pyrex volumetric flasks. Pyrex is opaque to light with wavelengths < 280 nm (Corning, Inc.), but the samples were not further protected from ambient light except for control experiments as specified in the text. All experiments were performed at ambient temperature and pressure.

2.2.2 UV-Vis Spectrophotometry

The UV-Vis absorption spectra of the reaction mixtures were measured using an HP 8453 UV-Visible Spectrophotometer with a 10 mm open-top quartz cuvette.

2.2.3 Surface Tension Measurements

Surface tension was measured using pendant drop tensiometry as described in Shapiro et al. (2009). Briefly, droplets of sample solution were suspended from the tip of a glass capillary tube using a 100 μL syringe mounted inside a chamber with quartz windows. Images were captured as described by Anastasiadis et al. (1987). (Anastasiadis et al., 1987) The method of Canny (1986) was implemented in MATLAB

7.0 (The MathWorks, Inc.) for edge detection. (Canny, 1986) Surface tension was calculated according to:

$$\sigma = \frac{\Delta\rho g d_e^2}{H} \quad (2.1)$$

where σ is surface tension, $\Delta\rho$ is the difference in density between the solution and the gas phase, g is acceleration due to gravity, d_e is the equatorial diameter of the droplet, and H is the shape factor. (Adamson and Gast, 1997) The method of several selected planes was used for determining H based on the diameter of the drop at five intervals along the drop axis. (Juza, 1997) Solution density was measured using an analytical balance readable to within $\pm 10 \mu\text{g}$ (Denver Instruments).

2.2.4 Aerosol-CIMS

Aerosol-CIMS enables measurements of aerosol composition simultaneously with gas-phase composition, with the high sensitivity, selectivity, and fast time response of CIMS. (Hearn and Smith, 2004a; McNeill et al., 2007; McNeill et al., 2008; Hearn and Smith, 2006a) This technique allows speciated measurements of aerosol organics which are selective based on the choice of parent ion. Chemical ionization is a relatively soft ionization technique that results in low fragmentation of organics, thus simplifying their identification and quantification. Aerosol-CIMS has been used for laboratory studies of the oxidative aging of organic aerosols (Hearn and Smith, 2004b, 2005; Hearn et al., 2005; Hearn and Smith, 2007, 2006b; Hearn et al., 2007; McNeill et al., 2007; McNeill et al., 2008) and to characterize aerosols of unknown, complex chemical composition. (Hearn and Smith, 2006a)

Experiments were conducted using a custom-built Aerosol-CIMS apparatus. Analyte molecules were detected as the products of their interactions with I^- or $H_3O^+(H_2O)_n$ using a quadrupole mass spectrometer with high mass (≤ 1000 amu) capabilities (Extrel CMS). The two reagent ions used, I^- and $H_3O^+(H_2O)_n$, are complementary in their versatility ($H_3O^+(H_2O)_n$) and selectivity (I^-). A schematic of the experimental system is shown in Figure 2.1.

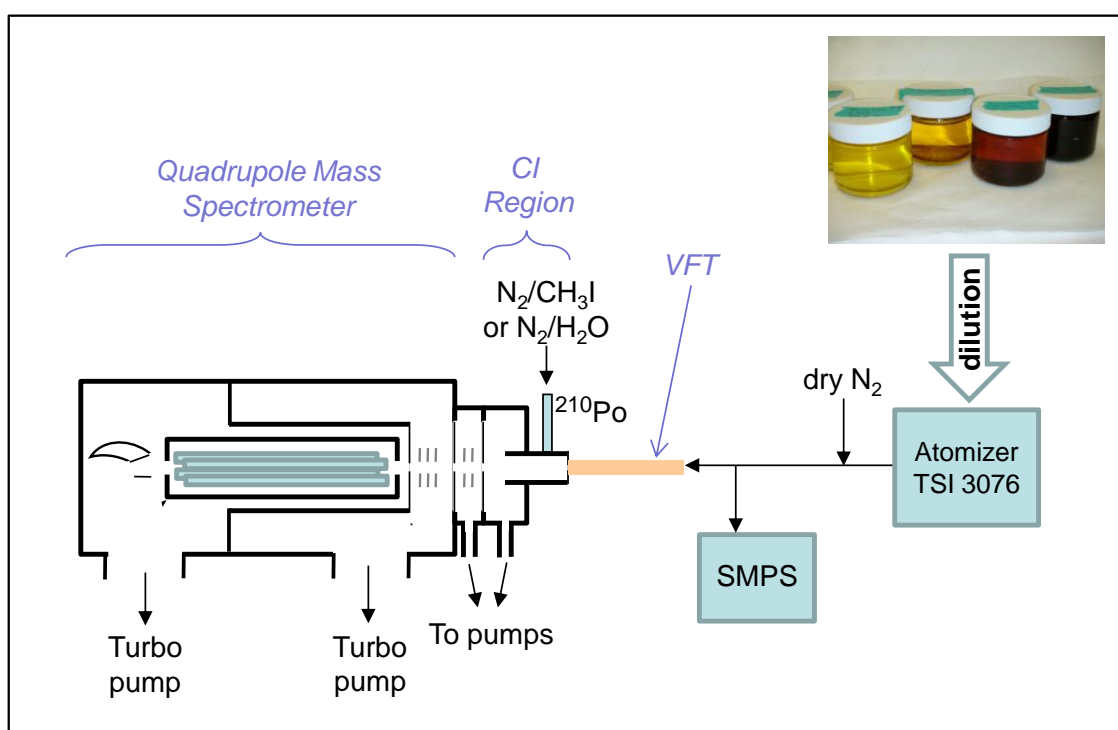


Figure 2.1. Schematic of Aerosol-CIMS setup for the detection of products formed during the reactions of methylglyoxal in aqueous solution with $(NH_4)_2SO_4$ or NaCl. SMPS: scanning mobility particle sizer, VFT: volatilization flow tube, CI: chemical ionization. See text for details.

Mixtures initially containing 1.62 M methylglyoxal and 3.1 M $(NH_4)_2SO_4$ or 5.1 M NaCl were prepared using Millipore water as described in the previous section. After

the desired reaction time had passed, the mixtures were diluted with Millipore water until the salt concentration was 0.2 M. Reaction time was generally >24 h, which was sufficient time for significant light absorption and surface tension depression to develop in the methylglyoxal/(NH₄)₂SO₄ solutions. Reaction kinetics at short times were investigated as follows: a small amount of reaction mixture initially containing 1.62 M methylglyoxal and 3.1 M (NH₄)₂SO₄ was diluted 2 min after mixing. Another sample of the same bulk reaction mixture was diluted 38 min after mixing. The mass spectra of these samples were measured using Aerosol-CIMS immediately after dilution.

Two control experiments were performed, the first in which a 0.2 M (NH₄)₂SO₄ solution at pH = 2 and the second in which a 0.05 M methylglyoxal solution was atomized and analyzed using Aerosol-CIMS. Additional control experiments to test the performance of Aerosol-CIMS in the high mass detection mode were performed using a solution of 0.2 M NaCl and 3.9 mM poly(ethylene glycol) (PEG) (Sigma Aldrich, 570-630 amu) in Millipore water. The instrument was calibrated using aerosol-phase succinic acid (C₄H₆O₄). Aerosols were generated by atomizing a solution of 0.001 M succinic acid in Millipore water. Since the liquid water content of the aerosol particles was not known, we assume that the aerosol mass measured by the SMPS was comprised of 100% succinic acid and report the calculated sensitivity and detection limit values as lower and upper limits, respectively. The instrument sensitivity to aerosol-phase succinic acid was measured using the I⁻ detection scheme to be ≥100 Hz ppt⁻¹ with a detection limit of ≤ 0.01 μg m⁻³. Using the H₃O⁺·(H₂O)_n scheme, the sensitivity to succinic acid was ≥ 66 Hz ppt⁻¹ and the detection limit was ≤ 0.02 μg m⁻³.

The dilute solutions were aerosolized with N₂ using a constant output atomizer (TSI 3076), forming submicron particles. The aerosol stream was combined with a dry N₂ dilution flow, resulting in a relative humidity of 50-60% as measured with a hygrometer (Vaisala). The particle population was characterized using a scanning mobility particle sizer (SMPS) (Grimm Technologies, TSI). The aerosol had a lognormal size distribution with a typical geometric standard deviation of 1.8 and a mean volume-weighted particle radius of 119 ± 1 nm. Typical number concentrations were 7×10^4 cm⁻³. The aerosol stream passed through a 23 cm-long, 1.25 cm ID PTFE tube wrapped in heating tape in order to volatilize the organics before entering the chemical ionization region of the mass spectrometer. The external temperature of the inlet was maintained at 135 °C using a thermocouple and temperature controller (Staco Energy). No increase in signal was observed when the inlet temperature was increased to 160 °C. Some experiments were performed with no inlet heating in order to test for species which were volatile at room temperature.

Flow through the aerosol inlet into the chemical ionization region was maintained at 3 SLPM using a critical orifice. The chemical ionization (CI) region consists of a 3.5 cm ID stainless steel manifold which is 3.8 cm long. Pressure in the CI region is maintained at 45-55 Torr by a mechanical pump (Varian DS302). For the negative ion detection scheme, I⁻ reagent ions were generated by flowing dilute CH₃I (Alfa Aesar, 99.5%) in 3 SLPM N₂ (Tech Air, 99.999%) through a ²¹⁰Po ionizer (NRD). The ionizer was mounted perpendicular to the CI region. For detection with H₃O⁺(H₂O)_n, ions were generated by flowing a combined stream of 2 SLPM N₂ bubbled through Millipore water and 3 SLPM dry N₂ through the ionizer. Ion-neutral reaction times were 20-30 ms. For

the $\text{H}_3\text{O}^+(\text{H}_2\text{O})_n$ detection scheme, the predominant peaks in our spectra are $\text{H}_3\text{O}^+(\text{H}_2\text{O})_2$ at 55 amu and $\text{H}_3\text{O}^+(\text{H}_2\text{O})_3$ at 73 amu. The reagent ions react with the neutral species through proton transfer (Hearn and Smith, 2004a):



or ligand switching (Blake et al., 2009) :



and the species are then detected as the protonated analyte molecule or its cluster with H_2O . In the I^- detection scheme the analyte molecules form clusters with I^- via a ligand-switching reaction:



or they are ionized via proton abstraction:



Ions passed from the CI region through a 0.05 cm-ID charged orifice into a collisional dissociation chamber (CDC) which was maintained at 5 Torr by a mechanical pump (Varian DS402). Ions may be accelerated through this region using a series of biased cylindrical lenses in order to control clustering. The CDC is separated from the MS prechamber ($\sim 10^{-4}$ Torr) by a second charged orifice plate (ID = 0.05 cm). The prechamber contains an ion optics assembly (Extrel CMS) and is separated by a 0.2 cm-ID orifice from the final chamber ($\sim 10^{-7}$ Torr) which houses the 19 mm quadrupole and detector (Extrel CMS). The final two chambers are differentially pumped by identical turbomolecular pumps (Varian TV-301 Navigator) backed by a single mechanical pump

(Varian DS302). For regular operation the RF operating frequency for the mass spectrometer was 1.2 MHz; for high mass mode a 0.88 MHz RF supply was used (Extrel CMS).

2.2.5 DFT Calculations

Geometry optimizations and energy calculations were performed using Jaguar 6.0 (Schrodinger, Inc.) with the ChemBio3D interface (CambridgeSoft) in order to evaluate the UV-Vis absorption of potential products and the energetics of reaction pathways, and to evaluate the interactions of proposed product molecules with I^- for CIMS detection. Density functional theory (DFT) with the B3LYP functional and the cc-pVTZ(-f) basis set (Kendall et al., 1992) was used to predict the HOMO-LUMO energy difference (and thus UV-Vis absorption wavelengths) of proposed products. For purposes of comparison with Krizner et al. (Krizner et al., 2009) some additional calculations were performed with the 6-311G** basis set and Poisson-Boltzmann solvation (water solvent, $\epsilon = 80.37$, probe radius = 1.40 Å). The Gibbs free energy of solvated species was calculated using half the gas phase entropy following Krizner et al. (2009).

For the CIMS ion-molecule reaction calculations, Density functional theory was used with the B3LYP functional and the ERMLER2 basis set, which allows the treatment of iodine via the use of effective core potentials. (Lajohn et al., 1987) The free energy change for the ligand-switching reaction or proton abstraction was calculated. For the ligand switching reactions several geometries for the cluster of the analyte molecule with I^- were tested for each species, and in some cases several stable cluster geometries (local minima) were found. In each case, ΔG for the lowest-energy cluster geometry (global

minimum) is reported. The free energy values reported here are from the output of the 298.15 K vibrational frequency calculation and no further corrections were applied.

2.3 Results and Discussion

Solutions containing ≥ 0.16 M methylglyoxal and $(\text{NH}_4)_2\text{SO}_4$ became visibly colored immediately after mixing and became progressively darker in color with time. The color varied noticeably with initial methylglyoxal concentration; solutions with higher initial concentrations of methylglyoxal were darker in color.

2.3.1 UV-Vis Absorption

The products formed by methylglyoxal in aqueous solutions containing $(\text{NH}_4)_2\text{SO}_4$ or NH_4NO_3 absorb light at UV and visible wavelengths (ref. Figures 2.2-2.3).

2.3.1.1 Experimental Results

Aqueous methylglyoxal solutions with no salt have a broad absorbance peak at 290 nm at ambient temperatures. (Nemet et al., 2004) A kinetics study of 16.2 mM methylglyoxal in 3.1 M $(\text{NH}_4)_2\text{SO}_4$ (aq) (Figure 2.2a) shows that after a delay of ~ 1 hr, peaks grow in at 213 nm and 282 nm with roughly exponential time dependence. The measured absorbance of a solution of 1.62 M aqueous methylglyoxal and 3.1 M $(\text{NH}_4)_2\text{SO}_4$ initially increases upon mixing across all wavelengths (Figure 2.2b). This initial increase in baseline absorption could indicate either formation of at least one light-absorbing reaction intermediate that is consumed in later steps of the mechanism, or a

transient change in the bulk properties (e.g. refractive index, density) of the solutions. After 1 h, the absorption spectrum is saturated for $\lambda \leq 360$ nm, and the baseline at high wavelengths returns to < 0.5 AU. With increasing time, the saturated region of the spectrum extends to longer wavelengths and the tail shows increasing absorption at high wavelengths ($\lambda > 500$). Significant absorption at 550 nm is exhibited at < 1 h and after 12 h, with absorption at up to 700 nm developing within 2-3 days.

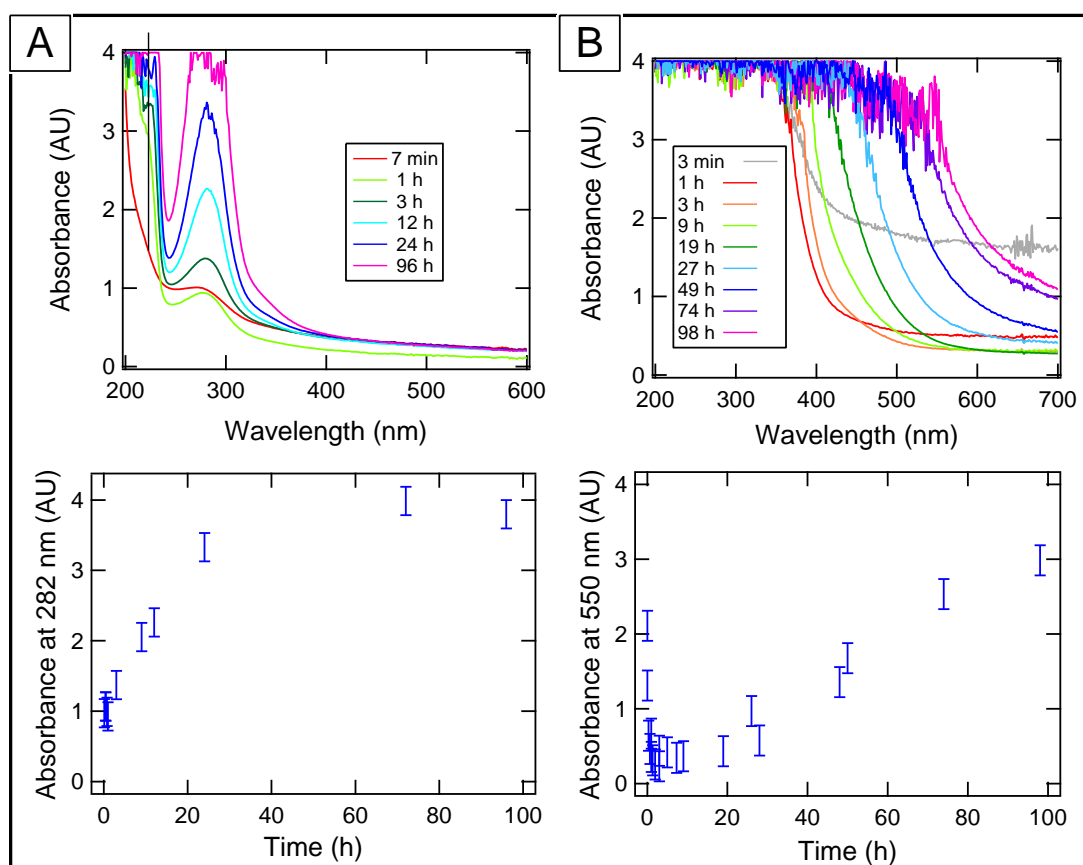


Figure 2.2. UV-Vis spectra of aqueous solutions containing 3.1M $(\text{NH}_4)_2\text{SO}_4$ and a) 16.2 mM methylglyoxal and b) 1.62 M methylglyoxal as a function of time after mixing. Absorbance is shown as a function of wavelength in the upper panels, and absorbance at selected wavelengths is shown in the lower panels. Error bars reflect uncertainty in the measured absorbances based on variation observed in the baseline signal.

The effect of initial methylglyoxal concentration on the UV-Vis spectra of solutions containing 3.1 M $(\text{NH}_4)_2\text{SO}_4$ 24 h after mixing is shown in Figure 2.3a. The absorbance at 282 nm after 3.0 h is linearly dependent on the initial methylglyoxal concentration. The effect of pH on the production of light-absorbing products in solutions initially containing 1.62 mM methylglyoxal and 3.1 M $(\text{NH}_4)_2\text{SO}_4$ is shown in Figure 2.3b. The absorbance at 282 nm of solutions initially containing 16.2 mM methylglyoxal 24 h after mixing is linearly dependent on the initial $(\text{NH}_4)_2\text{SO}_4$ concentration, as shown in Figure 2.3c.

Control samples containing 1.62 M methylglyoxal and 5.1 M NaCl or 1.18 M Na_2SO_4 exhibited UV-Vis spectra similar to aqueous methylglyoxal in the absence of salt after 24 h. A sample initially containing 1.62 M methylglyoxal and 3.1 M $(\text{NH}_4)_2\text{SO}_4$ was protected from light until analysis by covering the reaction vessel with aluminum foil, and the resulting spectrum at 24 h was identical to that of an unprotected solution with the same composition. This indicates that the reactions leading to light-absorbing compounds in this study are not photochemical.

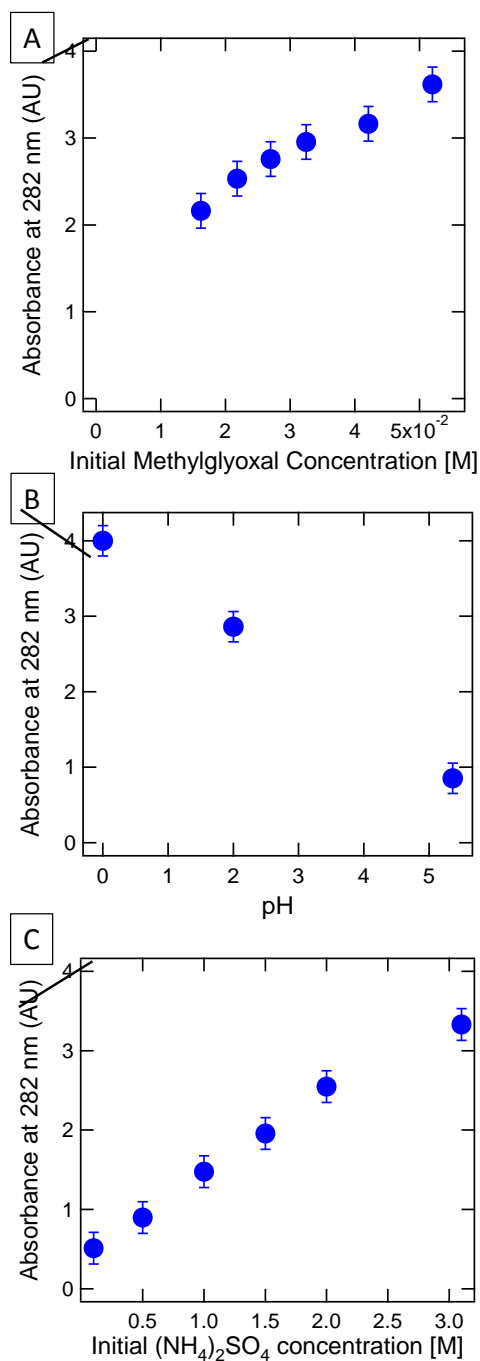
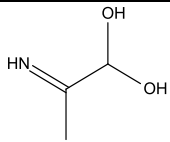
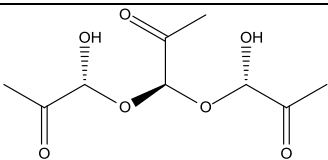
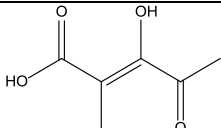


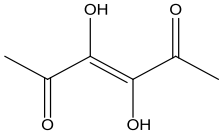
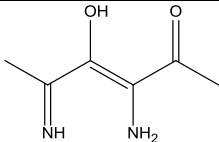
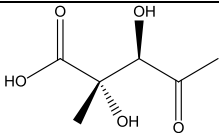
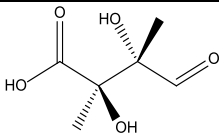
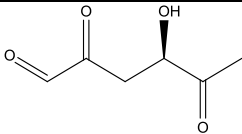
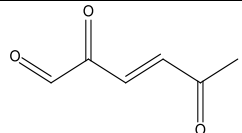
Figure 2.3. Absorbance at 282 nm of aqueous solutions containing a) 3.1 M $(\text{NH}_4)_2\text{SO}_4$ and varying initial concentrations of methylglyoxal, pH = 2.0(\pm 0.1), 3.0 hr after mixing. B) 3.1 M $(\text{NH}_4)_2\text{SO}_4$, 1.62 mM methylglyoxal, and varying pH 24 hr after mixing, and c) 16.2 mM methylglyoxal and varying initial concentrations of $(\text{NH}_4)_2\text{SO}_4$, 24 hr after mixing. Error bars reflect uncertainty in the measured absorbances based on variation observed in the baseline signal.

2.3.1.2 DFT Calculations

The results of our B3LYP/cc-pVTZ(-f) calculations of the HOMO-LUMO energy difference (and thus UV-Vis absorption wavelengths) of several proposed products are listed in Table 2.1. When molecules absorb light, their electrons may be promoted from the HOMO (highest occupied molecular orbital) to the LUMO (lowest unoccupied molecular orbital). The energy difference between these levels corresponds to the wavelength of absorption according to $E = hc/\lambda$ where E is the HOMO-LUMO energy difference, h is Planck's constant, c is the speed of light in vacuum, and λ is the wavelength.

Table 2.1. Proposed reaction products. Predictions for the energy of the gas phase HOMO-LUMO transition and the wavelength of UV-Vis absorption from DFT B3LYP/cc-pvtz(-f) simulations are shown. References are indicated by: 1) Nemet et al., 2004 2) Zhao et al., 2006 3) Krizner et al., 2009.

Molecule	Ref.	energy (eV)	λ (nm)
a) 	This work	6.757	183.5
b) 	1,2	5.728	216.5
c) 	This work	4.574	271.1

d)		This work	3.536	350.6
e)		This work	3.354	369.6
f)		This work	6.247	198.5
g)		This work	5.751	215.6
h)		3	3.872	320.2
i)		3	3.661	338.7

Our calculations were made for gas-phase molecules. Meller et al. (1991) reported that gas-phase methylglyoxal has an absorption peak at 280 nm. (Meller et al., 1991) Our B3LYP/cc-pVTZ(-f) calculations predict that gas-phase, unhydrated methylglyoxal has an absorption peak at 291.1 nm. Therefore we estimate that our predictions for these molecules in the absence of solvent effects are accurate to within ~12 nm. Further deviation between the theoretical results and experiment may result from solvent effects. The n to π^* excitation band characteristic of carbonyl compounds appears at ~290 nm and is known to shift toward lower wavelengths (blue shift) for a molecule in aqueous

solvent compared to the gas phase. (Skoog et al., 1997) For acetone this shift is approximately 12 nm, and for crotonaldehyde the shift is ~30 nm. (Bayliss and McRae, 1954) Therefore, we can estimate an error range of (-12 nm, +42 nm) for the predicted absorbances. Note that aqueous methylglyoxal solutions will contain a mixture of mono- and di-hydrated methylglyoxal, aldol condensation products, and hemiacetal oligomers (Krizner et al., 2009), so it is less straightforward to map the observed spectrum of aqueous methylglyoxal to the gas-phase absorbance of a single molecule for purposes of this discussion.

Referring to Scheme 2.1, Krizner et al. (2009) showed that aldol pathway (2) is thermodynamically favorable for aqueous methylglyoxal (they did not study pathway (1)). Our B3LYP/6-311G** calculations with Poisson-Boltzmann solvation show that $\Delta G = 10.5 \text{ kcal mol}^{-1}$ for the formation of the pathway (1) enol from singly hydrated methylglyoxal, close to Krizner et al.'s value of $11.9 \text{ kcal mol}^{-1}$ for the formation of the pathway (2) enol, suggesting that both enol species should be present in small quantities at equilibrium. Aldol addition via pathway (1) is likely to terminate after dimer or trimer formation due to the formation of organic acid or ketone end groups (e.g. species (c)-(g), Table 1). It is not energetically favorable for aldol addition at ketone end groups to continue via pathway 1 due to steric hindrance from the methyl group. Instead, these ketones may form an enol and follow pathway (2) for continuing aldol addition. Additionally, because of the methyl group, many of the products of aldol addition via pathway (1) cannot proceed with dehydration (e.g. species (g), Table 2.1). Pathway (2) results in carbonyl termination (e.g. species (h) and (i), Table 1) and therefore aldol condensation could propagate beyond the trimer.

Referring to Figure 2.2 (a), based on our B3LYP/cc-pvtz(-f) predictions, the species absorbing at 213 nm could correspond to an aldol addition product such as species (f) or (g) in Table 2.1. Acetals such as species (b) in Table 2.1 may also absorb at this wavelength. As described above, we estimate the error range of our theoretically predicted absorbances compared to the observed aqueous-phase spectra to be roughly (-12 nm, +42 nm). Therefore the absorbance band at 286 nm could correspond to a species predicted to absorb within the range $274 \text{ nm} < \lambda < 328 \text{ nm}$. Species which lie within this range include the pathway (2) aldol addition product species (h), which is predicted to absorb at 320 nm. Given the approximate nature of these lower and upper bounds, another candidate species could be species (c) which is predicted to absorb at 271.1 nm. Species (c) is the aldol condensation product corresponding to the aldol addition product (f). C=N bonds could also contribute to the observed absorbance.

2.3.2 Surface Tension

Solutions containing 3.1 M $(\text{NH}_4)_2\text{SO}_4$ and varying initial concentrations of methylglyoxal exhibit significant surface tension depression compared to 3.1 M $(\text{NH}_4)_2\text{SO}_4$ solutions without organics (ref. Figure 2.4).

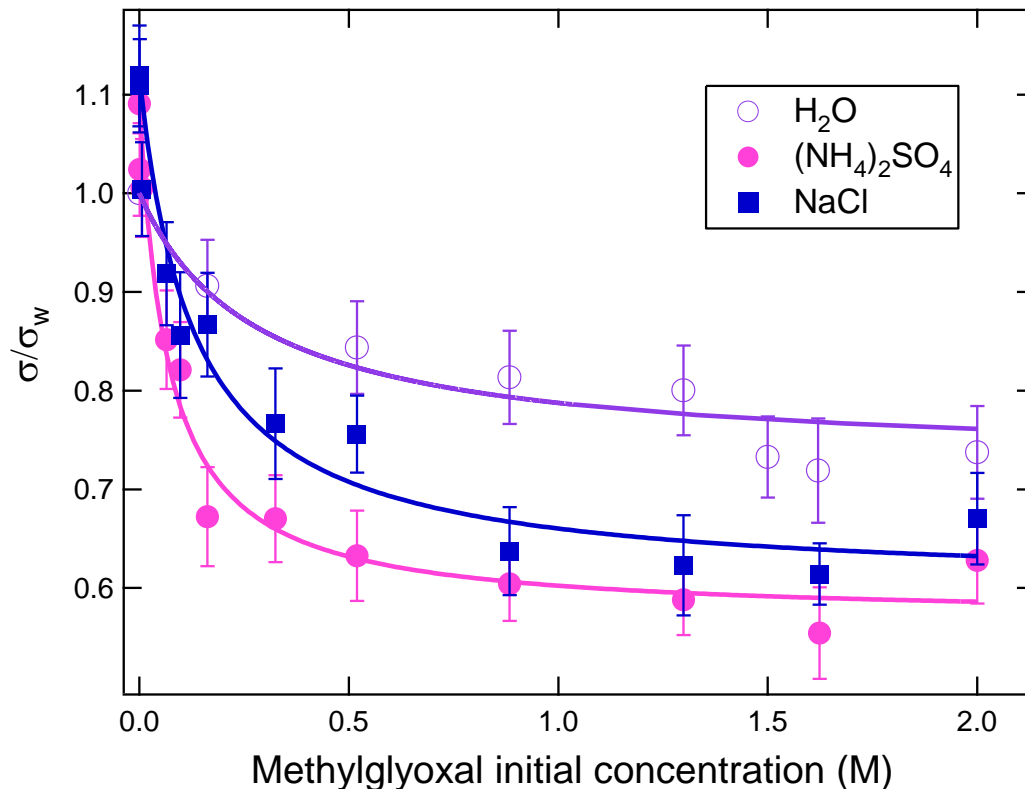


Figure 2.4. Results of pendant drop tensiometry measurements of aqueous mixtures as a function of initial methylglyoxal concentration for aqueous solution, 3.1 M (NH₄)₂SO₄ (aq), and 5.1 M NaCl (aq). The ratio of measured surface tension to the measured surface tension of Millipore water is shown. The measurements were made ≥ 24 h after mixing. Each point reflects the weighted average of five to eight measurements, and the error bars represent the standard deviation in the raw data. The best fit curve to each data set based on equation (2.6) is also shown.

The surface tension depression follows a Langmuir-like dependence on initial methylglyoxal concentration, with a minimum (saturation) surface tension, σ_{\min} , of 41 (± 2) dynes cm⁻¹ based on a fit to the data using the following equation:

$$\sigma = \sigma_0 - S \frac{bM_0}{1 + bM_0} \quad (2.6)$$

where σ is the surface tension, σ_0 is the surface tension of the solution with no methylglyoxal, M_0 is the initial methylglyoxal concentration, and S and b are fit parameters. Values of σ_0 for $(\text{NH}_4)_2\text{SO}_4$ (aq) and NaCl (aq) were taken from the International Critical Tables (2003). (Washburn) The physical interpretation of S is the surface tension depression when the surface is saturated, such that $\sigma_{\text{min}} = \sigma_0 - S$, and b is an equilibrium coefficient that describes surface-bulk partitioning. A time series was performed on a solution initially containing 1.62 M methylglyoxal and 3.1 M $(\text{NH}_4)_2\text{SO}_4$. The measured surface tension fluctuated for 2.5 hours before stabilizing at $45(\pm 1)$ dynes cm^{-1} , then slowly decreased over the next 21.5 h to the minimum value ($41(\pm 2)$ dynes cm^{-1}). Control experiments were performed in order to evaluate the role of $(\text{NH}_4)_2\text{SO}_4$. For aqueous methylglyoxal solutions with no salts present $\sigma_{\text{min}} = 52(\pm 3)$ dynes cm^{-1} . Therefore, while hydrated methylglyoxal and/or the oligomers it forms in aqueous solution are surface-active, the overall surface-tension lowering effect is less than when $(\text{NH}_4)_2\text{SO}_4$ is present in solution. Solutions containing 5.1 M NaCl and varying amounts of methylglyoxal follow a trend similar to that of the $(\text{NH}_4)_2\text{SO}_4$ solutions, with $\sigma_{\text{min}} = 43(\pm 2)$ dynes cm^{-1} (Figure 2.4).

Surface tension depression for methylglyoxal solutions containing 5.1 M NaCl or 3.1 M $(\text{NH}_4)_2\text{SO}_4$ is greater than that observed for aqueous methylglyoxal in the absence of salts. The observed enhancement in surface tension depression is likely to be a physical effect of the salts rather than an effect of especially surface-active products formed by a chemical reaction of methylglyoxal with the salts. High salt concentrations can result in a decreased critical micelle concentration due to charge screening, and thus cause enhanced film formation. (Li et al., 1998; Matijevic and Pethica, 1958) Salts can

also decrease the solubility of organics, commonly referred to as “salting out” (Setschenow, 1889), possibly resulting in surface film formation. Salts have commonly been observed to enhance the surface tension lowering effects of HULIS and organic diacids. (Asa-Awuku et al., 2008; Kiss et al., 2005; Shulman et al., 1996)

Glyoxal was previously observed not to be surface-active in hydrated form or to form surface-active products in aqueous $(\text{NH}_4)_2\text{SO}_4$ solutions. (Shapiro et al., 2009) Compared with glyoxal, the methyl group adds hydrophobicity to methylglyoxal and its oligomer products, increasing their surface activity.

2.3.3 Aerosol-CIMS

Representative Aerosol-CIMS mass spectra for the aqueous methylglyoxal, methylglyoxal/NaCl and methylglyoxal/ $(\text{NH}_4)_2\text{SO}_4$ systems using I^- or $\text{H}_3\text{O}^+(\text{H}_2\text{O})_n$ as the reagent ion are shown in Figures 2.5-2.8. The spectra represented in these figures have mass resolution of 1 amu except as noted; peak assignments were made using 0.5 amu resolution spectra.

2.3.3.1 Negative Ion Detection with I^-

A summary of proposed peak assignments for the mass spectra in Figure 2.5 using I^- as the reagent ion can be found in Table 2.2.

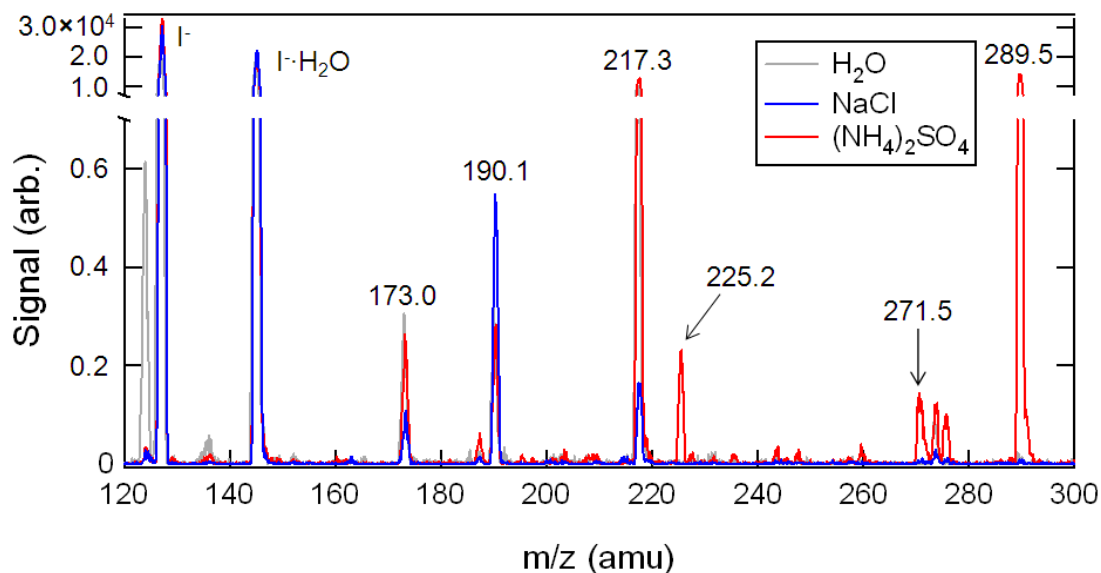
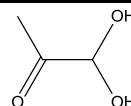
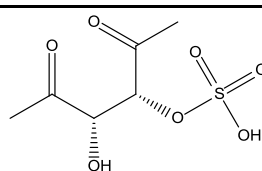
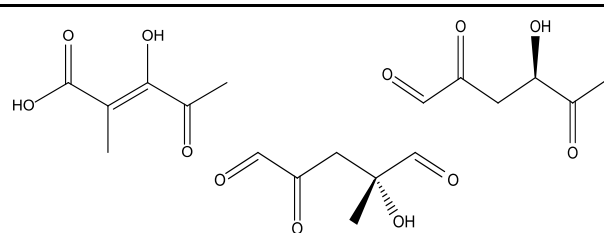
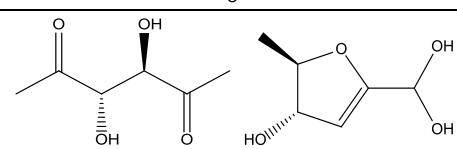
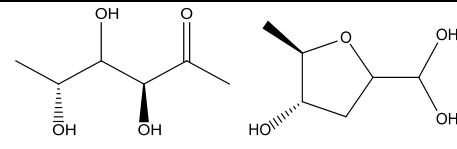
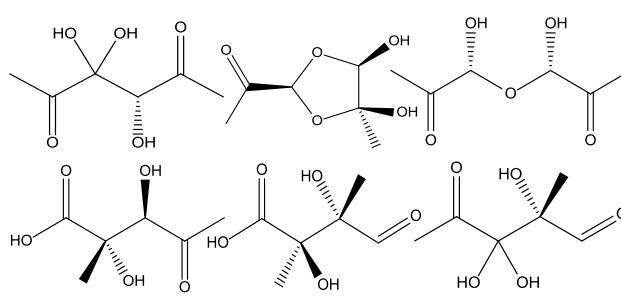


Figure 2.5. Negative-ion mass spectrum of aerosolized aqueous solutions initially containing methylglyoxal alone (grey) or with NaCl (blue) or $(\text{NH}_4)_2\text{SO}_4$ (red) (see text for details). Select product species were detected using I^- as the reagent ion. Peaks associated with I^- and its cluster with H_2O as well as the mass-to-charge ratios of product peaks are labeled.

Significant signal in the aqueous methylglyoxal control spectrum is observed at 173.0, 190.1, 217.3, and 273.5 amu. Most of the peaks in the methylglyoxal/ $(\text{NH}_4)_2\text{SO}_4$ mass spectrum are also found in the methylglyoxal/NaCl spectrum. Increased signal appears at 271.5, 273.5, and 289.5 amu in the methylglyoxal/ $(\text{NH}_4)_2\text{SO}_4$ spectrum. Peaks unique to methylglyoxal/ $(\text{NH}_4)_2\text{SO}_4$ include 225.2 and 275.6 amu. The peak at 217.3 amu is consistent with the cluster of I^- with singly hydrated methylglyoxal. The presence of multiple peaks >217.3 amu is indicative of dimer formation.

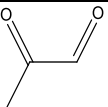
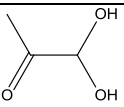
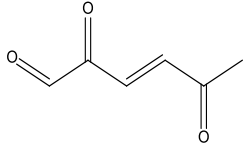
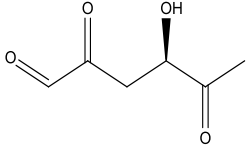
Table 2.2. Proposed peak assignments for Aerosol-CIMS mass spectra with I^- as the reagent ion. See text for details.

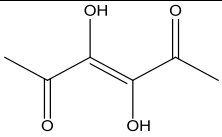
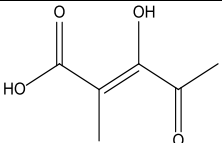
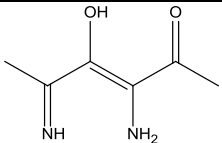
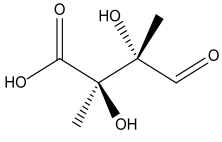
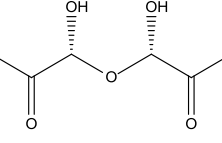
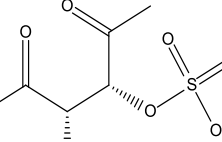
m/z (amu) ± 0.5 amu	Ion formula	Molecular formula	Possible Structure(s)
217.3	$I^-C_3H_6O_3$	$C_3H_6O_3$	
225.2	$C_6H_9O_7S^-$	$C_6H_{10}O_7S$	
271.5	$I^-C_6H_8O_4$	$C_6H_8O_4$	
273.5	$I^-C_6H_{10}O_4$	$C_6H_{10}O_4$	
275.6	$I^-C_6H_{12}O_4$	$C_6H_{12}O_4$	
289.5	$I^-C_6H_{10}O_5$	$C_6H_{10}O_5$	

2.3.3.1.1 DFT Calculations

I⁻ has previously been used as a reagent ion with Aerosol-CIMS to detect organic acids in aerosols. (McNeill et al., 2007; McNeill et al., 2008) Since the product species expected to be present in this reactive system (methylglyoxal, acetal/hemiacetal oligomers, aldol condensation oligomers) have not been previously detected via the I⁻ ionization scheme, we performed ab initio calculations in order to characterize the interaction of proposed product species with I⁻. The results are summarized in Table 2.3.

Table 2.3. Proposed reaction products. Predictions for the free energy change of the ligand switching reaction with I⁻H₂O to form a cluster with I⁻ based on DFT B3LYP/ERMLER2 calculations are shown. Strong clustering is indicated in bold.

Molecule	Molecular formula	Molecular weight (amu)	DFT ΔG (kJ mol ⁻¹) R + I ⁻ H ₂ O → I ⁻ R + H ₂ O
a) 	C ₃ H ₄ O ₂	72.1	-3.14
b) 	C ₃ H ₆ O ₃	90.1	-44.1
c) 	C ₆ H ₆ O ₃	126.1	-16.1
d) 	C ₆ H ₈ O ₄	144.1	-34.3

e)		$C_6H_8O_4$	144.1	-1.07
f)		$C_6H_8O_4$	144.1	-49.2
g)		$C_6H_{10}O_2N_2$	141.2	-7.77
h)		$C_6H_{10}O_5$	162.1	-65.2
i)		$C_6H_{10}O_5$	162.1	-65.7
j)		$C_6H_{10}O_7S$	226.2	H-abstraction from the sulfate group: -118.0

Our calculations show that the formation of clusters between I^- and several of the acetal and hemiacetal species proposed by Zhao et al. (2006) via ligand switching with $I^- \cdot H_2O$ is thermodynamically favorable, particularly when two or more hydroxyl moieties are available to interact with I^- simultaneously. This is also the case for hydrated methylglyoxal species. Non-hydrated methylglyoxal is not predicted to form strong clusters with or be ionized by I^- , and therefore we do not expect to detect it using this approach. Aldol addition products from either pathway (e.g. species (d) or (h) from Table

2.3), if present, should be detected as their clusters with I^- . The only aldol condensation products which we predict to form strong clusters with I^- are those species which terminate in a carboxylic acid group (e.g. species (f) from Table 2.3). We do not expect to observe products of aldol pathway 2 (ref. Scheme 2.1) such as species (c) from Table 2.3 with this ionization scheme.

2.3.3.1.2 Volatile Species

The peaks at 173.0, 190.1, and 217.3 amu were present in the same magnitude whether the volatilization inlet heat was turned on or off, indicating that these signals are associated with volatile species. The signal observed at 173.0 amu is consistent with formic acid (I^-HCOOH). Gas-phase formic acid has been previously observed to be an oxidation product of organic acids in aerosols; it was detected at this mass using Aerosol-CIMS with the same ionization scheme used here. (McNeill et al., 2008) The signal we observe at 190.1 amu is consistent with a molecular formula of $I^-CH_5O_2N$, but it is more likely due to the water cluster of the formic acid peak.

2.3.3.1.3 (Hemi)acetals and Aldol Condensation Products

The peak at 271.5 amu is attributed to the molecular formula $I^-C_6H_8O_4$, which could correspond to the pathway 1 aldol condensation dimers or pathway 2 aldol addition products (ref. Scheme 2.1 and Table 2.2). 289.5 amu is consistent with $I^-C_6H_{10}O_5$, and therefore can be matched to acetal and hemiacetal dimers proposed by others (Loeffler et al., 2006; Nemet et al., 2004; Zhao et al., 2006) or pathway 1 aldol addition products. Small amounts of signal at both of these masses are present in the methylglyoxal/NaCl

spectrum, and temperature control experiments indicate that these species are semivolatile.

Since succinic acid, an organic diacid, is expected to cluster strongly with I^- we may assume that the instrument sensitivity to succinic acid (100 Hz ppt^{-1}) is an upper limit for the sensitivity to these species. Using this assumption, we estimate lower bounds for the production rates of the species at 271.5 and 289.5 to be $\geq 10^{-3} \text{ M min}^{-1}$ and $\geq 10^{-2} \text{ M min}^{-1}$, respectively.

The peaks at 273.5 and 275.6 amu are assigned the molecular formulas $I^-C_6H_{10}O_4$ and $I^-C_6H_{12}O_4$ respectively. These molecular formulas, since they each contain six carbons, are consistent with the addition of two methylglyoxal monomers. Possible structures are shown in Table 2.2, but the formation mechanisms of these species in the methylglyoxal/ $(NH_4)_2SO_4$ system are not known.

2.3.3.1.4 Sulfur-Containing Species

The peak at 225.2 amu features a satellite peak at 227.2 amu with an abundance roughly consistent with the expected 95:4 ratio of the stable isotopes of sulfur ^{32}S and ^{34}S (Figure 2.6), suggesting a compound containing sulfur.

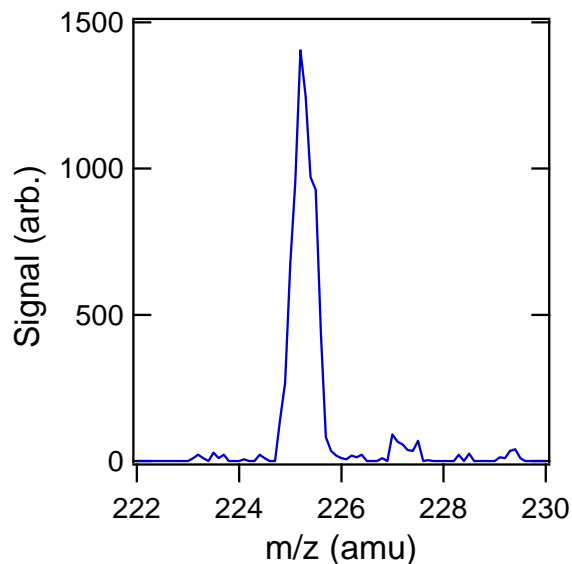


Figure 2.6. Detail of a 0.5 amu-resolution negative ion mass spectrum of aerosolized methylglyoxal/(NH₄)₂SO₄ solution. A peak at 225.2 amu and a satellite peak at 227.2 amu are shown.

Either a molecule with a molecular weight of 226.2 amu (in the case of proton abstraction) or 98.3 amu (in the case of a cluster with I⁻) would be consistent with the 225.2 amu mass-to-charge ratio. The species with m/z 225.2 was observed to be nonvolatile at room temperature. One possible molecular formula for this species is C₆H₉O₇S⁻. The proposed structure for the C₆H₉O₇S⁻ organosulfate species is shown in Table 2.1. Our DFT calculations predict that proton abstraction from the sulfate group by I⁻, rather than clustering via the ligand-switching reaction, is thermodynamically favorable for this species. Kinetics studies show that the signal at 225.2 amu develops within approximately 30 min of mixing. Assuming an upper limit sensitivity of 100 Hz ppt⁻¹ for this species we can estimate a production rate of $\geq 4 \times 10^{-3}$ M min⁻¹.

H₂SO₄ may cluster with I⁻ or undergo proton abstraction. I⁻H₂SO₄, if present, would also appear at 225.2 amu and display a satellite peak at 227.2 amu. In order to test

for this possibility a control experiment was performed in which a 0.2 M $(\text{NH}_4)_2\text{SO}_4$ solution at $\text{pH} = 2$ (similar to the conditions of the solutions with methylglyoxal) was atomized and analyzed using Aerosol-CIMS. There was no peak at 225.2 amu in the spectrum of the control, suggesting that the observed peak in the methylglyoxal/ $(\text{NH}_4)_2\text{SO}_4$ spectrum cannot be attributed to inorganic sulfate or sulfuric acid. Hearn and Smith (2006b) previously used Aerosol-CIMS with SF_6^- as the parent ion and a volatilization temperature of 220°C to detect aerosol sulfate (as HSO_4^- , 97 amu). (Hearn and Smith, 2006a) We observed a small (~ 300 cps) peak at 97 amu in the methylglyoxal/ $(\text{NH}_4)_2\text{SO}_4$ spectra but not in the control experiment. We note that organosulfates have previously been observed to decompose during negative ion mass spectrometry to generate HSO_4^- . (Attygalle et al., 2001)

2.3.3.2 Positive Ion Detection Using $\text{H}_3\text{O}^+(\text{H}_2\text{O})_n$

$\text{H}_3\text{O}^+(\text{H}_2\text{O})_n$ is commonly used to detect VOCs, including methylglyoxal (Blake et al., 2009; Zhao et al., 2006) and has been used to detect volatilized aerosol organics including levoglucosan from tobacco and wood smoke, limonene SOA (Hearn and Smith, 2004a) and pyridine (Thornberry et al., 2009). Table 2.4 lists the proposed peak assignments for the spectra in Figure 2.7 which were obtained using $\text{H}_3\text{O}^+(\text{H}_2\text{O})_n$ as the reagent ion.

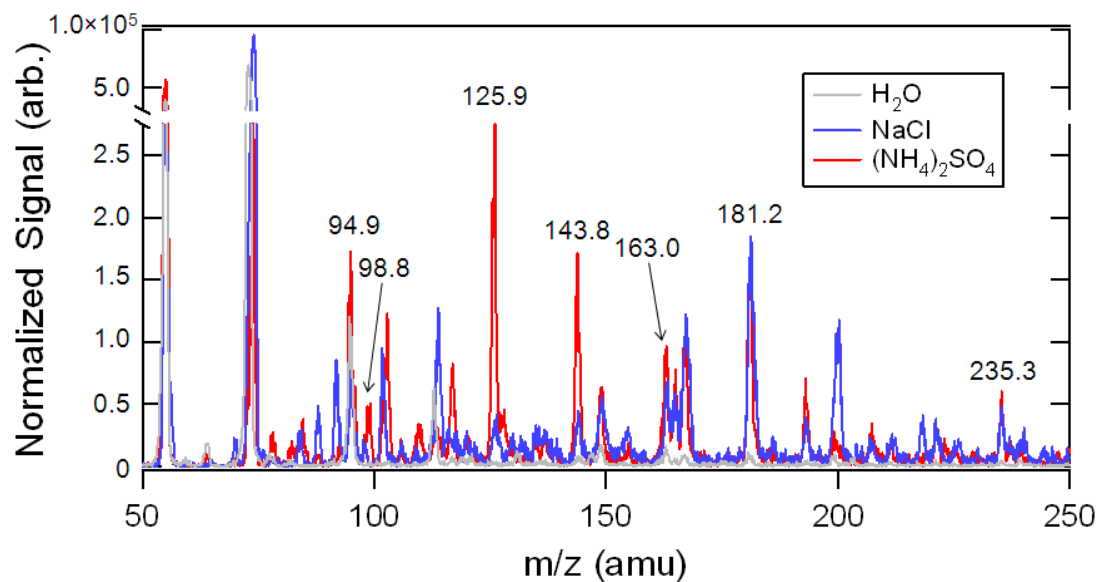
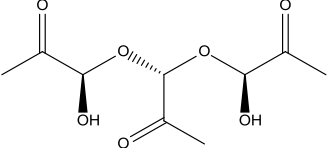


Figure 2.7. Positive ion mass spectrum of aerosolized aqueous solutions initially containing methylglyoxal alone (grey) or with NaCl (blue) or $(\text{NH}_4)_2\text{SO}_4$ (red). $\text{H}_3\text{O}^+(\text{H}_2\text{O})_n$ was the chemical ionization reagent. The mass-to-charge ratios of select product peaks are labeled.

Table 2.4. Proposed peak assignments for Aerosol-CIMS mass spectra with $\text{H}_3\text{O}^+(\text{H}_2\text{O})_n$ as the reagent ion. See text for details.

m/z (amu) ± 0.5 amu	Ion formula	Molecular formula	Possible Structure(s)
125.9	$\text{C}_6\text{H}_8\text{O}_2\text{N}^+$	$\text{C}_6\text{H}_7\text{O}_2\text{N}$	
143.8	$\text{C}_6\text{H}_{10}\text{O}_3\text{N}^+$ $\text{C}_6\text{H}_8\text{O}_2\text{N}^+\cdot\text{H}_2\text{O}$	$\text{C}_6\text{H}_9\text{O}_3\text{N}$ $\text{C}_6\text{H}_7\text{O}_2\text{N}$	

163.0	$C_6H_{11}O_5^+$	$C_6H_{10}O_5$	
	$C_6H_9O_4^+ + H_2O$	$C_6H_8O_4$	
165.0	$C_6H_{13}O_5^+$	$C_6H_{12}O_5$	
	$C_6H_{11}O_4^+ + H_2O$	$C_6H_{10}O_4$	
167.1	$C_6H_{15}O_5^+$	$C_6H_{14}O_5$	
	$C_6H_{13}O_4^+ + H_2O$	$C_6H_{12}O_4$	
181.2	$C_6H_{13}O_6^+$	$C_6H_{12}O_6$	
	$C_6H_{11}O_5^+ + H_2O$	$C_6H_{10}O_5$	

235.3	$C_9H_{15}O_7^+$	$C_9H_{14}O_7$	
-------	------------------	----------------	--

More peaks appear in these spectra than in those obtained using I^- as a reagent ion because proton transfer via $H_3O^+(H_2O)_n$ is favorable for a wider variety of organics than ligand switching or proton abstraction via I^- is. The aqueous methylglyoxal control spectrum features peaks at 94.9 amu and 112.9 amu. Signal at 94.9, 98.8, 125.9, 143.8, and 163.0 is significantly higher in the methylglyoxal/ $(NH_4)_2SO_4$ spectrum as compared to methylglyoxal/NaCl or aqueous methylglyoxal. Other notable peaks include 165.0, 167.1, 181.2, and 235.3 amu. The peaks at $m/z \leq 167.1$ amu (except for 98.8 amu) were present in the mass spectrum when the volatilization inlet was not heated, indicating that these signals are associated with volatile or semivolatile species.

Methylglyoxal has been detected previously using proton transfer mass spectrometry. (Zhao et al., 2006) In our experiment, the expected m/z for methylglyoxal coincided with that of one of the parent ions, $H_3O^+(H_2O)_3$, at 73.1 amu. Water clusters of methylglyoxal or the hydrated forms would correspond with $H_3O^+(H_2O)_4$ and $H_3O^+(H_2O)_5$ at 91.1 and 109.0 amu, respectively. A small signal is observed at 109.0 amu.

The peak at 94.9 amu is consistent with a molecular formula of $C_2H_7O_4^+$. This is likely a decomposition product or fragment of a larger compound.

2.3.3.2.1 (Hemi)acetals and Aldol Condensation Products

The peak at 125.9 amu is consistent with the molecular formula $C_6H_8O_2N^+$, corresponding to a type 2 aldol condensation product with a single imine substitution. The peak at 143.8 amu is consistent with a water cluster or aldol addition precursor of that species, or else a type 1 aldol condensation product with one amine or imine substitution. No peaks corresponding to these products were observed using the I^- detection scheme. As stated previously, our ab initio calculations showed that products of aldol pathway 2 would not likely be detected using I^- . Small amounts of signal at 125.9 amu and 143.8 amu are observed in the methylglyoxal/NaCl spectrum; since N-substitution would not be possible in the methylglyoxal/NaCl system, we will therefore consider this identification of C-N species to be tentative.

The peak at 163.0 amu corresponds to $C_6H_{11}O_5^+$; the species which appear at 289.5 amu in the I^- spectrum should appear at this mass. Alternatively, it could be the water cluster of $C_6H_9O_4^+$, the type 1 aldol condensation or type 2 aldol addition products which were observed at 271.5 amu in the I^- spectrum. Acetal and hemiacetal species also appear at 181.2 and 235.3 amu (see Table 2.4).

The peaks at 165.0 and 167.1 amu correspond to $C_6H_{13}O_5^+$ and $C_6H_{15}O_5^+$, respectively, or the water clusters of $C_6H_{11}O_4^+$ and $C_6H_{13}O_4^+$. These molecular formulas are consistent with methylglyoxal dimers but the structure and formation mechanism are not known for these species.

2.3.3.2.2 Sulfur-Containing Products

No peak at 227 amu, which would correspond to $C_6H_{11}O_7S^+$, was observed in the methylglyoxal/ $(NH_4)_2SO_4$ spectrum as detected using $H_3O^+(H_2O)_n$. To our knowledge organosulfates have not been previously detected using proton transfer ionization.

A peak was observed at 98.8 amu, but no satellite peak was present at 100.8 amu. The signal did not appear in the methylglyoxal/NaCl spectrum. Control experiments confirmed that no peak appeared at 98.8 amu when acidified $(NH_4)_2SO_4$ without methylglyoxal was present in the atomizer solution. Proton transfer ionization is not expected to allow detection of inorganic sulfate or sulfuric acid at this mass. Molecular formulas consistent with this mass-to-charge ratio include $C_6H_{11}O^+$, $C_5H_7O_2^+$, or $C_4H_3O_3^+$.

2.3.3.2.3 High-Molecular-Weight Species

In order to test our ability to detect high-molecular-weight organics with the Aerosol-CIMS technique, we analyzed aerosols containing NaCl and PEG (570-630 amu) in high-mass mode. We observed two sets of peaks separated by $44(\pm 1)$ amu (one ethylene oxide unit): (475.8, 518.9, 563.7, 607.4, and 651.5) and (502.4, 546.6, 590.9, 635.1). This is consistent with the observations of Bogan et al. (2007). (Bogan et al., 2007)

For methylglyoxal/ $(NH_4)_2SO_4$ we observed peaks from 536.6-759.5 amu in high-mass mode using $H_3O^+(H_2O)_n$ as the reagent ion (see Figure 2.8).

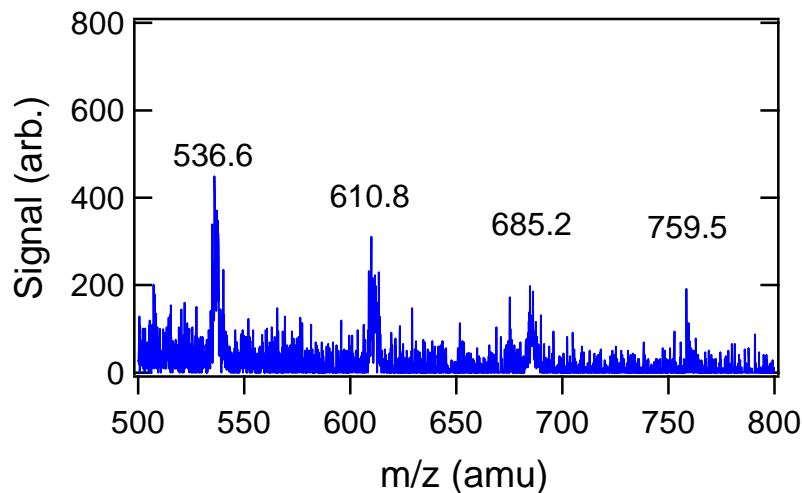


Figure 2.8. Detail of a positive ion mass spectrum of an aerosolized methylglyoxal/ $(\text{NH}_4)_2\text{SO}_4$ solution. Spectrum was taken in high-mass mode with $\text{H}_3\text{O}^+(\text{H}_2\text{O})_n$ as the reagent ion.

The peaks were separated by 74 amu, which could correspond to a unit of $\text{C}_3\text{H}_6\text{O}_2$. We did not observe non-background signal for $m/z > 300$ amu when using I^- as the reagent ion. We previously observed that glyoxal forms oligomers of 500-600 amu in aqueous solution when ammonium sulfate is present. (Shapiro et al., 2009) Kalberer et al. (2004) observed oligomers up to ~ 750 amu for aqueous methylglyoxal using LDI-MS.

2.3.3.3 Role of NaCl from Aerosol-CIMS Data

Hemiacetal species have been observed by others to be present in aqueous methylglyoxal solutions in the absence of salts. (Nemet et al., 2004) Aldol condensation was also predicted to be favorable in aqueous methylglyoxal solutions by Barsanti and Pankow (2005) and Krizner et al. (2009). Therefore, the observation of several common peaks in the spectra of the aqueous methylglyoxal control, methylglyoxal/NaCl, and

methylglyoxal/(NH₄)₂SO₄ is to be expected. Comparison of the aqueous methylglyoxal control and methylglyoxal/NaCl spectra suggests that NaCl may enhance the formation of hemiacetal species, which are not light-absorbing.

2.3.4 Mechanism

The evidence from our UV-Vis and Aerosol-CIMS studies together with our ab initio calculations points to aldol condensation as the mechanism for formation of light-absorbing products in this system. We observed mass spectra consistent with aldol addition and aldol condensation products, and these species were shown via our ab initio calculations to be consistent with the observed UV-Vis absorption spectra. The calculations of Barsanti and Pankow (2005) and Krizner et al. (2009) suggested that aldol condensation should be favorable for methylglyoxal in aerosols, and it has long been known that methylglyoxal undergoes aldol condensation in the presence of amino acids to form brown products. (Enders and Sigurdsson, 1943)

The results of our UV-Vis studies indicate that the formation of light-absorbing products is enhanced by the presence of NH₄⁺ and H₃O⁺. Our Aerosol-CIMS data also provides supporting evidence that the presence of NH₄⁺ increases the formation of aldol addition and condensation products. H₃O⁺ is a well-known catalyst for aldol condensation. (Casale et al., 2007; Jang et al., 2002; Nozière and Esteve, 2007) Nozière and coworkers have recently shown that NH₄⁺ is a catalyst for aldol condensation of ketones or aldehydes. (Nozière and Cordova, 2008) The most likely point of participation of both NH₄⁺ and H₃O⁺ in the aldol condensation mechanism is the initial step when the carbonyl is protonated before attack by the enol. A protonated carbonyl can also lead to a

number of subsequent reactions besides aldol condensation, including hemiacetal formation or amine substitution. (Nozière et al., 2009b) Two recent studies report the formation of C-N compounds by glyoxal when NH_4^+ is present in the aqueous phase under acidic conditions (Galloway et al., 2009; Nozière et al., 2009b), and both propose mechanisms involving ammonia and iminium intermediates. The low pH in this study will result in low equilibrium NH_3 concentrations. However, the protonation of a carbonyl by NH_4^+ as proposed here and by Nozière et al. (2009b) would result in the generation of a short-lived NH_3 molecule proximal to the reaction site. Nozière et al. (2009b) reported that the iminium pathway was active for glyoxal in ammonium-containing solutions down to pH 4.8 (the lowest pH studied).

2.3.5 Kinetics

The data in Figure 2.3 demonstrate a linear dependence for the absorbance at 282 nm on initial methylglyoxal concentration and initial ammonium sulfate concentration, respectively, when $\text{pH} = 2$. This is consistent with the protonation of methylglyoxal by ammonium being the rate-limiting step in the formation of light-absorbing dimers. The inverse dependence of product formation on pH is consistent with acid-catalyzed aldol condensation occurring in parallel with the ammonium-facilitated process. The following model can be used to describe this system:

$$\frac{d[P]}{dt} = k_A [MG][\text{NH}_4^+] + k_B [MG][\text{H}_3\text{O}^+] = -\frac{d[MG]}{dt} \quad (2.7)$$

$$\frac{d[\text{NH}_4^+]}{dt} = -k_A [MG][\text{NH}_4^+] \quad (2.8)$$

$$\frac{d[H_3O^+]}{dt} = -k_B^{\text{II}} [MG][H_3O^+] \quad (2.9)$$

Here, MG represents methylglyoxal and P represents light-absorbing products. This model can be used to describe the kinetic data in Figure 2.2 or the concentration-dependent data in Figure 2.3. A fit to the data can yield the bimolecular rate constants k_A^{II} and k_B^{II} if the molar absorptivity of the absorbing species are known. Referring to the UV-Vis absorption data in Figure 2.3(b), and assuming that the species responsible for the observed absorption at 282 nm are dimers of methylglyoxal and therefore their maximum concentration in the solution is half the initial concentration of methylglyoxal, a lower bound for the molar absorptivity of the products absorbing at 282 nm is $\epsilon \geq 4938 \text{ Lmol}^{-1}\text{cm}^{-1}$. We used POLYMATH 6.10 to numerically integrate eqs (2.7)-(2.9). We find that the data in Figures 2-3 can be described by this model with $k_A^{\text{II}} \leq 5 \times 10^{-6} \text{ M}^{-1} \text{ min}^{-1}$ and $k_B^{\text{II}} \leq 10^{-3} \text{ M}^{-1} \text{ min}^{-1}$. This is consistent with the value we find ($k_A^{\text{II}} \leq 4.2(\pm 0.2) \times 10^{-6} \text{ min}^{-1}\text{M}^{-1}$) if we assume pseudo-first-order conditions and perform a weighted linear least squares fit to the data in Figure 2.3(c) according to:

$$[P] \propto [NH_4^+]_o (1 - \exp(-k_A^{\text{II}} [MG]_o t)) \quad (2.10)$$

Based on our Aerosol-CIMS/I data we estimated a lower bound for the production rate of the aldol addition and condensation products detected at 271.5 amu (ref. Table 2.1) to be $\geq 10^{-3} \text{ M min}^{-1}$. If protonation of the methylglyoxal monomer is the rate-limiting step for formation of these products eq. (2.7) should apply. Aerosol particles will become concentrated relative to the atomizer solution as the 100% RH atomizer output equilibrates to 60% RH. Following Tang and Munkelwitz (1994), an ammonium sulfate concentration of ~65 wt%, or 14 M, will be reached at 60% RH. Assuming the

same proportional increase in concentration for methylglyoxal and H_3O^+ we find $[\text{MG}]_0 = 7.32 \text{ M}$ and $[\text{H}_3\text{O}^+]_0 = 0.045 \text{ M}$. Applying eq. (2.7) and the bimolecular rate constants we derived based on the UV-Vis data ($k_A^{\text{II}} \leq 5 \times 10^{-6} \text{ M}^{-1} \text{ min}^{-1}$ and $k_B^{\text{II}} \leq 10^{-3} \text{ M}^{-1} \text{ min}^{-1}$) we find that at these high salt concentrations $k_A^{\text{II}}[\text{NH}_4^+][\text{MG}]$ exceeds $k_B^{\text{II}}[\text{H}_3\text{O}^+][\text{MG}]$ by a factor of 3, allowing us to approximate the production rate by $dP/dt \approx k_A^{\text{II}}[\text{NH}_4^+][\text{MG}]$. Using this and the measured production rate of $\geq 10^{-3} \text{ M min}^{-1}$ we find a lower bound of $k_A^{\text{II}} \geq 5 \times 10^{-6} \text{ M}^{-1} \text{ min}^{-1}$. Coupling this with the upper bound obtained using the UV-Vis data, we conclude that $k_A^{\text{II}} \approx 5 \times 10^{-6} \text{ M}^{-1} \text{ min}^{-1}$.

2.4 Conclusions and Atmospheric Implications

The results of this study show that the ammonium ion plays an active role in the chemistry of methylglyoxal in aqueous aerosol mimics. This chemistry represents a new potential pathway for heterogeneous SOA formation.

We have made tentative identifications of an organosulfate product and C-N containing species using Aerosol-CIMS. To our knowledge, organosulfate formation by methylglyoxal in ammonium sulfate aerosols has not been observed previously, although Liggio et al. (2005 a,b) and Galloway et al. (2009) identified organosulfate products in ammonium sulfate aerosols exposed to gas-phase glyoxal. Organosulfates have been identified in ambient aerosol. (Gao et al., 2006; Gómez-González et al., 2008; Iinuma et al., 2007; Lukács et al., 2009; Russell et al., 2009; Surratt et al., 2008; Surratt et al., 2007) Lukács et al. (2009) observed that organosulfate mass concentrations were at a maximum for submicron aerosol size fractions, suggesting a link between organosulfate formation and heterogeneous SOA formation pathways. If C-N species form in this system, this

could contribute to the nitrogen-containing aerosol organics which have been observed in ambient aerosol. (Aiken et al., 2008; Denkenberger et al., 2007; Lin et al., 2010; Gilardoni et al., 2009)

To our knowledge, the concentrations of the methylglyoxal reaction products we have proposed here have not been measured in atmospheric aerosol samples. Kawamura and coworkers have measured methylglyoxal monomer and related compounds (glyoxal, ketocarboxylic acids, and dicarboxylic acids) in ambient aerosols. (Ho et al., 2007; Kawamura et al., 1996; Kawamura and Yasui, 2005; Kundu et al., 2010; Sempère and Kawamura, 1994) Methylglyoxal was found to comprise roughly 0.005-0.05% of aerosol mass in urban environments. (Ho et al., 2007; Kawamura and Yasui, 2005) Assuming a particle density of 1 g cm^{-3} this corresponds to an in-particle methylglyoxal concentration range of 0.7 mM to 7 mM.

A typical ammonium sulfate concentration in an aqueous atmospheric aerosol particle at 60% RH is $\sim 65 \text{ wt}\%$ (Tang and Munkelwitz, 1994), or 14 M, with $0 \leq \text{pH} \leq 5$ (Keene et al., 2004; Zhang et al., 2007b), resulting in pseudo-first-order rate coefficients of $k_A^I = 1.4 \times 10^{-4} \text{ min}^{-1}$ and $10^{-8} \text{ min}^{-1} \leq k_B^I \leq 10^{-3} \text{ min}^{-1}$ for the loss of methylglyoxal through reaction with NH_4^+ and H_3O^+ , respectively. Given an aerosol-phase methylglyoxal concentration of 7 mM, this corresponds to a production rate of $10^{-6} \text{ M min}^{-1}$ (at $\text{pH} = 5$) to $8 \times 10^{-6} \text{ M min}^{-1}$ (at $\text{pH} = 0$). Based on our reaction model this corresponds to 0.7 to 6 mM of light-absorbing products formed after 12 hours (up to 86% conversion of methylglyoxal to products).

What we have observed for the methylglyoxal/ $(\text{NH}_4)_2\text{SO}_4$ system is another example of aerosol-phase chemistry which may increase the absorption index of

atmospheric aerosols with increasing aerosol age. These results add to the growing body of evidence that SOA formation and aging may be a source of “brown carbon” in atmospheric aerosols. Brown carbon, including the products observed here, does not absorb as strongly as black carbon at high wavelengths (~550 nm and higher) and therefore its contribution to aerosol absorption in this range may be minor in comparison. (Andreae and Gelencsér, 2006) However, the absorption of UV radiation by brown carbon has the potential to reduce tropospheric O₃ levels. (Jacobson, 1999, 2002) Based on our calculated molar absorptivity of $\epsilon_{282} \geq 4938 \text{ Lmol}^{-1}\text{cm}^{-1}$ and our estimated production rate of 0.7 to 6 mM light-absorbing products formed after 12 hours, we estimate that the contribution to the dimensionless absorption coefficient at 282 nm from methylglyoxal reaction products is $A_{282, \text{MG}} = \lambda\epsilon_{282}/4\pi \sim 10^{-5}$. On a per-mole basis, the light-absorbing products observed here are stronger absorbers in the range 250-400 nm than pyruvic or oxalic acids (Lund Myhre and Nielsen, 2004) or the light-absorbing products of glyoxal in aqueous ammonium sulfate solutions observed by Shapiro et al. (2009).

Our observation of surface tension depression is consistent with observations of surface tension depression by HULIS in ambient aerosol samples. (Asa-Awuku et al., 2008; Kiss et al., 2005; Salma et al., 2006; Taraniuk et al., 2007) Referring to Figure 2.4, based on our estimated in-particle methylglyoxal concentration of 7 mM, and assuming that the particles are primarily composed of ammonium sulfate, this corresponds to surface tension depression of approximately 8% due to methylglyoxal in urban particles. We note that, since methylglyoxal will react in the particle to form potentially surface-active products, this value likely underestimates the total amount of surface tension

depression associated with methylglyoxal uptake to the particle. Decreased aerosol surface tension may affect the cloud nucleation ability of the aerosol. The ability of an aerosol particle to activate at a given supersaturation condition depends on the amount of solute present in the particle (i.e. its dry diameter) and the surface tension of the droplet at the point of activation. The Kohler curve that describes this process is given by (Köhler, 1936; Seinfeld and Pandis, 1998):

$$s = \frac{A}{D_p} - \frac{B}{D_p^3} \quad (2.10)$$

with

$$A = \frac{4M_w\sigma}{RT\rho_w} \text{ and } B = \frac{6n_sM_w}{\pi\rho_w}$$

where s is the supersaturation, D_p is the diameter of the aqueous droplet, M_w is the molecular weight of water and ρ_w is its density, R is the gas constant, T is temperature, σ is surface tension, and n_s is the number of moles of solute. Surface tension depression in aqueous aerosols by methylglyoxal SOA material could therefore result in increased CCN activation due to its effect on the parameter A . It has been suggested that this effect may be partially compensated for by the effect of surface-active organic solute partitioning from the bulk to the gas-aerosol interface, thereby reducing the bulk solute concentration (and the value of B). (Sorjamaa et al., 2004) However, in a heterogeneous SOA formation scenario the bulk solute content of the particle is expected to be

dominated by salt. Furthermore, in order to maintain Henry's law equilibrium, gas-phase methylglyoxal will continuously be taken up at the aerosol surface as it is consumed by particle-phase reactions. Therefore we assume here that the effect of methylglyoxal and its reaction products on equilibrium CCN activity is purely surface-tension based. For particles of a given size, this effect can be expressed as:

$$s_c^* = \left(\frac{\sigma}{\sigma_w} \right)^{3/2} s_c \quad (2.11)$$

where s_c^* is the critical supersaturation, σ_w and σ are the surface tension of water and the particle, respectively, and s_c is the critical supersaturation for a particle with the surface tension of water. (Engelhart et al., 2008b) Based on 7 mM methylglyoxal in the particle, we estimate $\sigma/\sigma_w \sim 1.01$, compared to $\sigma/\sigma_w = 1.09$ for a saturated ammonium sulfate solution (see Figure 2.4). Using eq. 2.11, this corresponds to a critical supersaturation ~11% lower than that of a pure ammonium sulfate particle. CCN activation measurements are planned in order to confirm this effect. We note that the relevant surface tension is that of the droplet at the moment of activation, at which point the surfactant concentration will be lower than that in the aqueous aerosol at lower relative humidities, especially for larger particles. A film of surface-active organics coating an aqueous particle may also affect the kinetics of particle equilibration with the surrounding water vapor, thereby affecting cloud droplet growth rate and cloud droplet number. (Archer and La Mer, 1955; Chuang et al., 1997; Feingold and Chuang, 2002; Garland et al., 2005; Rosano and La Mer, 1956; Ruehl et al., 2009)

The small size, and thus high surface area-to-volume ratio of a submicron aerosol particle means that, compared to the bulk solutions used here, a greater fraction of the

total surfactant molecules present in the aerosol will partition to the interface. This will effectively decrease surface coverage for a given surfactant concentration and increase the critical micelle concentration (CMC). (McNeill et al., 2006) Based on this effect, we would expect the minimum surface tension in an aerosol particle to be similar to what was observed here, but the plateau region of the surface tension curve may not be reached until higher methylglyoxal concentrations. However, this effect may be balanced by the fact that the small size of aerosol particles also leads to supersaturated salt concentrations which were not accessible in this study. (Tang and Munkelwitz, 1994; Tang et al., 1997; Tang, 1997) The CMC lowering effect of the salt and the increased “salting-out” may counteract the size effect.

Kroll et al. (2005) reported negligible particle growth when ammonium sulfate particles were exposed to ~960 ppb of methylglyoxal in aerosol chamber experiments on a timescale of several hours, and attributed this to the Henry’s law coefficient of methylglyoxal, which is low relative to that of glyoxal. (Betters and Hoffmann, 1988b; Zhou and Mopper, 1990) Surface film formation such as is suggested by our surface tension measurements, even at submonolayer coverages (i.e. concentrations below the CMC), can also inhibit the reactive uptake of gas-phase species into the aerosol. (Anttila et al., 2006; Folkers et al., 2003; McNeill et al., 2006; McNeill et al., 2007; Stemmler et al., 2008; Thornton and Abbatt, 2005) Film formation upon uptake of methylglyoxal to the aerosol could result in suppressed VOC uptake (and therefore suppressed SOA formation and particle growth).

Finally, we have demonstrated here that Aerosol-CIMS using I^- and $\text{H}_3\text{O}^+(\text{H}_2\text{O})_n$ as the parent ions is suitable for the detection of the products of heterogeneous SOA

formation by α -dicarbonyls, and high molecular weight organics up to 759 amu. This technique can be extended to aerosol chamber studies and, when coupled with a suitable aerosol collection or concentration technique, field studies.

CHAPTER 3: Oxidative aging of light-absorbing secondary organic aerosol material formed by methylglyoxal and glyoxal

3.1 Introduction

Water-soluble volatile organic compounds (WSVOCs) in the atmosphere may be absorbed by aqueous aerosol particles or cloud droplets. Once in the aqueous phase, these species can react to form secondary organic aerosol material (SOA). (Ervens et al., 2011; Lim et al., 2010) Water-soluble carbonyl compounds like glyoxal and methylglyoxal, which have both biogenic and anthropogenic sources, have been shown to be likely precursors for SOA formed via aqueous pathways. (Ervens et al., 2011; Lim et al., 2010; Sareen et al., 2010; Schwier et al., 2010; Shapiro et al., 2009)

The products of glyoxal and methylglyoxal reacting in aerosol mimics containing ammonium salts have been shown to include light-absorbing, surface-active, and high-molecular-weight oligomeric species. (Sareen et al., 2010; Schwier et al., 2010; Shapiro et al., 2009) Schwier et al. (2010) identified organic acids, hemi(acetals), aldol condensation products, and possible nitrogen and sulfur containing compounds as the products of methylglyoxal, glyoxal and ammonium sulfate aqueous solutions. (Schwier et al., 2010) Keutsch and coworkers have also identified the formation of imidazole species from the reaction of glyoxal in ammonium-containing solutions. (Galloway et al., 2009; Yu et al., 2011) Besides adding to organic aerosol mass in the atmosphere, these product species may affect aerosol optical properties and/or cloud droplet formation. (Li et al., 2011; Sareen et al., 2010; Schwier et al., 2010; Shapiro et al., 2009) Some could also potentially be used as tracer species for aqueous SOA formation chemistry. However,

their lifetimes in the oxidizing environment of the atmosphere, as well as the chemical identities and properties of their oxidation products, are largely unknown. Most of these product compounds would be highly vulnerable to oxidation by the hydroxyl radical (OH); unsaturated species such as aldol condensation products and imidazoles may also be oxidized by ozone (O_3). The formation of these SOA products will compete simultaneously with their oxidative degradation. Oxidation may result in re-volatilization of aerosol organic material, (Bertram et al., 2001; George et al., 2007; McNeill et al., 2008; Molina et al., 2004) although the aqueous-phase OH oxidation of glyoxal and methylglyoxal has been shown to be a source of SOA via the formation of lower-volatility organic acid products. (Ervens et al., 2011; Lee et al., 2011; Lim et al., 2010) Additionally, oxidation may decrease (through the breaking of C=C or C-N bonds) or increase (through the creation of carbonyls) light absorption by the oligomeric SOA products. (Nozière and Esteve, 2005; Sareen et al., 2010; Schwier et al., 2010; Shapiro et al., 2009)

In this study, we aim to quantify the products and kinetics of oxidative aging of secondary organic material formed via the aqueous reaction of methylglyoxal with ammonium sulfate. Aerosol flow tube reactors coupled to an Aerosol Chemical Ionization Mass Spectrometer (Aerosol-CIMS) for detection of gas and particle-phase organics were used for this purpose. Particles were collected on quartz windows before and after oxidation to characterize the effect of oxidation on the light-absorbing properties of these aerosols.

3.2 Methods

Oxidation experiments were performed using aerosol flow tube reactors coupled to a custom-built Aerosol-CIMS for product characterization and a scanning mobility particle sizer (SMPS, TSI) to monitor particle concentration.

3.2.1 Aerosol Generation

Aerosols were generated in a similar manner to that described in Sareen et al. (2010). Briefly, mixtures containing 1.62 M methylglyoxal (Sigma Aldrich or Acros Organics) or 2.21 M glyoxal (Fisher Scientific) and 3.1 M $(\text{NH}_4)_2\text{SO}_4$ were prepared using Millipore water (18.2 M Ω cm) and allowed to react for > 24 hours. The mixtures were then diluted with Millipore water to attain a salt concentration of 0.2 M. These dilute solutions were then aerosolized with N_2 using a constant output atomizer (TSI), mixed with a dry N_2 stream to maintain the relative humidity at 64 – 68% measured with a hygrometer (Vaisala), and then introduced into the reactor. Typical number concentrations were $1.2 \times 10^5 \text{ cm}^{-3}$ with mean surface area-weighted radius of 143 nm. The surface tension, light absorption properties, and product characterization for this system has been described in detail by Sareen et al. (2010). (Sareen et al., 2010)

3.2.2 Gas-phase Reactants

O_3 was generated by flowing 0.2-5 sccm of oxygen with a carrier gas of 200 sccm N_2 through a photocell containing a Hg pen-ray lamp (Jelight) operating at 185 nm. This produced O_3 concentrations ranging from 0.2 – 0.8 ppm. The concentration of O_3 generated was monitored using a UV absorption cell, 10 cm long with ¼” inlet and outlet ports for O_3 flow. Light from another Hg pen-ray lamp (Jelight) coated to primarily emit

254 nm passes through the cell and is detected by a photodiode (Hamamatsu) on the other end.

OH was formed *in situ* in an aerosol flow cell (described in the following section) by reacting O(¹D) with water, where O(¹D) is generated from the photolysis of O₃.



The concentration of OH generated was $\sim 9.5 \times 10^6$ molecules cm⁻³, as determined by calibration experiments with SO₂ following the procedure explained in McNeill et al. (2008). (McNeill et al., 2008)

3.2.3 Flow Reactors

The O₃ reactor setup is shown in Figure 3.1. O₃ oxidation experiments were performed in a similar manner as described by McNeill et al. (2007). (McNeill et al., 2007) The humidified aerosol stream was introduced through a perpendicular sidearm into a 7.5 cm ID, 55 cm long Pyrex flow tube. A 1/8" Teflon tube fitted inside a 0.25" OD stainless steel moveable injector was used to introduce the O₃/N₂ stream into the flow tube. The position of the injector was changed to vary the reaction times (0 to 23 sec) and hence attain kinetic information. The O₃ concentration in the reactor varied from 0.2 to 0.8 ppm. The relative humidity in the reactor was maintained at 62-67%.

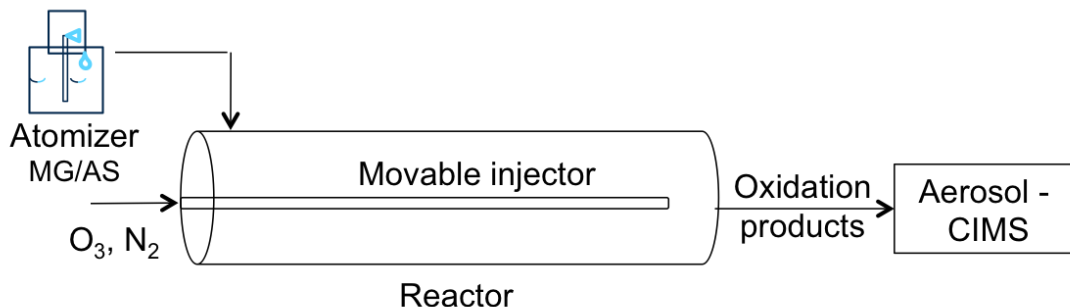


Figure 3.1. Schematic for O₃ setup.

The photolysis and OH reaction studies occurred in a continuous flow photocell reactor shown in Figure 3.2. The reactor consisted of a 25 cm long, 5 cm in diameter quartz photocell with a 1 cm inner sleeve. An ozone-free Hg pen-ray lamp (Jelight, 254 nm) was inserted into the inner sleeve. The reactor featured four different inlet ports placed at intervals of 8 cm that were used to vary the reaction times (0 to 10 sec). The humidified aerosol stream (RH ~ 62-67%) and the O₃/N₂ stream were introduced via separate ports to prevent the aerosols from being exposed to O₃ before entering the reactor. In a typical experiment, the aerosol stream was introduced via a perpendicular port at the back of the reactor, while the position of the O₃/N₂ stream was varied using the other ports on the reactor. Control experiments were also performed in this reactor in order to study the effect of photolysis on these aerosols in the absence of oxidants. All reactions were studied here under NO_x-free conditions.

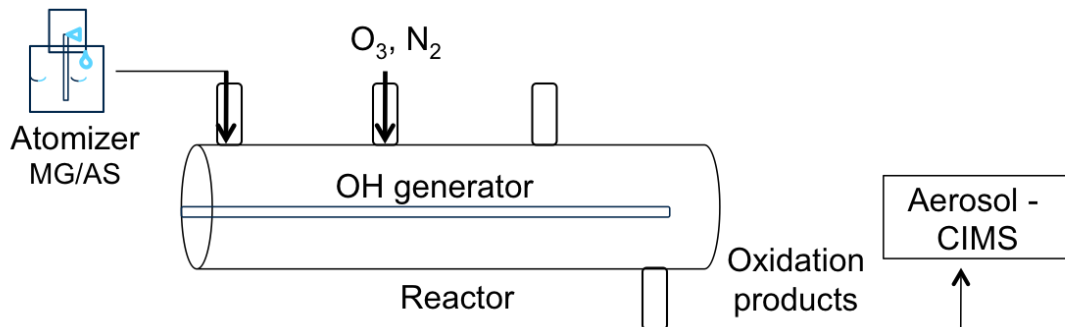


Figure 3.2. Schematic for OH setup.

3.2.4 Aerosol-CIMS Detection of Products

A custom-built chemical ionization mass spectrometer (CIMS) coupled to a volatilization flow tube inlet (Aerosol-CIMS) was used to monitor aerosol chemical composition during the oxidation experiments. The instrument and its operation were described in detail by Sareen et al. (2010). (Sareen et al., 2010) The effluent from the flow tube reactors was sent through a volatilization flow tube (VFT) kept at 135 °C in order to vaporize the particle-phase organic material for detection using CIMS. Some experiments were performed without applying heat to the inlet, in order to identify species which were volatile at room temperature. A quadrupole mass spectrometer (Extrel CMS) was used to detect the organics as the products of their reactions with the reagent ion, I⁻ or its clusters with water (see Sareen et al. (2010) for a full discussion of the relevant ion chemistry). An orifice was used downstream of the VFT to control the flow through the reactors and into the CIMS. Total flow was maintained at 2.3 SLPM through the O₃ reactor and 1.8 SLPM for the OH reactor. A fraction of this flow (0.3 SLPM) was sent to a scanning mobility particle sizer (SMPS) (TSI) to characterize the particle population.

3.2.5 Particle Collection and UV-Vis Spectrophotometry

The effect of oxidation on the UV-Visible light absorption of these particles was also studied by collecting particles before and after oxidation with 0.2 ppm O₃ by impaction on quartz windows (25 × 2 mm, Edmund Optics) using a custom-made impactor. The windows were held in place using a custom-made filter holder that was modified so that gases can escape while particles are collected on the windows. Prior to collection on the quartz windows, particles from the reactor were passed through a dryer, and the collection period was 90 min at a rate of 1.5 LPM. (Bones et al., 2010) UV-visible spectra of SOA material were measured immediately after particle collection. The impaction windows were placed in a custom-made holder that held them in position. Spectra were collected using a single beam spectrophotometer (HP 8453). A spectrum of the blank window was measured each time before particle collection and all subsequent spectra were baseline corrected at 1000 nm with respect to the blank window. Three trials were conducted for each experiment. The residence time in the O₃ reactor was 40 s for these experiments.

3.2.6 Heterogeneous Reaction Kinetics

Briefly, in a typical oxidation kinetics experiment, the Aerosol-CIMS is used to monitor the concentrations of the SOA products of interest. A previous study conducted in our group has characterized in detail the products of this reaction. (Sareen et al., 2010) Aerosols containing SOA products are exposed to O₃ or OH in their respective reactors. As mentioned earlier, for the O₃ flow tube reactor, the position of the injector through which O₃ is introduced is changed in order to achieve 5 different reaction times. To

change the reaction time in the OH reactor, the gas-phase oxidant can enter through 3 different ports. Various peaks are observed for changes in signal with reaction time.

The reactive uptake coefficient, γ , is calculated based on the measured rate constants for the reaction of the oxidants with individual SOA products. The signal decay for each peak is averaged for a given reaction time and plotted as a function of reaction time. The slope of the error-weighted linear least-squares fit gives the observed pseudo-first order-rate coefficient, k^I .

Assuming an aqueous-phase heterogeneous reaction between O_3 and the SOA products, the loss rate of the organic that gets depleted can be expressed as:

$$\frac{d[\text{Org}]_{\text{aq}}}{dt} = -k^{II}[\text{O}_3]_{\text{aq}}[\text{Org}]_{\text{aq}} = -k^{II}HP_{O_3}[\text{Org}]_{\text{aq}} \quad (3.3)$$

where $[\text{Org}]_{\text{aq}}$ is the concentration of the organic, and $[\text{O}_3]_{\text{aq}}$ is the concentration of the oxidant, H is the Henry's Law solubility constant for O_3 ($\sim 0.013 \text{ M atm}^{-1}$), (Müller and Heal, 2002) and P_{O_3} is the partial pressure of O_3 in the gas phase.

Since the diffuso-reactive length (the characteristic distance the O_3 molecule diffuses within the particle before it reacts, $l = \sqrt{\frac{D}{k^{II}[\text{Org}]}}$) is greater than the radius of the particles, we can assume a uniform distribution of the oxidant through the particle. Hence, the reaction rate is not limited by in-particle diffusion of the oxidant and Eq. 3.3 can be simplified to:

$$\frac{d[\text{Org}]_{\text{aq}}}{dt} = -k^I[\text{Org}]_{\text{aq}} \quad (3.4)$$

where $k^I = k^{II}HP_{O_3}$ is the pseudo-first-order rate constant.

Finally, k^I can be related to the reactive uptake coefficient using the following equation (Hearn et al., 2005):

$$\gamma = \frac{4RT}{\omega_{P_{O_3}}} \frac{r}{3} k^I [\text{Org}]_{\text{aq}} \quad (3.5)$$

where R is the gas constant, T is the temperature, ω is the mean speed of the oxidant molecules, and r is the radius of the particles.

3.3 Results and Discussion

The photolysis and heterogeneous reactions of O_3 and OH with aqueous SOA formed by methylglyoxal or glyoxal and $(NH_4)_2SO_4$ was observed to result in an increase in aerosol light absorption, and the formation of volatile organic acid products.

3.3.1 Ozonolysis Products for SOAs from $(NH_4)_2SO_4$ and Methylglyoxal

Table 3.1 which has been adapted from Sareen et al. (2010) shows the different SOA product peaks detected with the Aerosol-CIMS using the I^- detection scheme and the observed change upon exposure to each oxidant. A prompt decrease of signal is observed at some of the higher masses upon exposure to O_3 , accompanied by an increase of signal at some lower masses, indicative of O_3 reacting with the SOA products to form lower molecular weight products.

Table 3.1. Table adapted from Sareen et al. (2010) showing proposed peak assignments for Aerosol-CIMS mass spectra with I^- as the reagent ion for solutions containing methylglyoxal and $(NH_4)_2SO_4$. The up and down arrows in the two columns on the right indicate an increase or decrease, respectively, in signal at that mass when exposed to O_3 or OH. NC indicates no discernible change was seen with increasing reaction times.

m/z (amu) ± 0.5 amu	Ion formula	Molecular formula	Possible Structure(s)	O_3	OH
217.3	$I^-C_3H_6O_3$	$C_3H_6O_3$		↓	↑
225.2	$C_6H_9O_7S^-$	$C_6H_{10}O_7S$		↑	↑
271.5	$I^-C_6H_8O_4$	$C_6H_8O_4$		↓	↓
273.5	$I^-C_6H_{10}O_4$	$C_6H_{10}O_4$		NC	NC
275.6	$I^-C_6H_{12}O_4$	$C_6H_{12}O_4$		NC	NC
289.5	$I^-C_6H_{10}O_5$	$C_6H_{10}O_5$		↓	↓

Figure 3.3 shows an Aerosol-CIMS difference spectrum comparing the results for aerosols before and after exposure to 0.2 ppm of O₃ for 40 seconds in the flow tube reactor. The peaks that lie above the x-axis increase in the presence of O₃, whereas the peaks below the x-axis decrease. We see clear evidence that the (hemi)acetals and aldol condensation products at m/z 271.5 amu, 273.5 amu, and 289.5 amu decrease by ~90% when exposed to O₃. Additionally, as the exposure time increases, the peaks at 271.5 amu and 289.5 amu decrease further. The peaks at 273.5 amu and 275.6 amu did not show a clear trend with exposure time over the range of conditions studied here. Upon exposure to O₃, the peak at 217 amu also decreases by ~30%. This peak is attributed to either singly hydrated methylglyoxal or oxalic acid. These compounds are not expected to react with O₃, therefore, we attribute the decrease in signal to a shift in the aqueous-phase equilibrium caused by the oxidation of other SOA products.

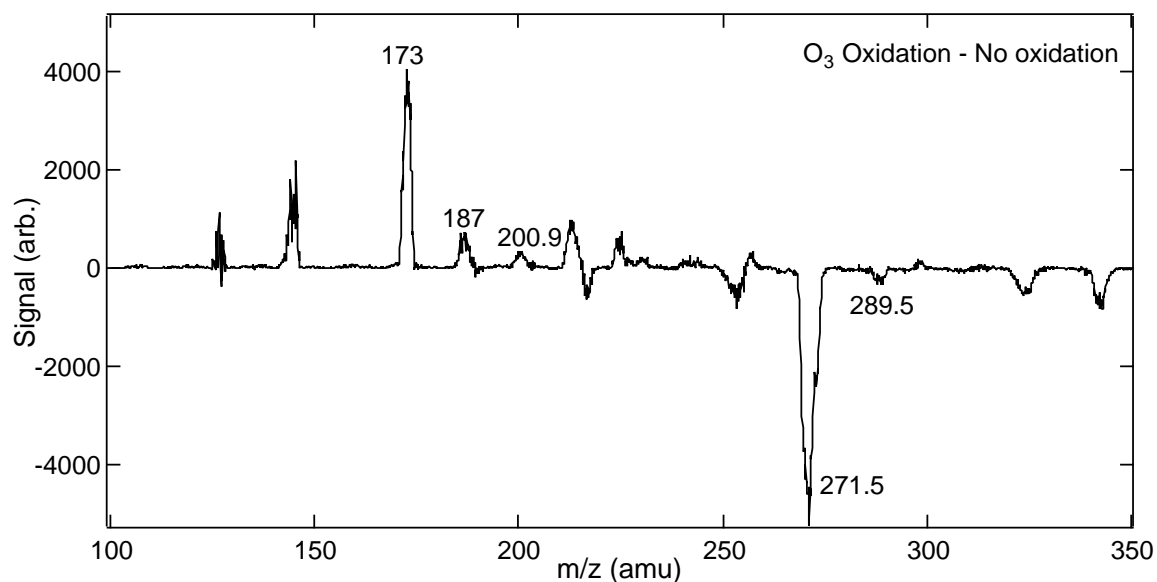
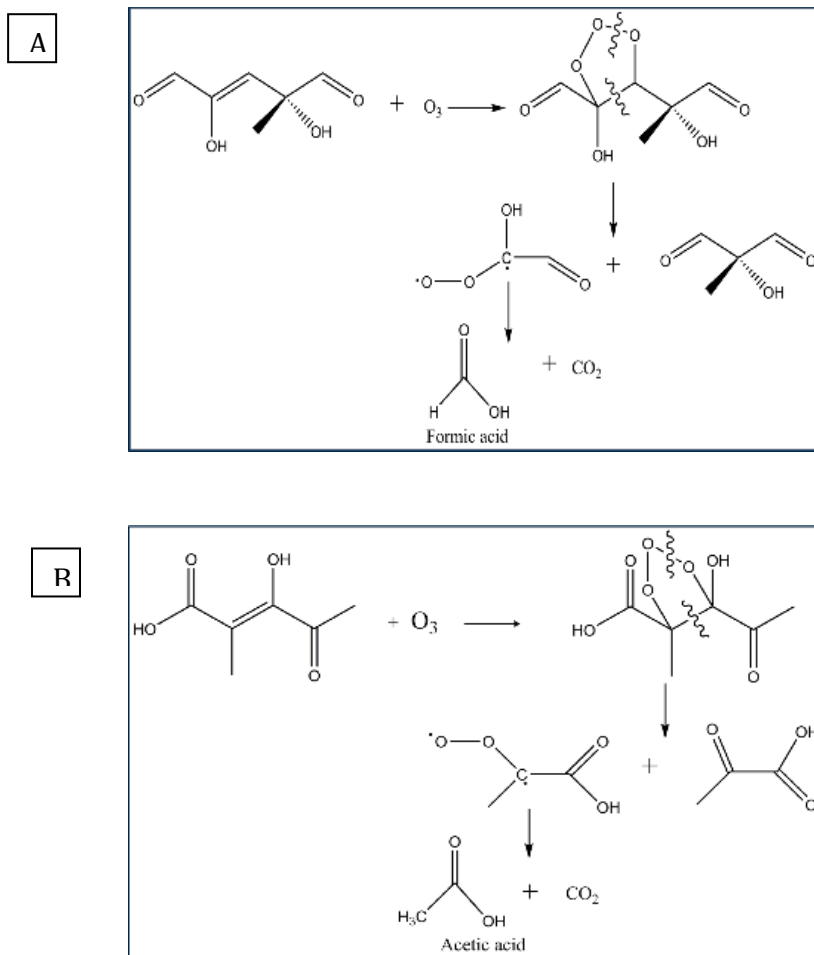


Figure 3.3. Spectrum showing the difference between (NH₄)₂SO₄ and methylglyoxal particles exposed to 0.2 ppm of O₃ and not being exposed to O₃.

Most of the compounds that undergo ozonolysis break down into smaller, more volatile organic acids. One such possible pathway is shown in scheme 3.1, where the aldol condensation product with a formula $C_6H_8O_4$ at m/z 271.5 amu, undergoes ozonolysis to form formic and acetic acids, along with CO_2 .

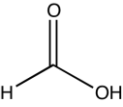
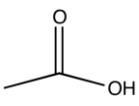
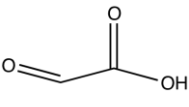
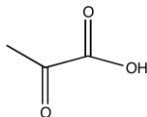


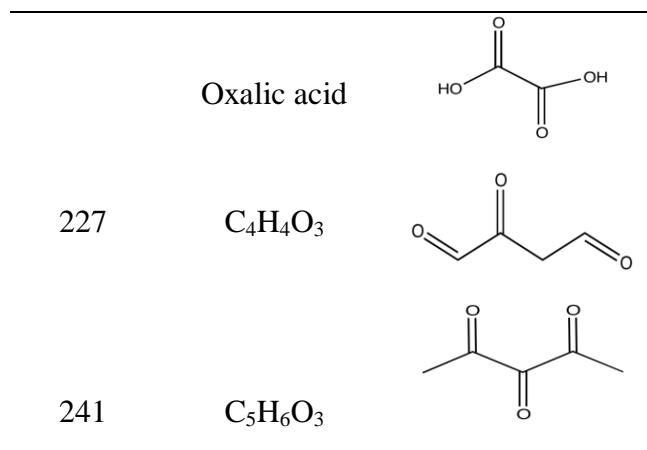
Scheme 3.1. Ozonolysis of the product at 271.5 amu leads to the formation of (a) formic acid and CO_2 and/or (b) acetic acid and CO_2 .

Figure 3.3 shows a significant increase in the formic acid peak at 173 amu upon ozonolysis, consistent with our proposed reaction mechanisms. An increase in 187 amu

and 200.9 amu as seen in the figure represents an increase in acetic acid and glyoxylic acid, respectively, both of which are predicted to form under ozonolysis of the compounds with formula $C_6H_8O_4$ and $C_6H_{10}O_5$ observed at m/z 271.5 amu and 289.5 amu. A broad peak that encompasses masses from 213 amu to 215 amu corresponds to oxopropanedial (213 amu) and pyruvic acid (215 amu) respectively, products from the reaction of O_3 with the peak at 271.5 amu. Similar mechanisms are also seen for the ozonolysis of the hemi(acetal) and aldol condensation products observed at m/z 289.5 amu, breaking to form compounds like formic acid, acetic acid, methanol, and formaldehyde, amongst others. Table 3.2 lists the various oxidation products and their structures that were observed in our system.

Table 3.2. Compounds formed upon the ozonolysis, photolysis, and/or OH oxidation of the SOA products of $(NH_4)_2SO_4$ and methylglyoxal.

m/z [amu]	Chemical name	Structure
173	Formic acid	
187	Acetic acid	
200.9	Glyoxylic acid	
215-217	Pyruvic acid	



3.3.2 Kinetics of Ozonolysis

Figure 3.4 shows the signal decay for a sample peak traced at 271.5 amu plotted against the reaction times to attain k' values.

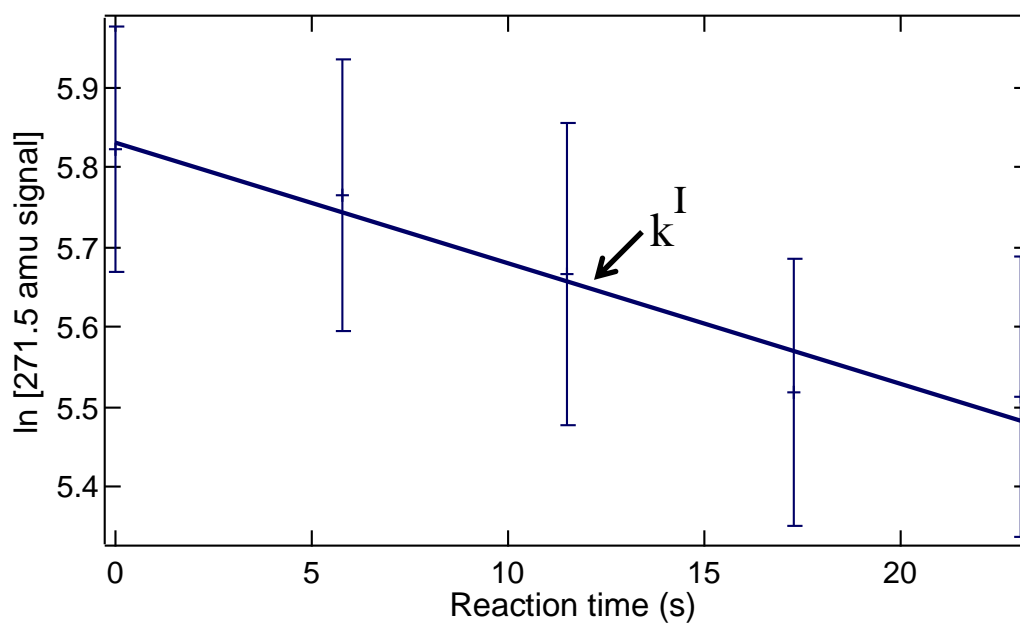


Figure 3.4. Loss of the peak at 271.5 amu as a function of reaction time in the presence of O₃. The line represents the error-weighted linear least-squares fit to the experimental data.

The values for average k^I , γ , and τ , the lifetime of the specific species in the atmosphere are listed in Table 3.3.

Table 3.3. Kinetic parameters for the ozonolysis of the SOA products of $(\text{NH}_4)_2\text{SO}_4$ and methylglyoxal.

m/z [amu]	k^I [s^{-1}]	γ	τ_{atm} [hr]
271.5	0.003	1.37×10^{-8}	0.95
289.5	1.7×10^{-4}	1.16×10^{-10}	16.8

Ozone concentrations were varied between 0.2 ppm and 0.8 ppm. No clear trend for the rate constant with ozone concentrations over this concentration range was seen for most of the traced peaks. The peak at 271.5 amu, showed a slight increase in k^I with increasing ozone concentrations as seen in Figure 3.5.

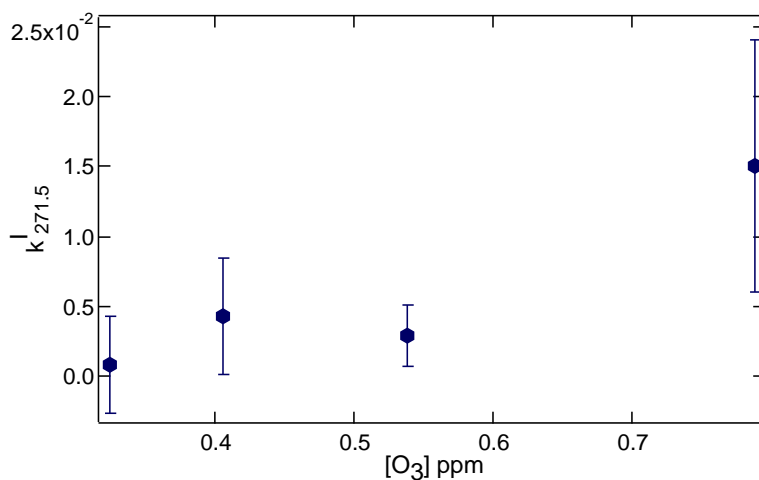
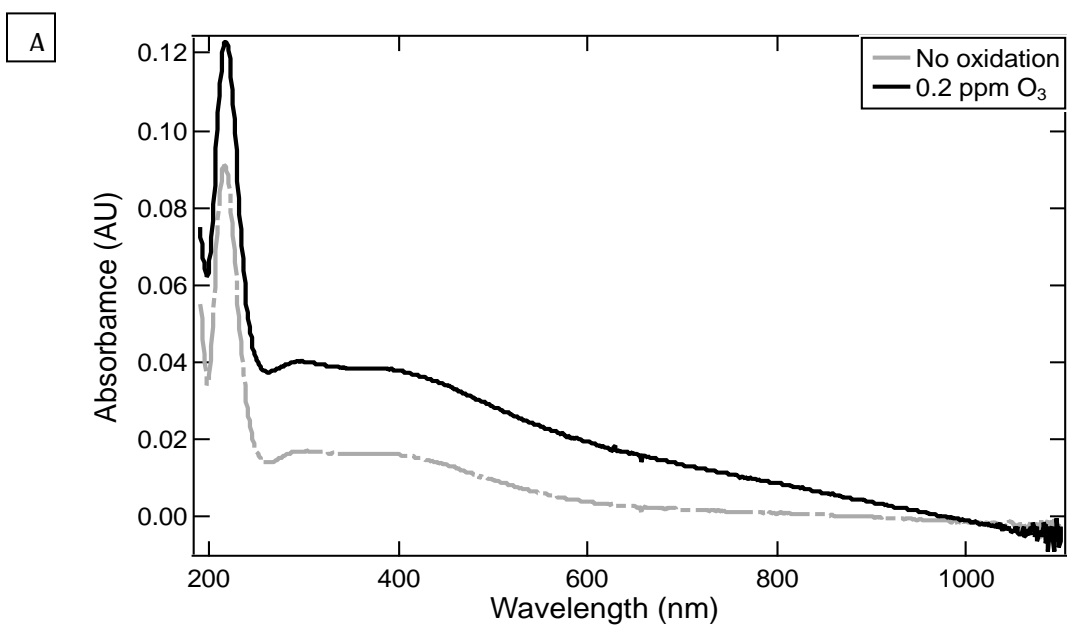


Figure 3.5. Average k^I values for the peak at 271.5 amu over varying ozone concentrations.

3.3.3 Changes in UV-Vis Absorption with Ozonolysis

$(\text{NH}_4)_2\text{SO}_4$ and methylglyoxal SOA products exposed to 0.2 ppm O_3 for 40 seconds in the flow tube reactor show an increase in light absorption over UV and visible wavelengths as shown in Figure 3.6a. Two main peaks appear in the spectrum: a strong peak at 216 nm and another around 282 nm, both of which are representative of the presence of carbonyls. (Sareen et al., 2010) This result suggests that the formation of new carbonyl groups upon oxidation has a greater impact on particle light absorption than the breakdown of C=C bonds.



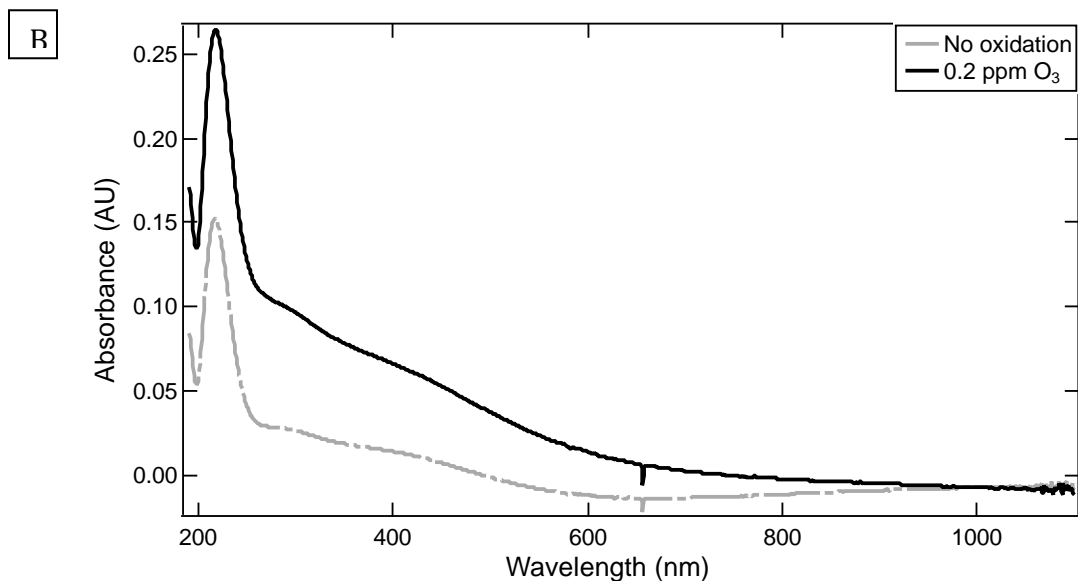


Figure 3.6. UV-Vis spectra of $(\text{NH}_4)_2\text{SO}_4$ and a) glyoxal SOA particles exposed to 0.2 ppm of O_3 b) methylglyoxal SOA particles exposed to 0.2 ppm of O_3 .

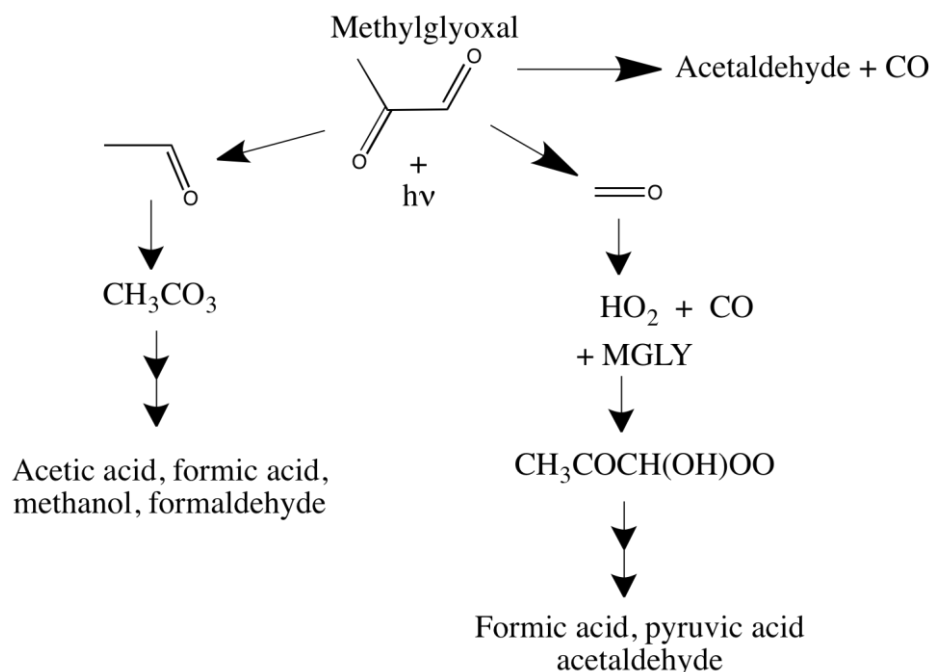
Similar results are observed for the products of the glyoxal/ $(\text{NH}_4)_2\text{SO}_4$ system (Figure. 3.6b). This spectrum has peaks at 216 nm and 277 nm. Table 3.4 lists the relative increase in absorption with oxidation at the specified peaks for both the methylglyoxal and glyoxal systems.

Table 3.4. Relative increase in absorption after oxidation.

	Wavelength (nm)	Oxidized/non-oxidized
Methylglyoxal	216	1.3 ± 0.06
	282	2.7 ± 1.2
Glyoxal	216	1.5 ± 0.2
	277	2.1 ± 0.9

3.3.4 Photolysis, OH Oxidation Products and Kinetics of SOAs from $(\text{NH}_4)_2\text{SO}_4$ and Methylglyoxal

In the OH reactor, we have three processes that can possibly affect the reaction chemistry: photolysis due to the OH lamp, reaction with O_3 , and reaction with OH. During the daytime, degradation via photolysis can be a major fate of organic compounds. Hence, before studying the effect of OH on these SOAs, we will conduct experiments to assess the impact of photolysis during the daytime on these SOAs. Our OH lamp transmits at wavelengths above 290 nm, which are relevant for the troposphere. In order to study photolysis, we observe the Aerosol-CIMS signals as the OH lamp is turned on and off without producing any OH. This allows us to study the effect of photolysis on the particles. We observe a significant influence on the particles due to photolysis. There is a large fraction of the formic acid and pyruvic acid peaks at 173 amu and 215 amu, respectively, which are primarily due to photolysis. The photooxidation pathway for methylglyoxal (Scheme 3.2), shows that it photolyzes to form these compounds in air.



Scheme 3.2. Photooxidation mechanism for methylglyoxal in air. (Barker, 1995)

Hence, even when methylglyoxal is present in a reactive aqueous system, it breaks down into similar products. We do not see a major change in the major SOA product peak at m/z 289.5 amu. The aldol condensation products at m/z 271.5 amu show a slight decrease in signal when is exposed to the lamp, implying that they may be photolyzing to a small extent. Table 3.5 lists the photolysis rate constants observed in our system for these peaks.

Table 3.5. Photolysis rate constants for the SOA products of $(\text{NH}_4)_2\text{SO}_4$ and methylglyoxal for our experimental setup.

m/z [amu]	k' [s^{-1}]
271.5	1.15×10^{-4}
289.5	1.22×10^{-5}

When oxidized by OH, the above-mentioned peaks decrease further as compared to purely by photolysis. Additionally, oxidation by OH leads to the formation of a wider range of compounds at a faster rate than that observed during ozonolysis. A decrease in the aldol condensation and (hemi)acetal products at m/z 271.5 amu and 289.5 amu with OH exposure is observed (Figure 3.7). Most of the compounds at these peaks get oxidized to form smaller compounds that we have mainly identified to be formic acid at 173 amu, acetic acid at 187 amu, glyoxylic acid at 200.9 amu, (and pyruvic acid at 215 amu) amongst others. The broader peak which encompasses 215-217 amu can be attributed to both pyruvic acid (215 amu) and oxalic acid or singly-hydrated methylglyoxal (217 amu), both of which are oxidation products. There is no distinct way of knowing which of the two compounds, oxalic acid or singly-hydrated methylglyoxal can the peak at 217 amu be attributed to as both have the same mass and both are expected to occur in the studied system. All the above oxidation products are expected to form in our system based on the reaction schemes we have determined when the compounds at 271.5 amu and 289.5 amu with formulae $C_6H_8O_4$ and $C_6H_{10}O_5$, respectively, are exposed to OH. Our reaction schemes have also shown that these higher molecular weight compounds can get oxidized to form methylglyoxal, which would correspond to the 199 amu peak we see with I^- in the Aerosol-CIMS spectra. An increase in peaks at 227 amu and 241 amu can be attributed to compounds with formulae $C_4H_4O_3$ and $C_5H_6O_3$, respectively, that we predict to form based on our reaction mechanisms.

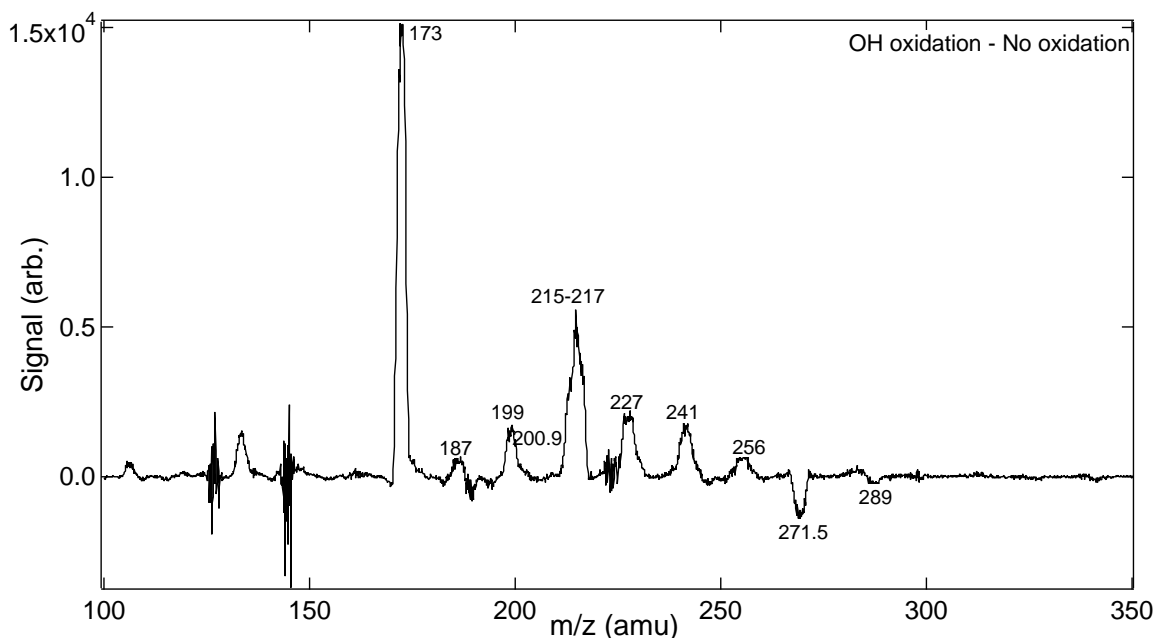


Figure 3.7. Spectrum showing the difference between $(\text{NH}_4)_2\text{SO}_4$ and methylglyoxal particles exposed to 9.5×10^6 molecules cm^{-3} of OH and not being exposed to OH.

Similar to the kinetic analysis for O_3 , the pseudo first-order rate constants and uptake coefficients for the reactive species in the system were determined by changing the reaction times in the reactor. As expected, the majority of the compound peaks decrease in intensity with increasing OH reaction time. Table 3.6 lists the rate data for these peaks. In the presence of OH, the aqueous SOA products have a lifetime in the atmosphere of a few seconds, much shorter than in the presence of O_3 , which is on the order of a few hours. Comparing the rate constants of the SOA products for the three processes that occur in the reactor, OH oxidation will be the dominant reaction, followed, by ozonolysis, and then photolysis.

Table 3.6. Kinetic parameters for the oxidation of the SOA products of $(\text{NH}_4)_2\text{SO}_4$ and methylglyoxal by OH.

m/z [amu]	k' [s^{-1}]	γ	τ_{atm} [sec]
271.5	0.0174	0.071	9.18
289.5	0.0133	0.027	23.9

3.3.5 Volatilization

The peaks at m/z 173 amu, 187 amu, 200.9 amu, and 215-217 amu have the same magnitude with and without the VFT indicating that the species present at these masses are volatile. The species at m/z 271.5 amu and 289.5 amu appear in the no heat temperature control experiments at a smaller magnitude, as also observed previously (Sareen et al., 2010), which tells us that they are semivolatile. We observe a distinct increase in signal at m/z 225.2 amu when the heating is turned on, suggesting the presence of a non-volatile species.

3.4 Conclusions and Atmospheric Implications

The results of this study provide insight into the fate of the secondary organic products formed in aqueous mixtures of $(\text{NH}_4)_2\text{SO}_4$ and methylglyoxal in the atmosphere. In the presence of oxidants like O_3 and OH, these products will degrade into smaller and more volatile organic compounds. Additionally, upon ozonolysis we observe an increase in light absorption by these particles.

As mentioned above, the photooxidation of aqueous SOA can be a potential source of more volatile organic compounds like formic acid, acetic acid, and glyoxylic acid in the atmosphere. SOAs formed from other aldehydes like glyoxal, acetaldehyde, formaldehyde, and glycoaldehyde could also undergo similar oxidation mechanisms, thereby making this pathway potentially important for the formation of the resulting volatile compounds. Additionally, Zhao et al. (2012) have shown that the reaction of H_2O_2 with glyoxal and methylglyoxal can lead to the formation of hydroxyhydroperoxide, which can then get photooxidized to form formic acid and acetic acid. (Zhao et al., 2012) Even at cloud relevant concentrations, the formation of these organic acids has been observed upon aqueous OH radical oxidation of methylglyoxal. (Tan et al., 2010) Recently, Paulot et al. (2011) highlighted that formic acid and acetic acid are the most abundant and ubiquitous trace gases in the atmosphere, yet their global budgets are underpredicted and there are major inconsistencies between model predictions and measurements. (Paulot et al., 2011) The aqueous phase oxidation of SOAs discussed in this study may contribute to the missing source of these volatile compounds in the atmosphere.

Reaction with OH radicals is a major fate of most organics in the atmosphere during the daytime in both clean and polluted environments. Given the rate constants and lifetimes for our reactions with OH, we would not expect SOAs formed from methylglyoxal to last for a significant time in the atmosphere during the day. However, in the night time, when there is no production of OH, these SOAs can last for a considerable time as their reactions with O_3 are comparatively slower. For instance, the SOA

compound at m/z 289.5 amu can last for ~17 hrs in the presence of only O_3 , which can be sufficient time to affect the physical and chemical properties of the aerosol.

Besides organic acids, similar to the fate of other hydrocarbons in the atmosphere, our results are consistent with reaction schemes which indicate that this oxidation chemistry is a source of HO_2 and CO_2 in the atmosphere. These reactions also regenerate OH and hence could be a potential source of OH.

Traditionally in atmospheric models SOA is treated as nonabsorbing, and usually scattering. (Dinar et al., 2008) Recent studies have shown that SOA is a potential source of brown carbon, including those which have glyoxal and methylglyoxal as precursors. (Bones et al., 2010; Nozière et al., 2009b; Sareen et al., 2010; Schwier et al., 2010; Shapiro et al., 2009) In our system, we observe a further increase in light absorption across all wavelengths when the light-absorbing products formed from methylglyoxal are exposed to O_3 . Even though brown carbon doesn't absorb as strongly as black carbon at wavelengths higher than 550 nm and contributes in a minor way to aerosol absorption, (Andreae and Gelencsér, 2006) its absorption has the potential to reduce tropospheric O_3 levels. (Jacobson, 1999, 2002) If these particles do indeed show increased light absorption in the atmosphere, then oxidized SOA from other aldehydes could also be a potential source of brown carbon which is not currently represented in atmospheric chemistry and climate models.

CHAPTER 4. Surfactants from the gas-phase promote cloud droplet formation

4.1 Introduction

Clouds, a key component of the climate system, form when water vapor condenses upon atmospheric particulates termed Cloud Condensation Nuclei (CCN). Variations in CCN concentrations can profoundly impact cloud properties, with important effects on local and global climate (IPCC, 2007). The ability of particles to act as CCN is affected by their chemical composition and dry particle size. Organic matter (OM) constitutes a significant fraction of tropospheric aerosol mass (Jimenez et al., 2009; IPCC, 2007), and can influence CCN activity by depressing surface tension, contributing solute, and influencing droplet activation kinetics by forming a barrier to water uptake at the surface (Feingold and Chuang, 2002). All CCN studies to date assume that surfactants are non-volatile and preexist in the CCN prior to activation.

The reactive uptake of volatile organic compounds (VOCs) by wet aerosols is a potentially important source of OM (Donaldson and Vaida, 2006; Ervens and Volkamer, 2010; Kroll et al., 2005). The α -dicarbonyl species glyoxal and methylglyoxal belong to this class; they are absorbed by wet aerosol particles (or cloud droplets) and undergo aqueous phase reactions to form low-volatility secondary organic aerosol (SOA) (Ervens and Volkamer, 2010; Tan et al., 2010). Recent studies have shown that the formation of SOA via the condensation of low-volatility VOC oxidation products, which are generally less hygroscopic than deliquescent inorganic salts, can affect the CCN activity of the seed

aerosol (Duplissy et al., 2008; Engelhart et al., 2008b; King et al., 2009; Prenni et al., 2007; VanReken et al., 2005; Engelhart et al., 2011). Few studies have focused on the impact of SOA generated in the aqueous phase on aerosol CCN activity (Bilde and Svenningsson, 2004; Cruz and Pandis, 2000; Prenni et al., 2001). SOA generated through aqueous-phase chemistry is likely to be highly oxygenated and surface active, hence making it more CCN active (Sareen et al., 2010; Schwier et al., 2010).

We studied the changes in the CCN activity of ammonium sulfate seed aerosols upon exposure to gas-phase methylglyoxal or acetaldehyde. A continuous flow streamwise thermal gradient CCN chamber (CFSTGC) was used downstream of a 3.5 m³ Teflon reaction chamber or an aerosol flow tube in order to determine the cloud-forming potential of these aerosols after various exposure times. The critical dry diameters observed for each experiment as a function of instrument supersaturation are compared to the (NH₄)₂SO₄ control in order to demonstrate the effect of the organics. A decrease in critical activation diameter at a given critical supersaturation indicates enhancement in CCN activity, and vice versa. We find that on the timescale of hours, methylglyoxal and/or acetaldehyde exposure enhances CCN activation beyond what is expected from equilibrium theory. To our knowledge, this is the first direct experimental evidence that the uptake of gas-phase organic precursors to atmospheric aerosol particles may lead to an enhancement in cloud droplet formation. These results further assert the importance of organics in determining the CCN activity of atmospheric aerosol particles. This study introduces the idea that volatile organics in the atmosphere may act as a reservoir of surfactants that can be taken up by aerosol particles and augment their CCN activity.

4.2 Methods

A schematic of the experimental setup is shown in Figure 4.1. A 0.2 M $(\text{NH}_4)_2\text{SO}_4$ solution was prepared using Millipore water and the pH was adjusted to 0 ± 0.1 or 2 ± 0.1 using H_2SO_4 , as the reactions which drive uptake are thought to be promoted by an acidic environment (Sareen et al., 2010). The solution was aerosolized with pure N_2 using a constant output atomizer (TSI). This aerosol stream was exposed to either gas-phase methylglyoxal (250 ppb or 8 ppb) and/or acetaldehyde (250 ppb or 8 ppb) in a continuous-flow 3.5 m³ Teflon aerosol chamber. The organic trace gas and $(\text{NH}_4)_2\text{SO}_4$ particles were added into the chamber together at a total flow rate of 13 LPM for a typical residence time of ~5 h. To characterize the time evolution of these processes, a residence time of 3 h was also tested using the chamber, and a glass flow tube (7.5 cm ID, 55 cm length) was used for a 3 min exposure time. Relative humidity inside the reactors was maintained between 62-67% as measured with a relative humidity meter (Vaisala) by passing the N_2 dilution flow through a bubbler filled with Millipore water. At the outlet of each reactor, the particles were passed through a diffusion dryer, a scanning mobility particle sizer (SMPS, TSI) and a CFSTGC (Droplet Measurement Technologies) to monitor particle concentration and CCN activity, respectively, using Scanning Mobility CCN Analysis (SMCA) (Moore et al., 2010). Total aerosol number concentrations in the chamber were $9.7\pm 0.3\times 10^5 \text{ cm}^{-3}$ (in the aerosol flow tube experiments, $1.5\pm 0.3\times 10^5 \text{ cm}^{-3}$). The size distribution had a mean volume-weighted particle radius of $231\pm 1.3 \text{ nm}$ with a geometric standard deviation of 1.4 (mean surface-weighted particle radius was $203\pm 1.7 \text{ nm}$ with a geometric standard deviation of 1.6).

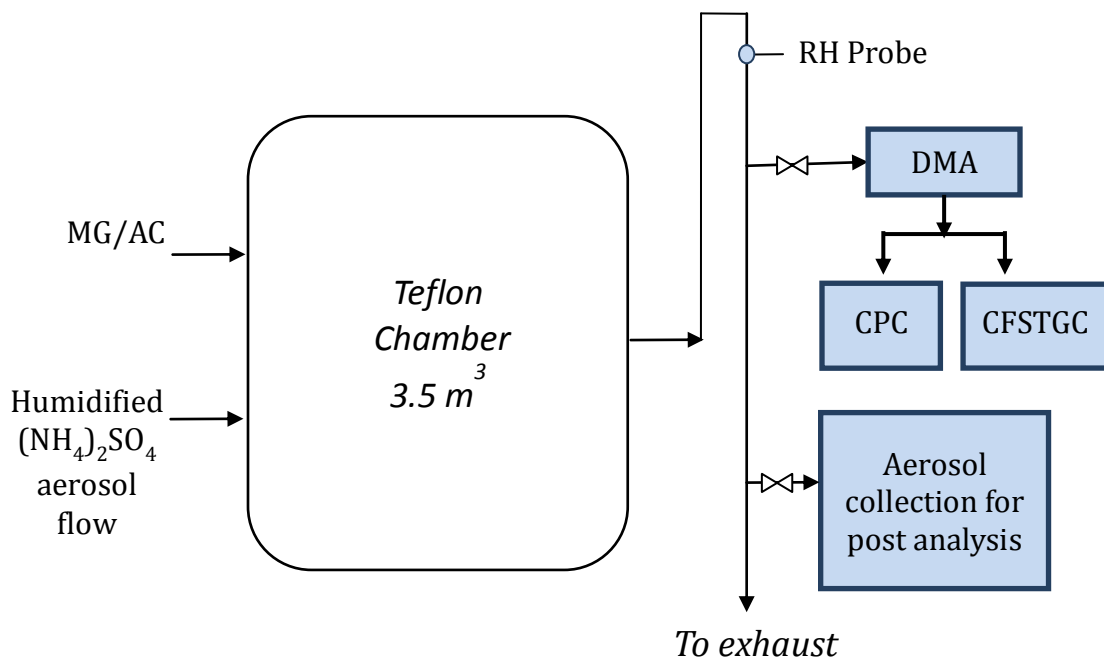


Figure 4.1. Schematic of the experimental setup. Gas phase methylglyoxal and/or acetaldehyde and ammonium sulfate seed aerosols are introduced into the chamber maintained at 62-67% RH. At the outlet, particles are analyzed using a SMPS and a CFSTGC.

The pure (NH₄)₂SO₄ solution was aerosolized, passed through a diffusion drier, and analyzed using SMCA to obtain the salt control. A control experiment with only the inorganic seed aerosol being introduced into the chamber was also conducted and analyzed, and the results consistent with the pure (NH₄)₂SO₄ solution data. Bulk aqueous solutions containing 0.5 M of the organic (methylglyoxal and/or acetaldehyde) with and without 3.1 M (NH₄)₂SO₄ were allowed to react for 24 h, and were then atomized and analyzed in a similar manner. For select experiments, the (NH₄)₂SO₄/methylglyoxal particles were passed through a heated stainless steel tube at 100°C upstream of the

SMPS/CFSTGC. No appreciable difference in the CCN activity spectra was observed with and without heating, suggesting that CCN activity in this system is not affected by volatilization biases (Asa-Awuku et al., 2009).

At the end of each chamber experiment, particles from the chamber were collected on Zeflour filters (Pall, 47 mm, 2.0 μm) for ~ 14 h at a pumping rate of 14 LPM, where 7 LPM was the chamber effluent and the rest of the flow consisted of dry N_2 in order to avoid deliquescence of the filter-sample aerosol. The water-soluble fraction of the collected particles was analyzed following the procedures of Asa-Awuku et al. (2010) (Asa-Awuku et al., 2010): the filters were extracted in 8 mL of pure water (18 M Ω) during a 1.25 h sonication process in a water bath heated to approximately 60°C. The filter extracts were then analyzed for WSOC concentration with a Total Organic Carbon (TOC) Turbo Siever analyzer, for soluble anion and cation composition with an Ion Chromatography system (Dionex DX-500); the CCN activity of the samples was measured by atomizing 3-5 mL of the extracted sample in a collision-type atomizer, drying the aerosol stream with two diffusion dryers, and analyzing using SMCA as described for the chamber experiments. The hygroscopicity of each filter extract was then determined with respect to a pure water blank. Gas-phase methylglyoxal was prepared as described previously by Kroll et al. (2005) (Kroll et al., 2005), except methylglyoxal was collected in a cold finger at -70 °C. While at this temperature, a 5 sccm or 0.5 sccm N_2 stream was passed through the cold finger for a final concentration of 250 ppb or 8 ppb methylglyoxal in the aerosol reaction chamber. Acetaldehyde was prepared by adding 99.9 wt% liquid acetaldehyde (Sigma Aldrich) to a cold finger under an oxygen-free environment and then passing a 1.4 sccm N_2 stream over it while the cold finger was kept

at -78 °C for a final concentration of 250 ppb or passing a 0.3 sccm N₂ stream over it while the cold finger was kept at -92 °C for a final concentration of 8 ppb.

4.3 Calculations

4.3.1 Cloud Droplet Number (CDN) Calculations

Computation of droplet number, N_c , is carried out with the Fountoukis and Nenes (FN; 2005) (Fountoukis and Nenes, 2005) droplet activation parameterization (augmented to account for depletion effects from Giant CCN; Barahona et al., 2010) (Barahona et al., 2010). FN is a comprehensive and efficient formulation, which has been evaluated extensively with numerical simulations (Barahona et al., 2010; Fountoukis and Nenes, 2005; Ghan, 2011), as well as in situ measurements (Fountoukis et al., 2007; Meskhidze et al., 2005). FN is based on the framework of an ascending adiabatic cloud parcel; N_c is determined by the maximum supersaturation, s_{\max} , which is controlled by the water vapor balance and is obtained by classifying the droplets by proximity to their critical diameter (“population splitting”). The effective water vapor uptake coefficient (which affects the water vapor mass transfer coefficient during droplet formation) is set to 0.06, following Fountoukis et al. (2007). (Fountoukis et al., 2007) The model was integrated for 2 years with present-day emissions of sulfur and sea salt; monthly, grid-by-grid CCN spectra are then derived from the simulations of the second year.

4.3.2 Kinetics of Methylglyoxal Hydration and Oligomerization

Methylglyoxal (MG) rapidly reacts with water in aqueous aerosols to form hydrated methylglyoxal (HMG) according to:



According to the density functional theory calculations of Krizner et al. (Krizner et al., 2009), the corrected free energy barrier for this process is 17.3 kcal mol⁻¹, and the preexponential factor is 5×10¹¹ M⁻¹s⁻¹, yielding a pseudo-first-order rate constant at 298 K of approximately 6 s⁻¹. Hence, the time required for methylglyoxal to be 98% converted to its singly hydrated form (Betterson and Hoffmann, 1988a) is ~0.7 s. The apparent enhancement in MG uptake due to hydration is already accounted for in the effective Henry's law constant reported by Betterson and Hoffmann (H^{*}=3.2×10⁴ M atm⁻¹) (Betterson and Hoffmann, 1988a).

The kinetics of methylglyoxal oligomerization in aqueous solutions containing NH₄⁺ and H₃O⁺ were presented by Sareen et al. (Sareen et al., 2010) It was found that the rate limiting step for the formation of oligomers was the protonation of singly hydrated MG by either NH₄⁺ or H₃O⁺, with second-order rate constants $k_{\text{H}_3\text{O}^+}^{\text{II}} \leq 10^{-3} \text{ M}^{-1} \text{ min}^{-1}$ and $k_{\text{NH}_4^+}^{\text{II}} = 5 \times 10^{-6} \text{ M}^{-1} \text{ min}^{-1}$. The conversion rate of HMG, is described by the following equation:

$$R = (k_{\text{H}_3\text{O}^+}^{\text{II}}[\text{H}_3\text{O}^+] + k_{\text{NH}_4^+}^{\text{II}}[\text{NH}_4^+])[\text{HMG}] \quad (4.2)$$

In the aerosol experiments presented here, [NH₄⁺]=28 M and [H₃O⁺]=7 M. Because the oligomerization reactions are relatively slow compared to the diffusional timescale in the

aerosol particle, $\tau=R^2/D$, where R is the characteristic length scale and D is the diffusion coefficient, we expect that the concentration of HMG in the particle is spatially uniform and maintained relatively constant via MG absorption from the gas phase according to Henry's Law. Based on a gas-phase MG concentration of 250 ppb, $[HMG]=8\times 10^{-3}$ M. After 3 hours of reaction, the total amount of MG sequestered as oligomeric products is between 2.02×10^{-4} M and 1.03×10^{-2} M. The total concentration of MG and products is then $0.031-6.06\times 10^{-4}$ mol C kg⁻¹ H₂O.

4.3.3 Inorganic:Organic Ratio

This ratio for the chamber filter extracts was calculated based on WSOC and IC analysis. The inorganic on the filter was 1.57×10^4 μ g and the water soluble organic matter was 18.928 μ g, giving a ratio of 829.4. For comparison, this ratio is also calculated for the particles in the chamber. Based on 250 ppb of methylglyoxal in the chamber and a Henry's Law constant of 3.2×10^4 M atm⁻¹, the in-particle concentration of methylglyoxal is 0.008 M. Following Tang and Munkelwitz (Tang and Munkelwitz, 1994), a 0.2 M ammonium sulfate atomizer solution will lead to an in-particle concentration of 14 M at 65 % relative humidity. The inorganic:organic ratio for the chamber based on these numbers is 3208.9.

4.3.4 Köhler Theory Analysis (KTA)

The following equations from Moore et al. (Moore et al., 2010) were used to infer surface tension of the particles:

$$\sigma = \left[\frac{\left(\frac{\rho_o}{M_o}\right)\varepsilon_o v_o + \frac{\rho_i}{M_i}\varepsilon_i v_i}{\frac{256(M_w)^2}{27(\rho_w)^2} \left(\frac{1}{RT}\right)^3 \omega^{-2}} \right]^{1/3} \quad (4.3)$$

where the subscripts i , o , and w refer to the inorganic, organic, and water respectively. M is the average molecular weight, ρ is the density, v is the effective van't Hoff factor, R is the universal gas constant, T is the median temperature of the CFSTGC column, σ is the surface tension, and ε is the mass fraction calculated as:

$$\varepsilon_i = \frac{\frac{m_i}{\rho_i}}{\frac{m_i}{\rho_i} + \frac{m_o}{\rho_o}} \quad (4.4)$$

ω , the fitted CCN activity factor, is determined from the critical supersaturation (S_c) and the critical dry activation diameter (d_d) using the equation:

$$S_c = \omega d_d^{-3/2} \quad (4.5)$$

4.3.5 Surface Tension of the Particle Based on Henry's Law

The surface tension of the aerosol particles can be estimated using the Szyszkowski-Langmuir equation:

$$\sigma = \sigma_0 - aT \ln(1 + bC) \quad (4.6)$$

where σ and σ_0 are the surface tension with and without the organics, respectively, T is temperature, C is the carbon content, and a and b are fit parameters. Although the particles studied here were composed of ammonium sulfate, we are interested in calculating the surface tension of the particle at the moment of activation. At that point,

the particle is composed mostly of water. Therefore, values for a and b are taken from the surface tension measurements done on a methylglyoxal and water solution using pendant drop tensiometry: $a=0.0244 \text{ dyn cm}^{-1} \text{ K}^{-1}$ and $b=3.050 \text{ kg water (mol C)}^{-1}$. σ_0 was tested in our laboratory using Millipore water and found to be $72.55 \text{ dyn cm}^{-1}$.

C is calculated based on the assumption that the droplet is in Henry's Law equilibrium with the gas phase, and that the total contribution of oligomeric products formed prior to activation is small. Hence based on 250 ppb of methylglyoxal in the chamber (and CFSTGC), we calculate an $8 \times 10^{-3} \text{ M}$ methylglyoxal concentration, or $0.0240 \text{ mol C (kg water)}^{-1}$. Plugging these values into the Szyszkowski-Langmuir equation gives a value of $72.02 \text{ dyn cm}^{-1}$ for the surface tension of the methylglyoxal and ammonium sulfate particles. Surface tension depression will lower the value of κ by a

factor of $\left(1 - \frac{\Delta\sigma}{\sigma_w}\right)^{-3}$

where $\Delta\sigma$ is the surface tension depression from that of pure water. In our case, the calculated surface tension value of $72.02 \text{ dyn cm}^{-1}$ will lead to a very small (2.2%) increase in κ .

For acetaldehyde, the constants a and b are taken from the surface tension measurements done on an acetaldehyde and water solution using pendant drop tensiometry: $a=0.0037 \text{ dyn cm}^{-1} \text{ K}^{-1}$ and $b=491.64 \text{ kg water (mol C)}^{-1}$ (Li et al., 2011). Based on 250 ppb of acetaldehyde in the chamber and a Henry's Law constant of 11.4 M/atm , the acetaldehyde concentration in a particle is $2.85 \times 10^{-6} \text{ M}$, or $5.7 \times 10^{-6} \text{ mol C (kg water)}^{-1}$. These values give a surface tension of $73.16 \text{ dyn cm}^{-1}$ for the surface tension

of the acetaldehyde and ammonium sulfate particles and will lead to a negligible change in κ of 0.01%.

4.3.6 Concentration of Methylglyoxal at the Moment of Activation

The critical wet diameter, D_c , is

$$D_c = \left(\frac{3*\kappa}{A} \right)^{0.5} d_d^{1.5} \quad (4.8)$$

where, κ is the hygroscopicity parameter, calculated from CCN activity data following Petters and Kreidenweis (Petters and Kreidenweis, 2007), and

$$A = \frac{4 \sigma M_w}{RT \rho_w} \quad (4.9)$$

Based on the amount of methylglyoxal in the chamber, 250 ppb, we can calculate the number of molecules of methylglyoxal at each d_d . Since the number of molecules is constant in the particle, it can be divided by the corresponding volume at D_c to get the concentration at the activated diameter.

4.3.7 Calibration of Supersaturation in the CCN Counter

The effective supersaturation in the CCN instrument depends on the flow rate, pressure and temperature gradient applied on the column (Lance et al., 2006). Scanning Mobility CCN Analysis (SMCA) with $(\text{NH}_4)_2\text{SO}_4$ calibration aerosol is used to determine

supersaturation for a given set of operating conditions, following the procedure of Moore et al. (2010) (Moore et al., 2010). Calibration aerosol is generated by atomizing an ammonium sulfate solution in pure water. Atomized droplets were dried in a silica gel dryer and sampled by a differential mobility analyzer (DMA; TSI 3081 Long DMA) that classifies the aerosol and then introduced into the CFSTGC and a Condensation Particle Counter (CPC; TSI 3010). The voltage applied to the DMA was scanned, and inversion of the time series of CCN and CPC counts yields the fraction of classified particles that act as CCN (“activation curve”). The dry mobility diameter for which half of the classified particles act as CCN, d_{50} , is used to characterize instrument supersaturation (being equal to the critical supersaturation of particles with dry diameter equal to d_{50}). Köhler theory is used to compute the effective instrument supersaturation, assuming the $(\text{NH}_4)_2\text{SO}_4$ particles have (at the point of activation) the surface tension and density of pure water, and a variable van’t Hoff factor is used as described in Moore et al. (2010) (Moore et al., 2010).

4.4 Results and Discussion

Figures 4.2 summarizes the results of the most relevant CCN activation experiments showing the change in critical activation diameters as compared to pure $(\text{NH}_4)_2\text{SO}_4$ for the various conditions tested. Figure 4.3 contains the supersaturation vs activation diameter plots for each individual condition tested in this study. After 3 minutes of exposure to 250 ppb methylglyoxal in the flow tube experiments, there is a negligible change in aerosol CCN activity. However, when aerosols are exposed to

methylglyoxal for longer periods in the chamber (3-5 h), their CCN activity is enhanced considerably.

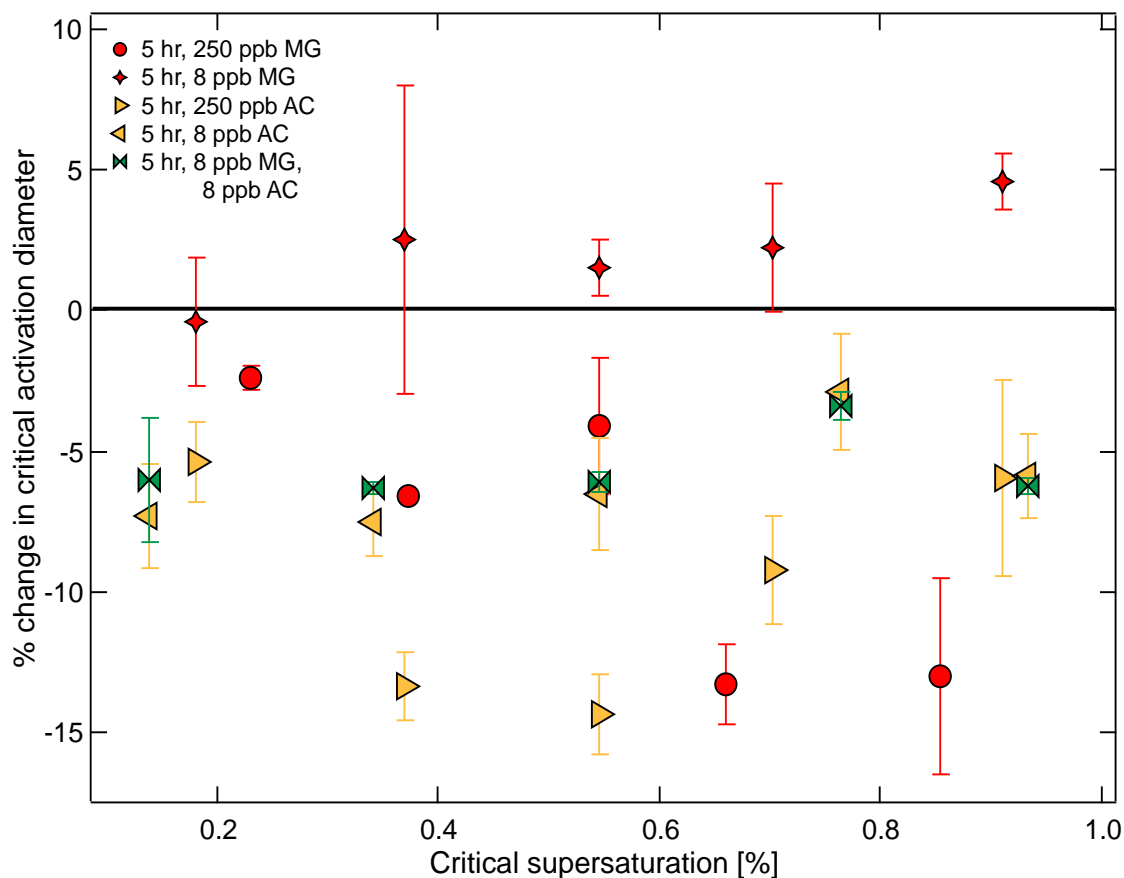
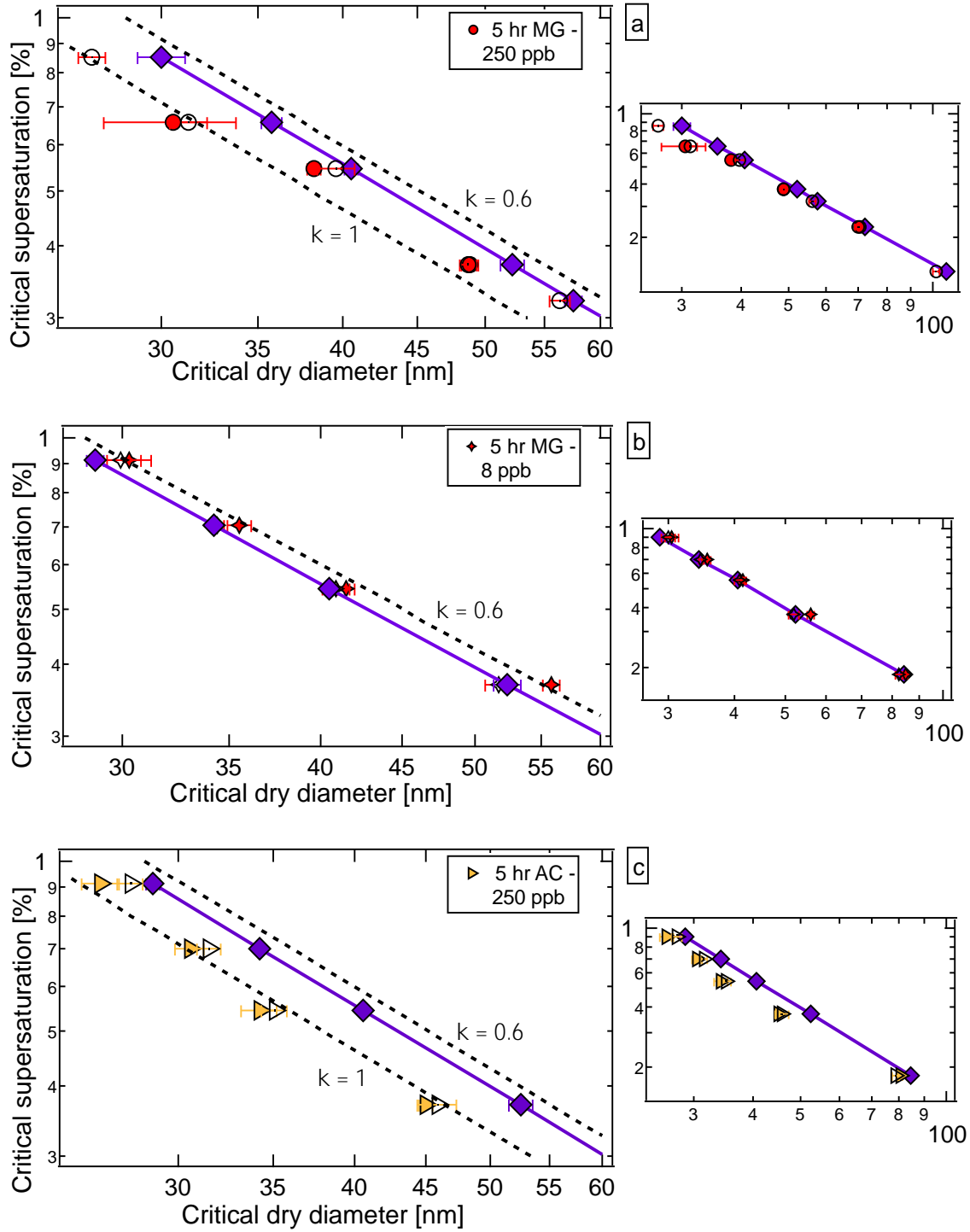
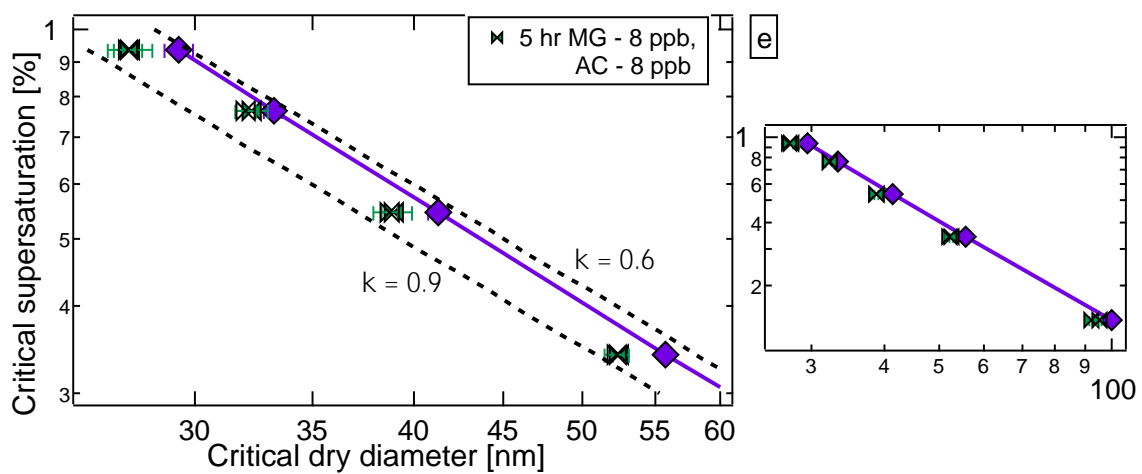
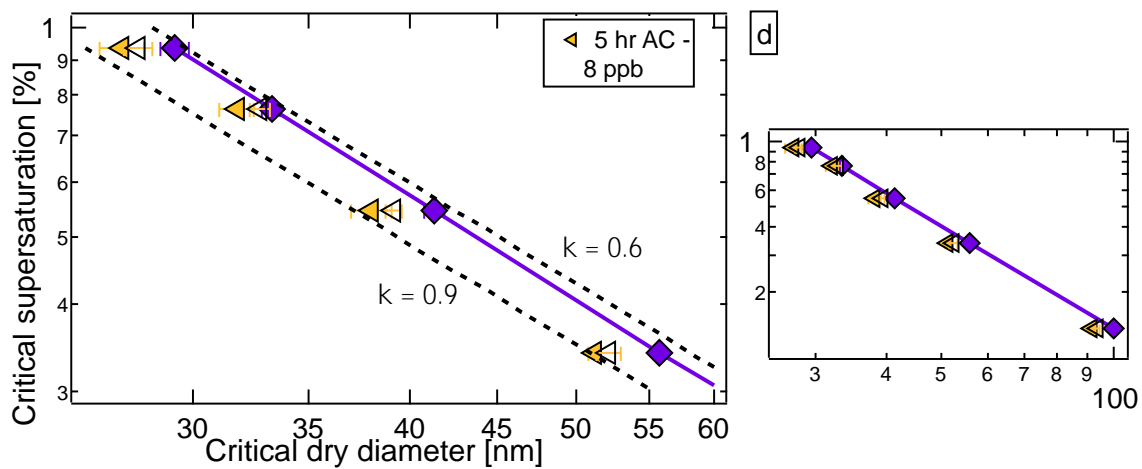


Figure 4.2. Cloud condensation nuclei (CCN) activity data. Humidified $(\text{NH}_4)_2\text{SO}_4$ aerosols were exposed to gas-phase methylglyoxal or acetaldehyde in a 3.5 m^3 Teflon reaction chamber. The critical dry diameters observed for each experiment as a function of instrument supersaturation are compared to the $(\text{NH}_4)_2\text{SO}_4$ control in order to demonstrate the effect of organics. A decrease in critical activation diameter at a given critical supersaturation indicates enhancement in CCN activity, and vice versa. The data shown here are the results for $(\text{NH}_4)_2\text{SO}_4$ particles exposed to 250 ppb and 8 ppb of methylglyoxal for 5 h, particles exposed to 250 ppb and 8 ppb of acetaldehyde for 5 h, and finally particles exposed to 8 ppb of methylglyoxal and 8 ppb of acetaldehyde for 5 h.





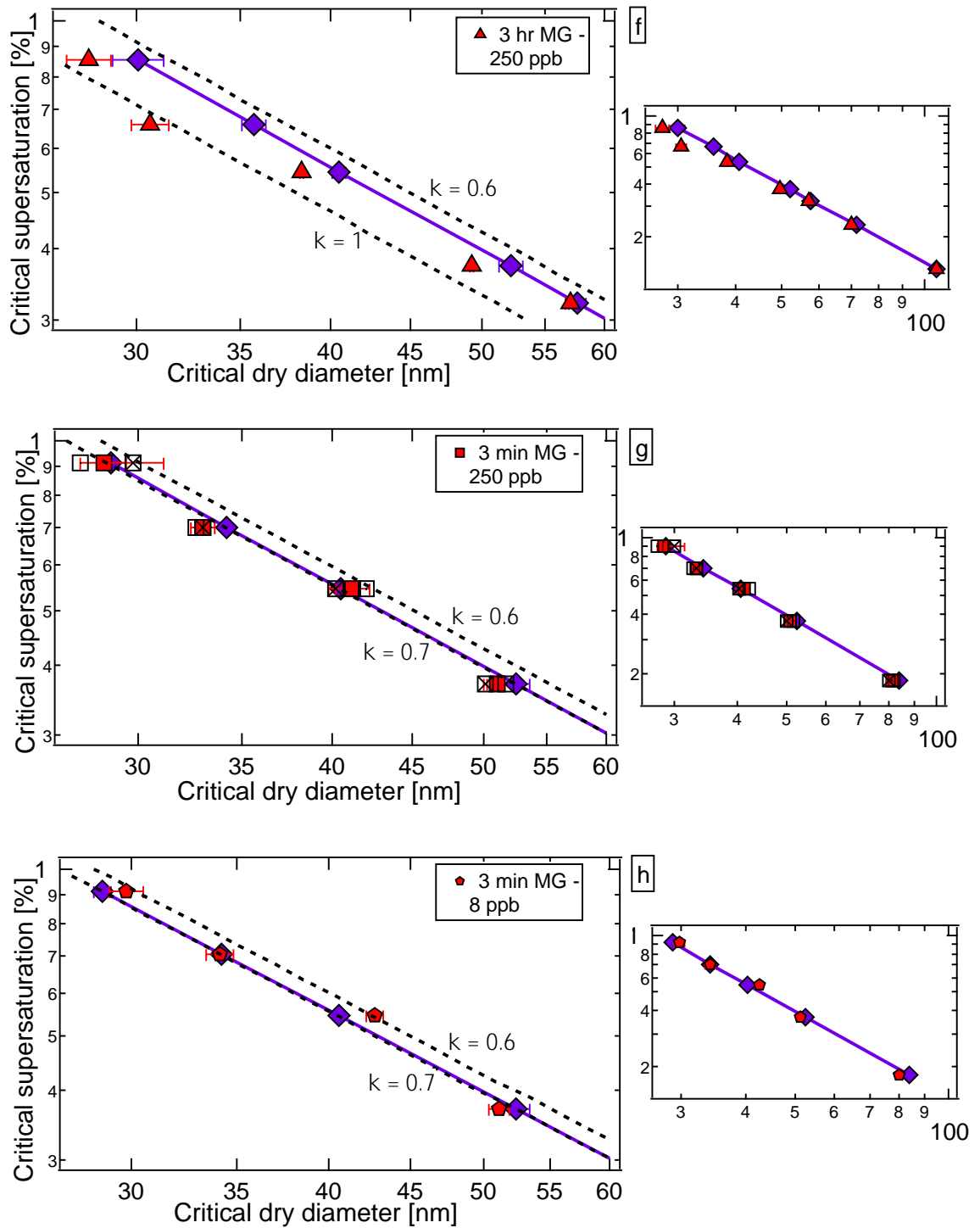


Figure 4.3. Cloud condensation nuclei (CCN) activity data. Humidified $(\text{NH}_4)_2\text{SO}_4$ aerosols were exposed to gas-phase methylglyoxal or acetaldehyde in a 3.5 m^3 Teflon reaction chamber or a glass flow tube for varying residence times. The critical dry diameters observed for each experiment as a function of instrument

supersaturation are compared to the $(\text{NH}_4)_2\text{SO}_4$ control (purple diamonds) in order to demonstrate the effect of organics. Closed and open symbols represent the first and second trials for each time point, respectively. The small graphs on the right side represent the entire range of supersaturations studied, whereas the main plots zoom in on the smaller diameters. The dashed lines show values of constant κ , ranging from our $(\text{NH}_4)_2\text{SO}_4$ control ($\kappa \sim 0.6$) to the maximum κ value observed for each experiment. Panels (a) and (b) show the results for particles exposed to 250 ppb and 8 ppb of methylglyoxal for 5 h, respectively. Panels (c) and (d) show the results for particles exposed to 250 ppb and 8 ppb of acetaldehyde for 5 h, respectively. In panel (e), particles were exposed to 8 ppb of methylglyoxal and 8 ppb of acetaldehyde for 5 h. In panel (f), particles were exposed to 250 ppb of methylglyoxal for 3 h. Panels (g) and (h) show the results for particles exposed to 250 ppb and 8 ppb of methylglyoxal for 3 min in the flowtube reactor, respectively.

For the conditions considered, methylglyoxal reduces the critical activation diameters of the inorganic seed aerosol on average by $6.36 \pm 0.05\%$ at the supersaturations studied (0.2% to 1.0%). For marine aerosols, where stratocumulus clouds (supersaturation ~ 0.1 -0.2%) are prevalent, a decrease in critical activation diameter within those supersaturation ranges can increase CCN concentrations by up to 54%. For continental aerosols, at supersaturations between 0.6-1.0%, typical of convective clouds, CCN concentrations can increase by up to 14% (Figure 4.4, 4.5) (Nenes and Seinfeld, 2003).

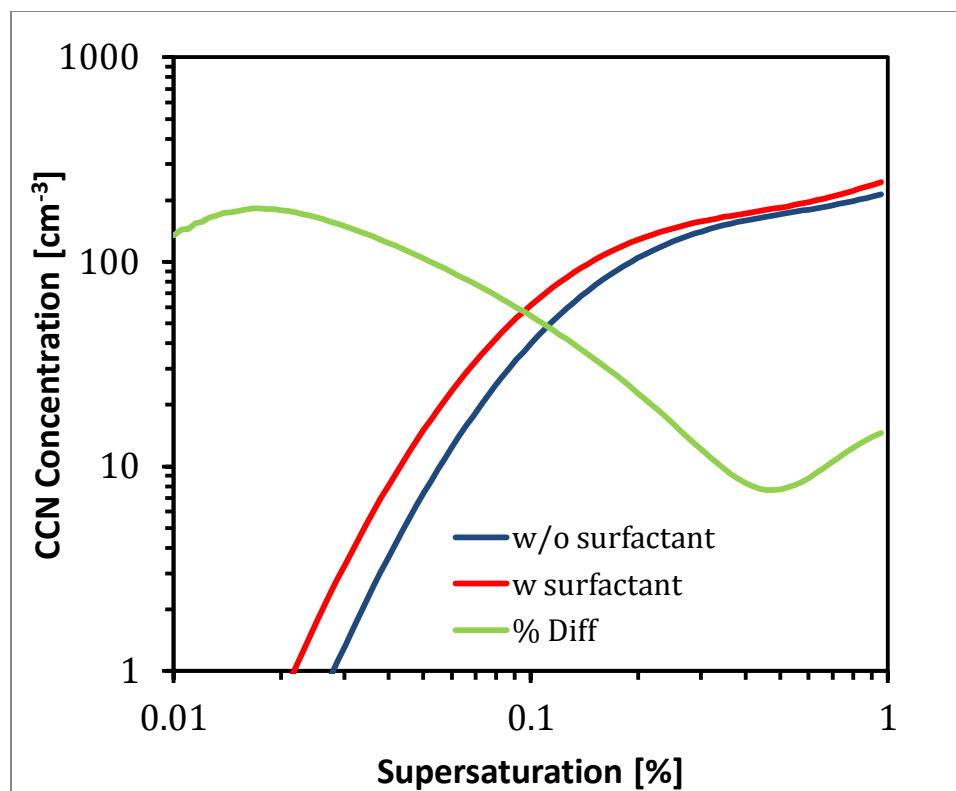


Figure 4.4. Change in CCN concentration when surfactant effects are included for marine aerosols. The blue line indicates CCN concentration without the effect of surfactants, the red line with the effect of surfactants, and the green line is the percent difference between the latter and the former. The CCN concentrations are calculated as a function of supersaturation using classical Köhler Theory, as described in Nenes and Seinfeld (Nenes and Seinfeld, 2003), using size distributions for marine aerosols given by Whitby (nuclei mode, median diameter: 0.010 μm , geometric standard deviation: 1.6) (Whitby, 1978).

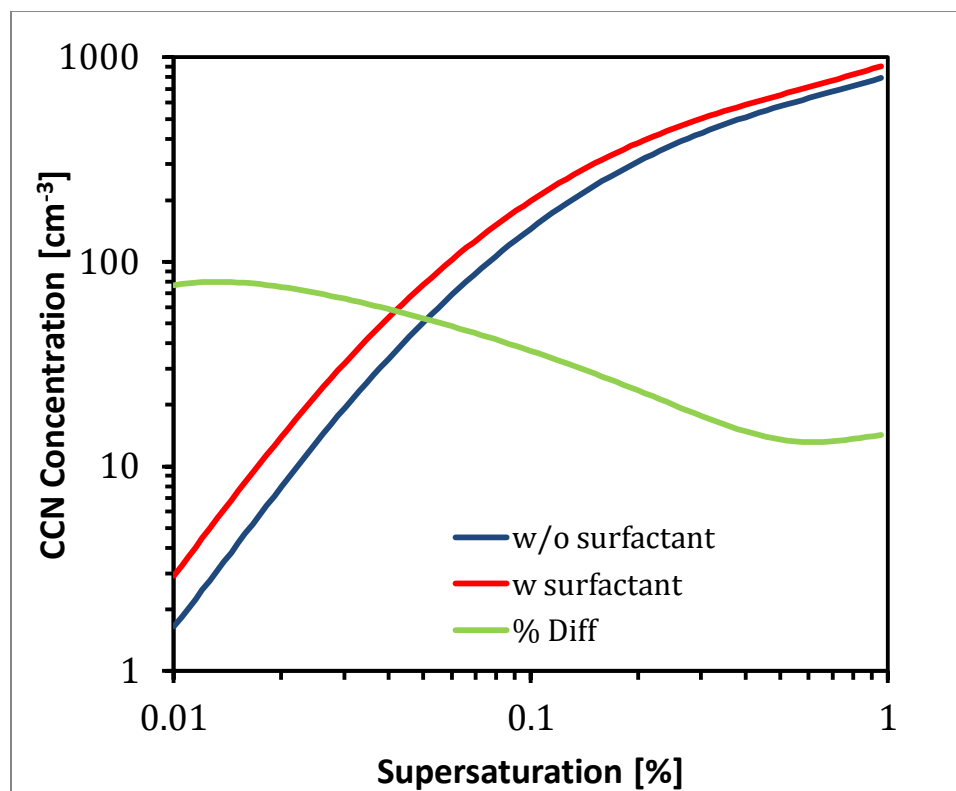


Figure 4.5. Change in CCN concentration when surfactant effects are included for continental aerosols. The blue line indicates CCN concentration without the effect of surfactants, the red line with the effect of surfactants, and the green line is the percent difference between the latter and the former. The CCN concentrations are calculated as a function of supersaturation using classical Köhler Theory, as described in Nenes and Seinfeld (Nenes and Seinfeld, 2003), using size distributions for continental aerosols given by Whitby (nuclei mode, median diameter: 0.016 μm , geometric standard deviation: 1.6) (Whitby, 1978).

More importantly, in the presence of such a surfactant, cloud droplet number concentrations (CDNC) can be enhanced by as much as 20% in the atmosphere as seen in Figure 4.6. The CDNC are calculated with the Fountoukis and Nenes (2005) (Fountoukis and Nenes, 2005) droplet activation parameterization (Supplementary Information) and are an upper limit based on our experimental results. At the supersaturation ranges of

stratocumulus clouds ($S_{\text{Max}} \sim 0.1-0.3$), this surfactant effect can increase CDNC by 10-15% for marine aerosols and by 15-20% for continental aerosols. It should be noted that stratocumulus clouds are most prevalent in the atmosphere and most sensitive to changes in microphysics, hence a 20% increase in CDNC can have a significant impact in the atmosphere.

Hydration of methylglyoxal in the aqueous phase occurs on a timescale of ~ 1 s (Krizner et al., 2009). The timescale of the methylglyoxal oligomerization reactions, which drive the uptake of methylglyoxal to the particle, is on the order of hours in saturated ammonium sulfate solutions (Sareen et al., 2010). This is consistent with our observations that a reaction time of up to 3 hours is required for the surfactant effect of the hydrated methylglyoxal and oligomers to become apparent in the CCN data. Full details of the timescale analysis are given Section 4.3.2.

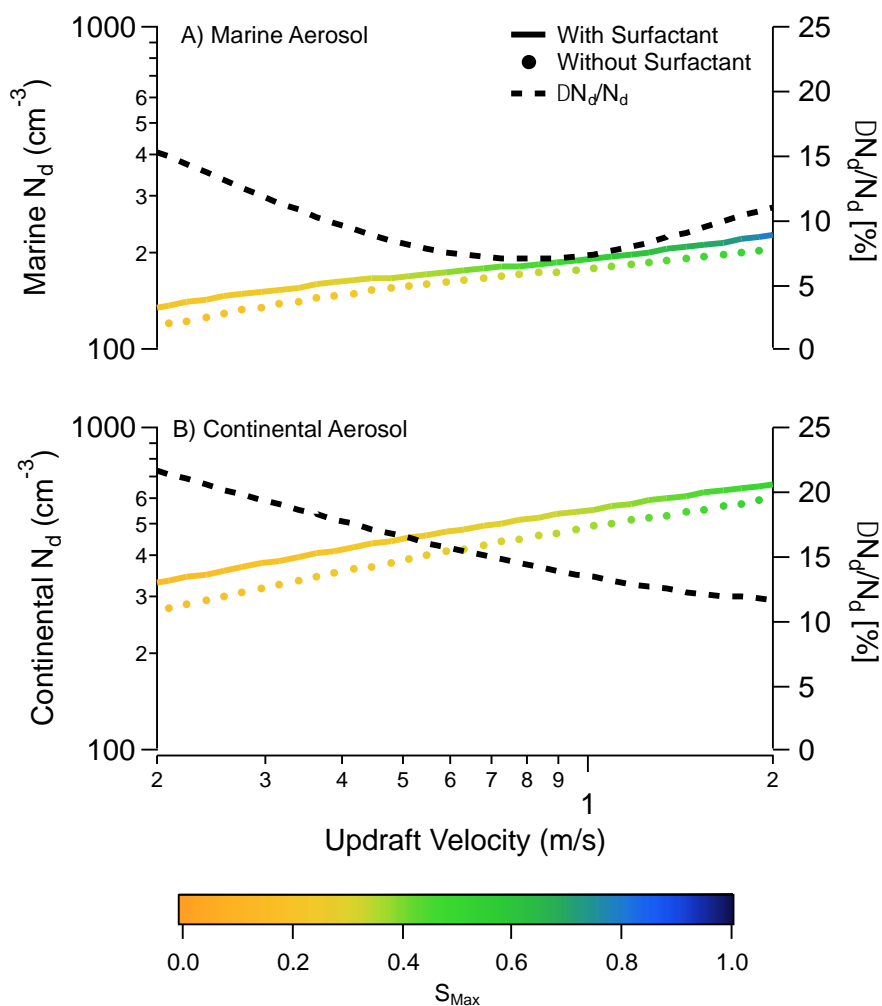


Figure 4.6. Cloud droplet number concentrations computed using a droplet activation parameterization by Fountoukis and Nenes (2005) (Fountoukis and Nenes, 2005) with and without the surfactant effects observed in this study. The “with surfactant” data is based on $\kappa=1$, which is the maximum enhancement we see in our experiments. The “without surfactant” data is based on $\kappa=0.6$, similar to that of $(\text{NH}_4)_2\text{SO}_4$. The maximum vertical velocity ranges from 0.2-2 m/s, typical to that of the atmosphere, and corresponds to supersaturation (S_{max}) of 0.1% – 1.0%. Panel (A) shows the marine aerosol case, panel (B) shows the continental aerosol case. An increase in cloud droplet number concentration (defined as $\Delta N_d/N_d$, right axis) of up to 20% is observed.

The observed critical supersaturation (S_c) deviates somewhat from the power law dependence on dry diameter (d_d) predicted by simple Köhler theory ($S_c \sim d_d^{-1.5}$); power law exponents range from -1.28 for the 5 h experiments to -1.51 for 3 min exposures (Table 4.1).

Table 4.1. Exponents of the power log fits for the SS vs dry diameter graphs for the various chamber experiments. As expected, these values deviate from the pure AS calibration curve.

Experiment	Average power log fits (exponent)
(NH ₄) ₂ SO ₄	-1.52 ± 0.03
5 hr 250 ppb MG	-1.34 ± 0.09
3 hr 250 ppb MG	-1.37
3 min 250 ppb MG	-1.42 ± 0.03
5 hr 8 ppb MG	-1.34 ± 0.09
3 min 8 ppb MG	-1.51
5 hr 250 ppb AC	-1.47 ± 0.06
5 hr 8 ppb AC	-1.59 ± 0.001
5 hr 8 ppb AC, 8 ppb MG	-1.57 ± 0.04

These deviations from Köhler theory at the longer timescales are consistent with the surfactant content in the particles increasing with time. In order to assess the influence of methylglyoxal, the CCN activation curve for each experiment is compared to that of pure (NH₄)₂SO₄ (Figures 4.2, 4.3). Larger deviations from this control curve are seen at high critical supersaturations (i.e., smaller critical dry size for activation). Such size-dependent deviations from Köhler theory are typical of aerosols containing surfactants (Moore et al., 2008), as the surfactants in particles activating at higher supersaturations (i.e. smaller particles) tend to be more concentrated at the critical wet diameter, resulting in a greater surface tension reduction than in particles which activate at lower supersaturations.

Table 4.2 lists the average apparent hygroscopicity parameter, κ (calculated from the CCN activity data following Petters and Kreidenweis (Petters and Kreidenweis, 2007)) for each experiment. For the 3 min flow tube experiments, the κ values (0.63 ± 0.18) are consistent with $(\text{NH}_4)_2\text{SO}_4$. Particles exposed for longer time scales however show an increase in κ (beyond that of pure $(\text{NH}_4)_2\text{SO}_4$) with increasing supersaturation, suggesting that the aerosol surface tension is lower than that of water (Ruehl et al., 2010). It should also be noted that a constant surface tension, that of water, was used to calculate κ and our observation of κ increasing at higher supersaturations is once again indicative of the presence of surfactants.

Table 4.2. Hygroscopicity parameter, κ , values for the different chamber and flowtube experiments for methylglyoxal (MG) and acetaldehyde (AC).

Experiment	Average κ
$(\text{NH}_4)_2\text{SO}_4$	0.60 ± 0.18
5 hr 250 ppb MG	0.81 ± 0.24
3 hr 250 ppb MG	0.74 ± 0.22
3 min 250 ppb MG	0.63 ± 0.18
5 hr 8 ppb MG	0.55 ± 0.16
3 min 8 ppb MG	0.59 ± 0.18
5 hr 250 ppb AC	0.81 ± 0.24
5 hr 8 ppb AC	0.72 ± 0.22
5 hr 8 ppb AC, 8 ppb MG	0.71 ± 0.19

Köhler Theory Analysis (KTA) (Asa-Awuku et al., 2010) was then used to infer the extent of surface tension depression (with respect to water) in the particles. The relative abundance of the organic and inorganic components were attained from water soluble organic carbon (WSOC) analysis and ion chromatography (IC) of aqueous

extracts of filter samples (obtained by pumping down the chamber for approximately 14 h following an exposure experiment with 250 ppb of methylglyoxal and 5h residence time). The ratio of inorganic:organic material in the filter extracts was 829, which is somewhat lower than that predicted based on Henry's Law uptake of methylglyoxal to the particles, 3209. This could be due to continued reactive uptake of the gas-phase organic on the filter during particle collection. KTA suggests that methylglyoxal and its reaction products suppress the surface tension of the aerosols to $65.1 \pm 0.8 \text{ dyn cm}^{-1}$ compared to $72.55 \text{ dyn cm}^{-1}$ for water.

Acetaldehyde is another VOC which has been shown to depress surface tension in bulk aqueous ammonium sulfate solutions (Li et al., 2011). Chamber experiments similar to those carried out with methylglyoxal were conducted using 250 ppb of acetaldehyde at an exposure time of 5 h. Acetaldehyde enhances CCN activity even more than methylglyoxal, reducing the critical activation diameters on average by $9.68 \pm 0.04\%$. Particles exposed to acetaldehyde become substantially more hygroscopic than pure ammonium sulfate, with κ values ranging from 0.62 to 1.00. κ is, in general, higher at high supersaturations, consistent with a surfactant-enhanced apparent hygroscopicity. The power law exponents deviate slightly from Köhler theory, averaging -1.47 ± 0.06 .

The gas-phase methylglyoxal, acetaldehyde, and particle concentrations used above exceed typical atmospheric concentrations (urban: 10^4 cm^{-3} , 2.5 ppb methylglyoxal, 4 ppb acetaldehyde (Grosjean et al., 1996; Hughes et al., 1998); wet-season Amazon: 10^2 cm^{-3} , 0.125 ppb methylglyoxal (Roberts et al., 2003; Fu et al., 2008), 0.5 ppb acetaldehyde (Kesselmeier et al., 2002)). Chamber experiments conducted at lower acetaldehyde and particle concentrations ($2.58 \times 10^4 \text{ cm}^{-3}$, 8 ppb acetaldehyde) with

a 5h residence time showed a depression in critical activation diameters by $6.01 \pm 0.02\%$ at the supersaturations studied (Figures 4.2, 4.3). However, experiments conducted at lower methylglyoxal and particle concentrations ($1.78 \times 10^4 \text{ cm}^{-3}$, 8 ppb methylglyoxal) showed CCN activity closer to that of ammonium sulfate. Recent studies of acetaldehyde and methylglyoxal mixtures in bulk ammonium sulfate solutions showed that cross-reactions lead to greater surface tension depression than predicted based on the single-species isotherms (Li et al., 2011). To represent a more atmospherically relevant environment, the combined effect of these aldehydes was also studied in the chamber; $2.33 \times 10^4 \text{ cm}^{-3}$ of ammonium sulfate were exposed to 8 ppb each of methylglyoxal and acetaldehyde for 5h. These experiments showed similar CCN enhancement to the low concentration acetaldehyde experiments. Unlike the bulk experiments of Li et al. (2011), no synergistic effect due to the mixed organics was observed. This suggests that the mechanisms of surface tension depression may be different in these two systems. For example, the formation of oligomer cross products may be more important to surface tension depression in the bulk system.

The wet diameter profiles of the activated droplets formed by the particles exposed to methylglyoxal and/or acetaldehyde at all time scales studied are similar to that of pure $(\text{NH}_4)_2\text{SO}_4$. These observations rule out the possibility of a kinetic barrier to water uptake to these particles on the timescale of the CCN measurements (Feingold and Chuang, 2002). However, the barrier action of a surfactant film towards the uptake of gas-phase species to the particle depends on the identity of the penetrating gas-phase molecules, so a barrier effect for the uptake of trace gases (with implications for aerosol heterogeneous chemistry) is a question for future study.

Methylglyoxal and acetaldehyde have low effective Henry's Law constants compared to that of glyoxal (Berterton and Hoffmann, 1988a). In accord with the observations of Kroll et al. (2005) (Kroll et al., 2005), we observed negligible particle growth when $(\text{NH}_4)_2\text{SO}_4$ particles with a diameter of 150 nm were size-selected using a differential mobility analyzer (DMA, TSI) and exposed to methylglyoxal in the chamber (Figure 4.7). This suggests that the organic species in this study reside at the gas-aerosol interface and induce the significant effects on CCN activity observed mainly by altering the properties of the particle surface. This is the first time that the presence of relatively insoluble VOCs has been shown to enhance aerosol CCN activity.

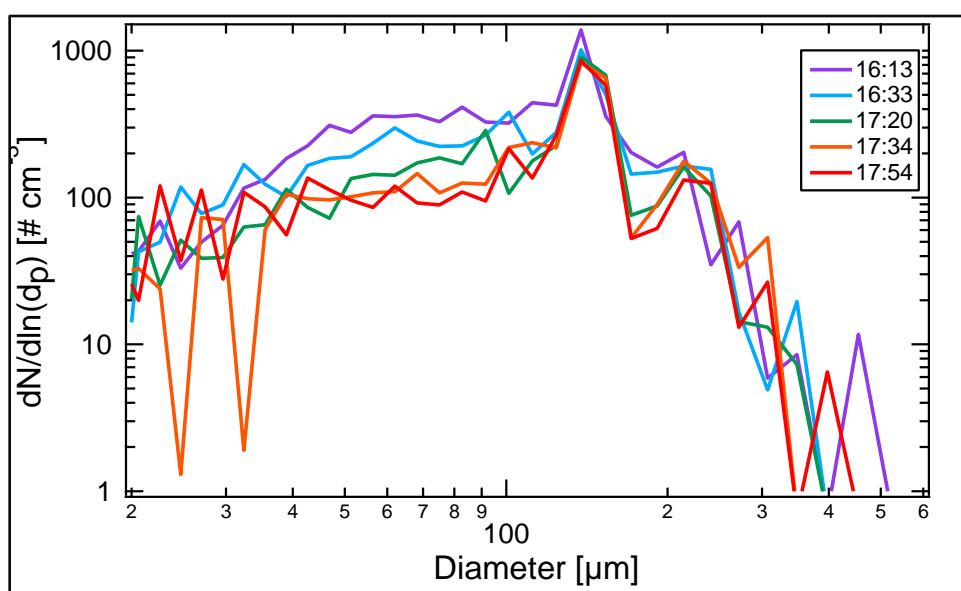


Figure 4.7. SMPS data showing the number size distribution of particles over time. 150 nm particles were size-selected using the DMA and put into the chamber. As can be seen, there is negligible particle growth.

If the total uptake of methylglyoxal to the particles is described by Henry's Law, then based on an effective Henry's Law constant of $H^*=3.2 \times 10^4 \text{ M atm}^{-1}$ (Berterton and Hoffmann, 1988a), and experimental surface tension data for aqueous bulk methylglyoxal

solutions (Sareen et al., 2010), the surface tension of the particles exposed to 250 ppb of methylglyoxal at the moment of activation is predicted to be $72.02 \text{ dyn cm}^{-1}$. This leads to a very small predicted change in κ (2.2% increase relative to pure ammonium sulfate). A similar calculation for acetaldehyde, which has a Henry's Law constant two orders of magnitude lower than that of methylglyoxal (Betterton and Hoffmann, 1988a), predicts an insignificant change in κ (0.01% increase). The fact that we observe a much greater enhancement in κ than these predictions suggests that surface adsorption may play a significant role in determining the aerosol surface tension, and thus CCN activity (Donaldson and Vaida, 2006; Djikaev and Tabazadeh, 2003). If surface-bulk repartitioning of the solute had been dominant, it would have depressed hygroscopicity further when compared to the pure inorganic. Romakkaniemi et al. (2011) modeled a similar system, specifically the reactive uptake of gas-phase methylglyoxal to $(\text{NH}_4)_2\text{SO}_4$ aerosol, allowing OH oxidation to take place (Romakkaniemi et al., 2011). They predicted that total reactive uptake of surface-active species into the aqueous phase may be enhanced by surface-bulk partitioning, especially for small particles, beyond what would be predicted based on Henry's Law alone. The significant differences between the model system of Romakkaniemi et al. and our study are that 1) the additional driving force for uptake of the aerosol-phase OH reaction with the organics is absent in our experiments and 2) they assume equilibration with the bulk.

Analysis of the CCN activity of atomized aqueous filter extracts provides insight into the hygroscopicity of the bulk material in the aerosol. By comparing this hygroscopicity to that of the chamber aerosol, we can deduce changes related to surface processes and nonequilibrium phenomena occurring in the chamber. We find that the

filter extracts show similar CCN activity to that of pure $(\text{NH}_4)_2\text{SO}_4$, but much less than that of particles exposed to methylglyoxal in the aerosol chamber for 3-5 h (Figure 4.8).

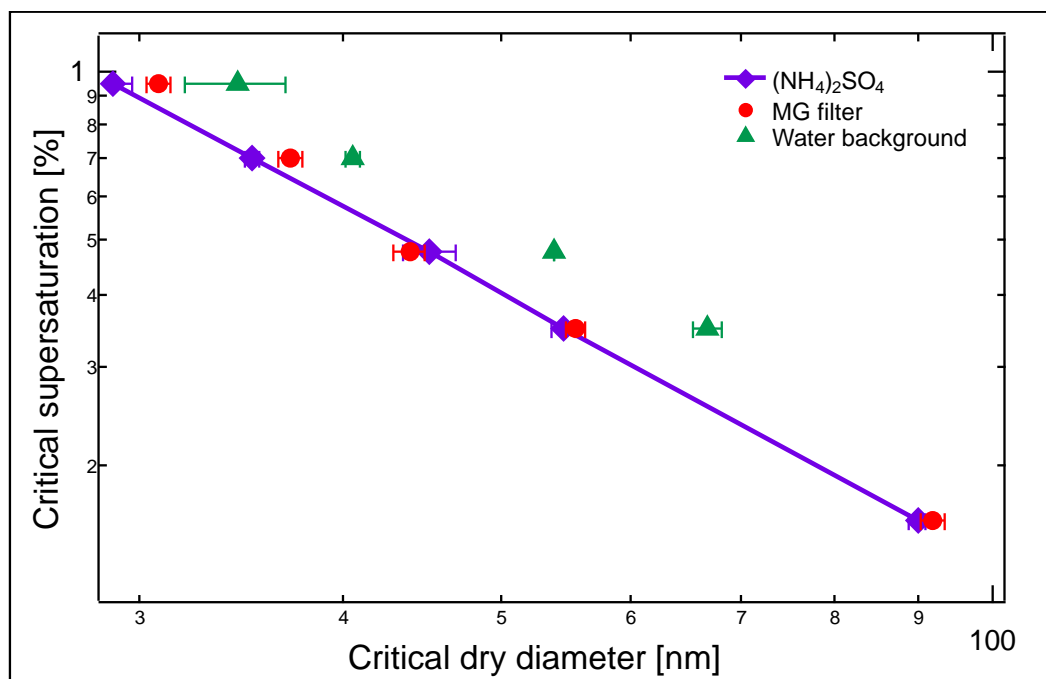


Figure 4.8. CFSTGC data of the extracted filter samples obtained by pumping down the chamber for ~14 h following the 5 h run. The dry diameters are compared to the $(\text{NH}_4)_2\text{SO}_4$ control.

Similar results were observed for aerosols formed by atomizing bulk aqueous solutions of 3.1 M $(\text{NH}_4)_2\text{SO}_4$ and 0.5 M methylglyoxal 24 h after mixing (previously shown to exhibit significant surface tension depression) (Sareen et al., 2010). Aerosols formed from atomized solutions of 0.5 M methylglyoxal and/or 0.5 M acetaldehyde and Millipore water exhibit decreased CCN activity compared to pure $(\text{NH}_4)_2\text{SO}_4$, typical of pure organic aerosols ($\kappa=0.12\pm 0.04$) and drastically different from the observed chamber aerosol hygroscopicity (Figure 4.9). In the chamber experiments, the estimated concentration of methylglyoxal in the particles at the moment of activation (using

Henry's Law) ranged from 1.17×10^{-5} – 3.22×10^{-5} M and for the filter extracts it was 1.24×10^{-4} – 4.53×10^{-5} M, orders of magnitude lower than for the atomized bulk solutions (1.59×10^{-2} – 2.86×10^{-3} M). This supports the notion that surface adsorption of methylglyoxal (not present in the atomized solution experiments) is key to the CCN enhancement seen in the particles sampled directly from the chamber, as the hygroscopicity of aerosol generated from bulk solutions never exceeds that of the pure salt.

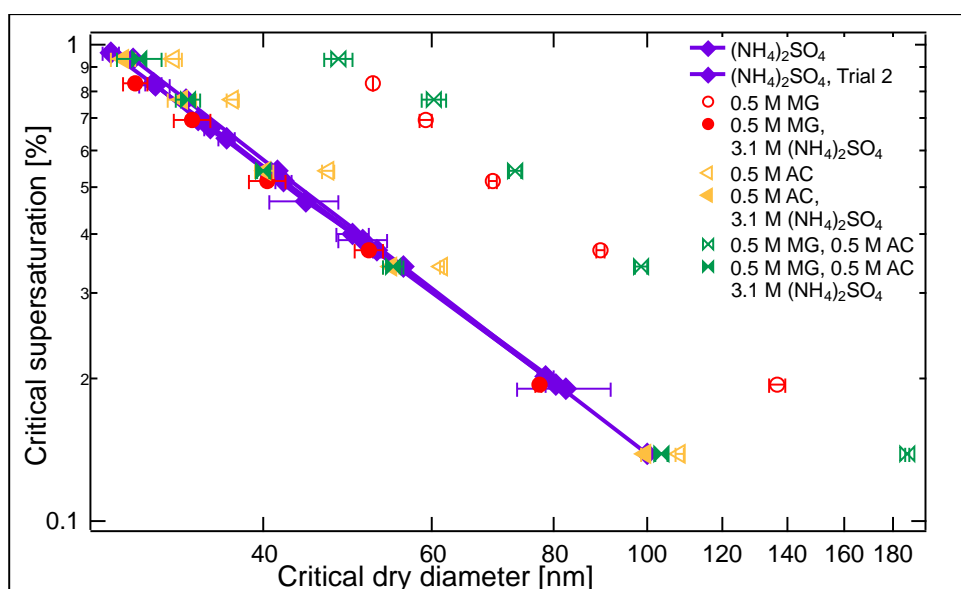


Figure 4.9. CFSTGC data from organics in solution compared to the $(\text{NH}_4)_2\text{SO}_4$ control. The plot includes: $(\text{NH}_4)_2\text{SO}_4$ solution, methylglyoxal solution, methylglyoxal / $(\text{NH}_4)_2\text{SO}_4$ solution, acetaldehyde solution, acetaldehyde / $(\text{NH}_4)_2\text{SO}_4$ solution, methylglyoxal / acetaldehyde solution, and methylglyoxal / acetaldehyde / $(\text{NH}_4)_2\text{SO}_4$ solution.

4.5 Conclusions

Here, we present direct evidence that two ubiquitous atmospheric trace gases, methylglyoxal and acetaldehyde, can also be significant sources of aerosol surfactants, through reactive uptake and potential formation of surface-active oligomers (Sareen et al., 2010). This effect is demonstrated by conduction chamber experiments to study how the uptake of two VOCs in the atmosphere, methylglyoxal and acetaldehyde, on $(\text{NH}_4)_2\text{SO}_4$ seed aerosols can affect their CCN activity. Significant enhancements in CCN activity, up to 15% reduction in critical dry diameter for activation, are observed over a timescale of hours, without any detectable limitation in activation kinetics. This reduction in critical diameter enhances the apparent particle hygroscopicity up to 65%, which can lead to a significant increase in cloud droplet number concentrations by up to 20%. At 250 ppb, both organics individually enhanced CCN activity. At more atmospherically relevant concentrations of 8 ppb, acetaldehyde depressed the critical activation diameters, whereas no change was seen with methylglyoxal. A mixture of the two organics at lower concentrations also showed enhancement in CCN activity. This is the first experimental study where such an effect has been demonstrated and it is likely that a similar effect may also be observed in ambient aerosols in the presence of a mixture of surface-active VOCs. Gas-phase surfactants may be an important and overlooked source of enhanced CCN activity in the atmosphere.

CHAPTER 5. Conclusions and Future Directions

The primary goal of this research has been to assess the role of methylglyoxal as a potential SOA precursor and its impacts on aerosol relevant physical and chemical properties, particularly optical properties and CCN activity. We have observed that the uptake of methylglyoxal on aqueous aerosols is a potentially significant source of light-absorbing SOA that can also enhance the CCN activity of the seed aerosol.

We show that methylglyoxal forms light-absorbing secondary organic material in aqueous ammonium sulfate and ammonium nitrate solutions mimicking tropospheric aerosol particles. The kinetics were characterized using UV-Vis spectrophotometry. The results suggest that the bimolecular reaction of methylglyoxal with an ammonium or hydronium ion is the rate-limiting step for the formation of light-absorbing species, with $k_{NH_4^+}^{II} = 5 \times 10^{-6} \text{ M}^{-1} \text{ min}^{-1}$ and $k_{H_3O^+}^{II} \leq 10^{-3} \text{ M}^{-1} \text{ min}^{-1}$. Evidence of aldol condensation products and oligomeric species up to 759 amu was found using chemical ionization mass spectrometry with a volatilization flow tube inlet (Aerosol-CIMS). Tentative identifications of carbon-nitrogen species and a sulfur-containing compound were also made using Aerosol-CIMS. Aqueous solutions of methylglyoxal, with and without inorganic salts, exhibit significant surface tension depression. These observations add to the growing body of evidence that dicarbonyl compounds may form secondary organic material in the aerosol aqueous phase, and that SOA formation via heterogeneous processes may affect seed aerosol properties.

As mentioned above, the aqueous-phase reaction products of methylglyoxal when NH_4^+ is present include species featuring unsaturated C=C bonds such as aldol condensation products and imidazoles which are likely to be vulnerable to oxidation by O_3 and OH in the atmosphere. In chapter 3, we summarized the results of kinetic studies of the O_3 and OH oxidation of methylglyoxal SOA products. Experiments were performed using aerosol flow tube reactors coupled with an Aerosol-CIMS for monitoring oxidation products. Particles were also collected on quartz windows to compare their UV-Visible absorption before and after oxidation. The oxidation of these particles leads to an increase in absorption and the formation of smaller, more volatile organic acids. In the presence of O_3 , methylglyoxal SOA can last for up to ~17 hrs in the atmosphere. With OH, which is highly reactive, the lifetime of these SOA is on the order of a few minutes.

We had observed that bulk solution studies of methylglyoxal and $(\text{NH}_4)_2\text{SO}_4$ depress surface tension of the solution, which has important implications for the CCN activity of aerosols. The effect of methylglyoxal and acetaldehyde on the CCN activity of $(\text{NH}_4)_2\text{SO}_4$ seed aerosols was studied inside our 3.5 m^3 aerosol chamber coupled to a CFSTGC to quantify the ability of a particle containing methylglyoxal to form a cloud. Significant enhancements in CCN activity, up to 15% reduction in critical dry diameter for activation, are observed over a timescale of hours, without any detectable limitation in activation kinetics. This reduction in critical diameter enhances the apparent particle hygroscopicity up to 65%, which can lead to a significant increase in cloud droplet number concentrations by up to 20%. This finding sheds importance on the role of gas-phase surfactants in the enhancement of CCN activity in the atmosphere, which has been

previously overlooked and hence not represented accurately in aerosol chemistry and climate models.

It is clear that the presence of methylglyoxal in the atmosphere has important implications for aerosol heterogeneous chemistry and the physical properties of particles. In our studies we have shown that glyoxal and mixtures of glyoxal and methylglyoxal are significant sources of light-absorbing SOA in the atmosphere. (Schwier et al., 2010; Shapiro et al., 2009) The atmosphere is a mixture of numerous trace gases, and in the future, additional experiments should be performed to study the various properties of aerosol mixtures at atmospherically relevant concentrations, in both the aerosol chamber and flow tube reactor. Chamber experiments with the CFSTGC should be conducted with a mixture of gases such as methylglyoxal, glyoxal, acetaldehyde, and formaldehyde amongst others. The Aerosol-CIMS should also be coupled with the chamber along with the CFSTGC to attain real-time composition data while monitoring the CCN activity of the aerosols. This will help us to gain an insight into the chemical mechanisms that may be causing a change in the CCN activity of the aerosols. Ambient air, which is most representative of our atmosphere may also be filtered to remove particles. This gas-phase stream can then be exposed to aerosols in the chamber, to attain a more realistic perspective of the processes that could be happening in the atmosphere.

The flow tube reactor experiments we have performed thus far have been at a constant relative humidity of 65%. Future experiments can be aimed at trying to study the effect of relative humidity on oxidation by O_3 and OH and consequently how it alters the light-absorption of the aged particles. In gas-particle partitioning models, SOAs are usually assumed to be liquid. Recently, this traditional view has been challenged by

observations of SOA adopting an amorphous solid state. (Virtanen et al., 2010) Relative humidity can play an important role in the physical state of the particle. Hence, conducting experiments at lower, dryer conditions and much higher, saturation conditions will be essential to gaining further insight into the chemistry of these aerosols.

In our bulk studies, we have observed that SOA formed from methylglyoxal as a precursor are light-absorbing. Relative to chamber experiments, bulk studies are easier to conduct and they provide insight into which processes and conditions may be important for the atmosphere. SOAs generated in the chamber (as done previously in chapter 4) through the interactions of trace organic gases and inorganic seed aerosol will provide us with a more realistic view of the atmosphere. Hence, SOAs can be generated in the chamber, particularly with glyoxal, and then exposed to oxidants like O_3 and OH at high and low NO_x regimes in the flow tube reactor. At the outlet, we obviously use the Aerosol-CIMS to measure composition. In addition, we can collect particles on filters to determine their UV-Vis absorption and additional composition information through Fourier Transform Infrared Spectroscopy (FTIR). The effect of oxidation on the CCN activity of these chamber-generated aerosols can also be determined by using the CFSTGC at the outlet of the flow tube reactor. Knowing the composition, optical properties, and CCN activity of these SOAs generated in the chamber, provides us with a more atmospherically relevant scenario which can then be easier to extrapolate and use in atmospheric chemistry and climate models and help reduce the uncertainties associated with aerosols.

References

Abbatt, J. P. D., Broekhuizen, K., and Kumal, P. P.: Cloud condensation nucleus activity of internally mixed ammonium sulfate/organic acid aerosol particles, *Atmos Environ*, 39, 4767-4778, Doi 10.1016/J.Atmosenv.2005.04.029, 2005.

Adamson, A. W., and Gast, A. P.: *Physical chemistry of surfaces*, xxi, 777 p, Wiley, New York, 1997.

Aiken, A. C., DeCarlo, P. F., Kroll, J. H., Worsnop, D. R., Huffman, J. A., Docherty, K. S., Ulbrich, I. M., Mohr, C., Kimmel, J. R., Sueper, D., Sun, Y., Zhang, Q., Trimborn, A., Northway, M., Ziemann, P. J., Canagaratna, M. R., Onasch, T. B., Alfarra, M. R., Prevot, A. S. H., Dommen, J., Duplissy, J., Metzger, A., Baltensperger, U., and Jimenez, J. L.: O/C and OM/OC ratios of primary, secondary, and ambient organic aerosols with high-resolution time-of-flight aerosol mass spectrometry, *Environ Sci Technol*, 42, 4478-4485, 2008.

Alexander, D. T. L., Crozier, P. A., and Anderson, J. R.: Brown carbon spheres in East Asian outflow and their optical properties, *Science*, 321, 833-836, 2008.

Altieri, K. E., Seitzinger, S. P., Carlton, A. G., Turpin, B. J., Klein, G. C., and Marshall, A. G.: Oligomers formed through in-cloud methylglyoxal reactions: Chemical composition, properties, and mechanisms investigated by ultra-high resolution FT-ICR mass spectrometry, *Atmos Environ*, 42, 1476-1490, 2008.

Anastasiadis, S. H., Chen, J. K., Koberstein, J. T., Siegel, A. F., Sohn, J. E., and Emerson, J. A.: The determination of interfacial-tension by video image-processing of pendant fluid drops, *Journal of Colloid and Interface Science*, 119, 55-66, 1987.

Andreae, M. O., and Gelencsér, A.: Black carbon or brown carbon? The nature of light-absorbing carbonaceous aerosols, *Atmos. Chem. Phys.*, 6, 3131-3148, 10.5194/acp-6-3131-2006, 2006.

Anttila, T., Kiendler-Scharr, A., Tillman, R., and Mentel, T. F.: On the reactive uptake of gaseous compounds by organic-coated aqueous aerosols: Theoretical analysis and application to the heterogeneous hydrolysis of N_2O_5 , *J. Phys. Chem. A.*, 110, 10435-10443, 2006.

Anttila, T., Kiendler-Scharr, A., Mentel, T. F., and Tillmann, R.: Size dependent partitioning of organic material: Evidence for the formation of organic coatings on aqueous aerosols, *J Atmos Chem*, 57, 215-237, Doi 10.1007/S10874-007-9067-9, 2007.

Archer, R. J., and La Mer, V. K.: The rate of evaporation of water through fatty acid monolayers, *Journal of Physical Chemistry*, 59, 200-208, 1955.

Asa-Awuku, A., Sullivan, A. P., Hennigan, C. J., Weber, R. J., and Nenes, A.: Investigation of molar volume and surfactant characteristics of water-soluble organic compounds in biomass burning aerosol, *Atmos Chem Phys*, 8, 799-812, 2008.

Asa-Awuku, A., Engelhart, G. J., Lee, B. H., Pandis, S. N., and Nenes, A.: Relating CCN activity, volatility, and droplet growth kinetics of β -caryophyllene secondary organic aerosol, *Atmos. Chem. Phys.*, 9 795-812, 2009.

Asa-Awuku, A., Nenes, A., Gao, S., Flagan, R. C., and Seinfeld, J. H.: Water-soluble SOA from alkene ozonolysis: Composition and droplet activation kinetics inferences from analysis of CCN activity, *Atmos. Chem. Phys.*, 10, 1585-1597, 2010.

Attygalle, A. B., Garcia-Rubio, S., Ta, J., and Meinwald, J.: Collisionally-induced dissociation mass spectra of organic sulfate anions, *Journal of the Chemical Society-Perkin Transactions 2*, 498-506, 2001.

Baker, J., Arey, J., and Atkinson, R.: Formation and reaction of hydroxycarbonyls from the reaction of OH radicals with 1,3-butadiene and isoprene, *Environ Sci Technol*, 39, 4091-4099, Doi 10.1021/Es047930t, 2005.

Bank, S., and Castillo, R.: Analysis of organic-matter from cloud particles, *Geophys Res Lett*, 14, 210-212, 1987.

Barahona, D., West, R. E. L., Stier, P., Romakkaniemi, S., Kokkola, H., and Nenes, A.: Comprehensively accounting for the effect of giant CCN in cloud activation parameterizations, *Atmos. Chem. Phys.*, 10, 2467-2473, 10.5194/acp-10-2467-2010, 2010.

Barker, J. R.: *Progress and problems in atmospheric chemistry*, 1995.

Barsanti, K. C., and Pankow, J. F.: Thermodynamics of the formation of atmospheric organic particulate matter by accretion reactions - 2. Dialdehydes, methylglyoxal, and diketones, *Atmos Environ*, 39, 6597-6607, 2005.

Bayliss, N. S., and McRae, E. G.: Solvent effects in the spectra of acetone, crotonaldehyde, nitromethane and nitrobenzene, *The Journal of Physical Chemistry*, 58, 1006-1011, 10.1021/j150521a018, 1954.

Bertram, A. K., Ivanov, A. V., Hunter, M., Molina, L. T., and Molina, M. J.: The reaction probability of OH on organic surfaces of tropospheric interest, *The Journal of Physical Chemistry A*, 105, 9415-9421, 10.1021/jp0114034, 2001.

Betterton, E. A., and Hoffmann, M. R.: Henry's law constants of some environmentally important aldehydes, *Environmental Science & Technology*, 22, 1415-1418, 10.1021/es00177a004, 1988a.

Betterton, E. A., and Hoffmann, M. R.: Henry law constants of some environmentally important aldehydes, *Environ Sci Technol*, 22, 1415-1418, 1988b.

Bilde, M., and Svenningsson, B.: CCN activation of slightly soluble organics: The importance of small amounts of inorganic salt and particle phase, *Tellus B*, 56, 128-134, 10.1111/j.1600-0889.2004.00090.x, 2004.

Blake, R. S., Monks, P. S., and Ellis, A. M.: Proton-transfer reaction mass spectrometry, *Chem.Rev.*, 109 861-896, 2009.

Bogan, M. J., Patton, E., Srivastava, A., Martin, S., Fergenson, D. P., Steele, P. T., Tobias, H. J., Gard, E. E., and Frank, M.: Online aerosol mass spectrometry of single

micrometer-sized particles containing poly(ethylene glycol), *Rapid Communications in Mass Spectrometry*, 21, 1214-1220, 10.1002/rcm.2953, 2007.

Bones, D. L., Henricksen, D. K., Mang, S. A., Gonsior, M., Bateman, A. P., Nguyen, T. B., Cooper, W. J., and Nizkorodov, S. A.: Appearance of strong absorbers and fluorophores in limonene-O₃ secondary organic aerosol due to NH₄⁺-mediated chemical aging over long time scales, *J. Geophys. Res.*, 115, D05203, 10.1029/2009jd012864, 2010.

Brown, S. S., Ryerson, T. B., Wollny, A. G., Brock, C. A., Peltier, R., Sullivan, A. P., Weber, R. J., Dube, W. P., Trainer, M., Meagher, J. F., Fehsenfeld, F. C., and Ravishankara, A. R.: Variability in nocturnal nitrogen oxide processing and its role in regional air quality, *Science*, 311, 67-70, Doi 10.1126/Science.1120120, 2006.

Canny, J.: A computational approach to edge detection, *IEEE Trans. Pattern Analysis and Machine Intelligence*, 8, 679-714, 1986.

Carlton, A. G., Turpin, B. J., Lim, H. J., Altieri, K. E., and Seitzinger, S.: Link between isoprene and secondary organic aerosol (SOA): Pyruvic acid oxidation yields low volatility organic acids in clouds, *Geophys Res Lett*, 33, Artn L06822
Doi 10.1029/2005gl025374, 2006.

Carlton, A. G., Turpin, B. J., Altieri, K. E., Seitzinger, S. P., Mathur, R., Roselle, S. J., and Weber, R. J.: CMAQ model performance enhanced when in-cloud secondary organic aerosol is included: Comparisons of organic carbon predictions with measurements, *Environ Sci Technol*, 42, 8798-8802, 2008.

Casale, M. T., Richman, A. R., Elrod, M. J., Garland, R. M., Beaver, M. R., and Tolbert, M. A.: Kinetics of acid-catalyzed aldol condensation reactions of aliphatic aldehydes, *Atmos Environ*, 41, 6212-6224, 2007.

Chuang, P. Y., Charlson, R. J., and Seinfeld, J. H.: Kinetic limitations on droplet formation in clouds, *Nature*, 390, 594-596, 1997.

Corrigan, C. E., and Novakov, T.: Cloud condensation nucleus activity of organic compounds: A laboratory study, *Atmos Environ*, 33, 2661-2668, 10.1016/s1352-2310(98)00310-0, 1999.

Cruz, C. N., and Pandis, S. N.: A study of the ability of pure secondary organic aerosol to act as cloud condensation nuclei, *Atmos Environ*, 31, 2205-2214, 10.1016/s1352-2310(97)00054-x, 1997.

Cruz, C. N., and Pandis, S. N.: The effect of organic coatings on the cloud condensation nuclei activation of inorganic atmospheric aerosol, *J. Geophys. Res.*, 103, 13111-13123, 10.1029/98jd00979, 1998.

Cruz, C. N., and Pandis, S. N.: Deliquescence and hygroscopic growth of mixed inorganic-organic atmospheric aerosol, *Environmental Science & Technology*, 34, 4313-4319, 10.1021/es9907109, 2000.

De Haan, D. O., Corrigan, A. L., Smith, K. W., Stroik, D. R., Turley, J. J., Lee, F. E., Tolbert, M. A., Jimenez, J. L., Cordova, K. E., and Ferrell, G. R.: Secondary organic aerosol-forming reactions of glyoxal with amino acids, *Environ Sci Technol*, 43, 2818-2824, 2009a.

De Haan, D. O., Tolbert, M. A., and Jimenez, J. L.: Atmospheric condensed-phase reactions of glyoxal with methylamine, *Geophys Res Lett*, 36, doi:10.1029/2009GL037441, 2009b.

Denkenberger, K. A., Moffet, R. C., Holecek, J. C., Rebotier, T. P., and Prather, K. A.: Real-time, single-particle measurements of oligomers in aged ambient aerosol particles, *Environ Sci Technol*, 41, 5439-5446, 2007.

Dinar, E., Riziq, A. A., Spindler, C., Erlick, C., Kiss, G., and Rudich, Y.: The complex refractive index of atmospheric and model humic-like substances (HULIS) retrieved by a cavity ring down aerosol spectrometer (CRD-AS), *Faraday Discussions*, 137, 279-295, 2008.

Djikaev, Y. S., and Tabazadeh, A.: Effect of adsorption on the uptake of organic trace gas by cloud droplets, *J. Geophys. Res.*, 108, 4689, 10.1029/2003jd003741, 2003.

Donaldson, D. J., and Vaida, V.: The influence of organic films at the air-aqueous boundary on atmospheric processes, *Chemical Reviews*, 106, 1445-1461, 10.1021/cr040367c, 2006.

Duplissy, J., Gysel, M., Alfarra, M. R., Dommen, J., Metzger, A., Prevot, A. S. H., Weingartner, E., Laaksonen, A., Raatikainen, T., Good, N., Turner, S. F., McFiggans, G., and Baltensperger, U.: Cloud forming potential of secondary organic aerosol under near atmospheric conditions, *Geophys.Res.Lett.*, 35, L03818, 2008.

Ekström, S., Nozière, B., and Hansson, H. C.: The cloud condensation nuclei (CCN) properties of 2-methyltetrols and C3-C6 polyols from osmolality and surface tension measurements, *Atmos. Chem. Phys.*, 9, 973-980, 10.5194/acp-9-973-2009, 2009.

El Haddad, I., Yao, L., Nieto-Gligorovski, L., Michaud, V., Temime-Roussel, B., Quivet, E., Marchand, N., Sellegri, K., and Monod, A.: In-cloud processes of methacrolein under simulated conditions - Part 2: Formation of secondary organic aerosol, *Atmos. Chem. Phys.*, 9, 5107-5117, 10.5194/acp-9-5107-2009, 2009.

Enders, C., and Sigurdsson, S.: The chemistry of humic acid formation under physiological conditions, v. Announcement: The introductory phase of the humic acid formation. A aldol condensation from methylglyoxal, *Berichte der Deutschen Chemischen Gesellschaft*, 76, 562-565, 1943.

Engelhart, G. J., Asa-Awuku, A., Nenes, A., and Pandis, S. N.: CCN activity and droplet growth kinetics of fresh and aged monoterpene secondary organic aerosol, *Atmos Chem Phys*, 8, 3937-3949, 2008a.

Engelhart, G. J., Asa-Awuku, A., Nenes, A., and Pandis, S. N.: CCN activity and droplet growth kinetics of fresh and aged monoterpene secondary organic aerosol, *Atmos.Chem.Phys.*, 8 3937-3949, 2008b.

Engelhart, G. J., Moore, R. H., Nenes, A., and Pandis, S. N.: Cloud condensation nuclei activity of isoprene secondary organic aerosol, *J. Geophys. Res.*, 116, D02207, 10.1029/2010jd014706, 2011.

Ervens, B., and Volkamer, R.: Glyoxal processing by aerosol multiphase chemistry: Towards a kinetic modeling framework of secondary organic aerosol formation in aqueous particles, *Atmos.Chem.Phys.*, 10, 8219-8244, 2010.

Ervens, B., Turpin, B. J., and Weber, R. J.: Secondary organic aerosol formation in cloud droplets and aqueous particles (aqSOA): A review of laboratory, field and model studies, *Atmos. Chem. Phys.*, 11, 11069-11102, 10.5194/acp-11-11069-2011, 2011.

Facchini, M. C., Mircea, M., Fuzzi, S., and Charlson, R. J.: Cloud albedo enhancement by surface-active organic solutes in growing droplets, *Nature*, 401, 257-259, 1999.

Feingold, G., and Chuang, P. Y.: Analysis of the influence of film-forming compounds on droplet growth: Implications for cloud microphysical processes and climate, *J Atmos Sci*, 59, 2006-2018, 10.1175/1520-0469(2002)059<2006:aotiof>2.0.co;2, 2002.

Folkers, M., Mentel, T. F., and Wahner, A.: Influence of an organic coating on the reactivity of aqueous aerosols probed by the heterogeneous hydrolysis of N_2O_5 , *Geophys Res Lett*, 30, Artn 1644 Doi 10.1029/2003gl017168, 2003.

Fountoukis, C., and Nenes, A.: Continued development of a cloud droplet formation parameterization for global climate models, *J. Geophys. Res.*, 110, D11212, 10.1029/2004jd005591, 2005.

Fountoukis, C., Nenes, A., Meskhidze, N., Bahreini, R., Conant, W. C., Jonsson, H., Murphy, S., Sorooshian, A., Varutbangkul, V., Brechtel, F., Flagan, R. C., and Seinfeld, J. H.: Aerosol-cloud drop concentration closure for clouds sampled during the International Consortium for Atmospheric Research on Transport and Transformation 2004 campaign, *J. Geophys. Res.*, 112, D10S30, 10.1029/2006jd007272, 2007.

Fu, T. M., Jacob, D. J., Wittrock, F., Burrows, J. P., Vrekoussis, M., and Henze, D. K.: Global budgets of atmospheric glyoxal and methylglyoxal, and implications for formation of secondary organic aerosols, *J. Geophys. Res.*, 113, D15303, 2008.

Fu, T. M., Jacob, D. J., and Heald, C. L.: Aqueous-phase reactive uptake of dicarbonyls as a source of organic aerosol over eastern North America, *Atmos Environ*, 43, 1814-1822, 2009.

Fuzzi, S., Andreae, M. O., Huebert, B. J., Kulmala, M., Bond, T. C., Boy, M., Doherty, S. J., Guenther, A., Kanakidou, M., Kawamura, K., Kerminen, V. M., Lohmann, U., Russell, L. M., and Poschl, U.: Critical assessment of the current state of scientific knowledge, terminology, and research needs concerning the role of organic aerosols in the atmosphere, climate, and global change, *Atmos Chem Phys*, 6, 2017-2038, 2006.

Galloway, M. M., Chhabra, P. S., Chan, A. W. H., Surratt, J. D., Flagan, R. C., Seinfeld, J. H., and Keutsch, F. N.: Glyoxal uptake on ammonium sulphate seed aerosol: Reaction products and reversibility of uptake under dark and irradiated conditions, *Atmos.Chem.Phys.*, 9, 3331-3345, 2009.

Gao, S., Surratt, J. D., Knipping, E. M., Edgerton, E. S., Shahgholi, M., and Seinfeld, J. H.: Characterization of polar organic components in fine aerosols in the southeastern United States: Identity, origin, and evolution, *J. Geophys. Res.*, 111, D14314, 10.1029/2005jd006601, 2006.

Garland, R. M., Wise, M. E., Beaver, M. R., Dewitt, H. L., Aiken, A. C., Jimenez, J. L., and Tolbert, M. A.: Impact of palmitic acid coating on the water uptake and loss of ammonium sulfate particles, *Atmos Chem Phys*, 5, 1951-1961, 2005.

George, I. J., Vlasenko, A., Slowik, J. G., Broekhuizen, K., and Abbatt, J. P. D.: Heterogeneous oxidation of saturated organic aerosols by hydroxyl radicals: Uptake kinetics, condensed-phase products, and particle size change, *Atmos. Chem. Phys.*, 7, 4187-4201, 10.5194/acp-7-4187-2007, 2007.

Ghan, S.: Droplet nucleation: Physically-based parameterizations and comparative evaluation, *Journal of Advances in Modeling Earth Systems*, 3, 33 pp., 10.1029/2011ms000074, 2011.

Gilardoni, S., Liu, S., Takahama, S., Russell, L. M., Allan, J. D., Steinbrecher, R., Jimenez, J. L., De Carlo, P. F., Dunlea, E. J., and Baumgardner, D.: Characterization of organic ambient aerosol during MIRAGE 2006 on three platforms, *Atmos. Chem. Phys.*, 9, 5417-5432, 10.5194/acp-9-5417-2009, 2009.

Gómez-González, Y., Surratt, J. D., Cuyckens, F., Szmigielski, R., Vermeylen, R., Jaoui, M., Lewandowski, M., Offenberg, J. H., Kleindienst, T. E., Edney, E. O., Blockhuys, F., Van Alsenoy, C., Maenhaut, W., and Claeys, M.: Characterization of organosulfates from the photooxidation of isoprene and unsaturated fatty acids in ambient aerosol using liquid chromatography/(-) electrospray ionization mass spectrometry, *Journal of Mass Spectrometry*, 43, 371-382, 2008.

Grosjean, D., Grosjean, E., and Williams, E. L.: Atmospheric chemistry of unsaturated alcohols, *Environ Sci Technol*, 27, 2478-2485, 1993.

Grosjean, D., Grosjean, E., and Moreira, L. F. R.: Speciated ambient carbonyls in Rio de Janeiro, Brazil, *Environ Sci Technol*, 36, 1389-1395, 10.1021/es0111232, 2002.

Grosjean, E., Grosjean, D., Fraser, M. P., and Cass, G. R.: Air quality model evaluation data for organics. 2. C1 - C14 carbonyls in Los Angeles air, *Environmental Science & Technology*, 30, 2687-2703, 10.1021/es950758w, 1996.

Havers, N., Burba, P., Lambert, J., and Klockow, D.: Spectroscopic characterization of humic-like substances in airborne particulate matter, *J Atmos Chem*, 29, 45-54, 1998.

Heald, C. L., Jacob, D. J., Park, R. J., Russell, L. M., Huebert, B. J., Seinfeld, J. H., Liao, H., and Weber, R. J.: A large organic aerosol source in the free troposphere missing from current models, *Geophys Res Lett*, 32, Artn L18809 Doi 10.1029/2005gl023831, 2005.

Hearn, J. D., and Smith, G. D.: A chemical ionization mass spectrometry method for the online analysis of organic aerosols, *Analytical Chemistry*, 76, 2820-2826, 10.1021/ac049948s, 2004a.

Hearn, J. D., and Smith, G. D.: Kinetics and product studies for ozonolysis reactions of organic particles using aerosol CIMS, *J Phys Chem A*, 108, 10019-10029, Doi 10.1021/Jp0404145, 2004b.

Hearn, J. D., Lovett, A. J., and Smith, G. D.: Ozonolysis of oleic acid particles: Evidence for a surface reaction and secondary reactions involving Criegee intermediates, *Phys Chem Chem Phys*, 7, 501-511, Doi 10.1039/B414472d, 2005.

Hearn, J. D., and Smith, G. D.: Measuring rates of reaction in supercooled organic particles with implications for atmospheric aerosol, *Phys Chem Chem Phys*, 7, 2549-2551, 2005.

Hearn, J. D., and Smith, G. D.: Reactions and mass spectra of complex particles using aerosol CIMS, *International Journal of Mass Spectrometry*, 258, 95-103, 10.1016/j.ijms.2006.05.017, 2006a.

Hearn, J. D., and Smith, G. D.: A mixed-phase relative rates technique for measuring aerosol reaction kinetics, *Geophys. Res. Lett.*, 33, L17805, 10.1029/2006gl026963, 2006b.

Hearn, J. D., Renbaum, L. H., Wang, X., and Smith, G. D.: Kinetics and products from reaction of Cl radicals with dioctyl sebacate (DOS) particles in O₂: A model for radical-initiated oxidation of organic aerosols, *Phys Chem Chem Phys*, 9, 2007.

Hearn, J. D., and Smith, G. D.: Ozonolysis of mixed oleic acid/*n*-docosane particles: The roles of phase, morphology, and metastable states, *The Journal of Physical Chemistry A*, 111, 11059-11065, 10.1021/jp0755701, 2007.

Henning, S., Rosenørn, T., D'Anna, B., Gola, A. A., Svenningsson, B., and Bilde, M.: Cloud droplet activation and surface tension of mixtures of slightly soluble organics and inorganic salt, *Atmos. Chem. Phys.*, 5, 575-582, 10.5194/acp-5-575-2005, 2005.

Ho, K. F., Cao, J. J., Lee, S. C., Kawamura, K., Zhang, R. J., Chow, J. C., and Watson, J. G.: Dicarboxylic acids, ketocarboxylic acids, and dicarbonyls in the urban atmosphere of China, *J. Geophys. Res.*, 112, D22S27, 10.1029/2006jd008011, 2007.

Huff Hartz, K. E., Rosenorn, T., Ferchak, S. R., Raymond, T. M., Bilde, M., Donahue, N. M., and Pandis, S. N.: Cloud condensation nuclei activation of monoterpene and sesquiterpene secondary organic aerosol, *J. Geophys. Res.*, 110, D14208, 2005.

Hughes, L. S., Cass, G. R., Gone, J., Ames, M., and Olmez, I.: Physical and chemical characterization of atmospheric ultrafine particles in the Los Angeles area, *Environmental Science & Technology*, 32, 1153-1161, 10.1021/es970280r, 1998.

Iinuma, Y., Muller, C., Berndt, T., Boge, O., Claeys, M., and Herrmann, H.: Evidence for the existence of organosulfates from beta-pinene ozonolysis in ambient secondary organic aerosol, *Environ Sci Technol*, 41, 6678-6683, 2007.

IPCC: *Ipcc, 2007: Climate change 2007: The physical science basis. Contribution of working group I to the fourth assessment report of the Intergovernmental Panel on Climate Change*, 996, 2007.

Jacob, D. J.: Heterogeneous chemistry and tropospheric ozone, *Atmos Environ*, 34, 2131-2159, 2000.

Jacobson, M. C., Hansson, H. C., Noone, K. J., and Charlson, R. J.: Organic atmospheric aerosols: Review and state of the science, *Rev. Geophys.*, 38, 267-294, 10.1029/1998rg000045, 2000.

Jacobson, M. Z.: Isolating nitrated and aromatic aerosols and nitrated aromatic gases as sources of ultraviolet light absorption, *J Geophys Res-Atmos*, 104, 3527-3542, 1999.

Jacobson, M. Z.: Control of fossil-fuel particulate black carbon and organic matter, possibly the most effective method of slowing global warming, *J Geophys Res-Atmos*, 107, 2002.

Jang, M., Czoschke, N. M., Lee, S., and Kamens, R. M.: Heterogeneous atmospheric aerosol production by acid-catalyzed particle-phase reactions, *Science*, 298, 814-817, 10.1126/science.1075798, 2002.

Jang, M. S., and Kamens, R. M.: Atmospheric secondary aerosol formation by heterogeneous reactions of aldehydes in the presence of a sulfuric acid aerosol catalyst, *Environ Sci Technol*, 35, 4758-4766, Doi 10.1021/Es010790s, 2001.

Jimenez, J. L., Canagaratna, M. R., Donahue, N. M., Prevot, A. S. H., Zhang, Q., Kroll, J. H., DeCarlo, P. F., Allan, J. D., Coe, H., Ng, N. L., Aiken, A. C., Docherty, K. S., Ulbrich, I. M., Grieshop, A. P., Robinson, A. L., Duplissy, J., Smith, J. D., Wilson, K. R., Lanz, V. A., Hueglin, C., Sun, Y. L., Tian, J., Laaksonen, A., Raatikainen, T., Rautiainen, J., Vaattovaara, P., Ehn, M., Kulmala, M., Tomlinson, J. M., Collins, D. R., Cubison, M. J., E, Dunlea, J., Huffman, J. A., Onasch, T. B., Alfarra, M. R., Williams, P. I., Bower, K., Kondo, Y., Schneider, J., Drewnick, F., Borrmann, S., Weimer, S., Demerjian, K., Salcedo, D., Cottrell, L., Griffin, R., Takami, A., Miyoshi, T., Hatakeyama, S., Shimojo, A., Sun, J. Y., Zhang, Y. M., Dzepina, K., Kimmel, J. R., Sueper, D., Jayne, J. T., Herndon, S. C., Trimborn, A. M., Williams, L. R., Wood, E. C., Middlebrook, A. M., Kolb, C. E., Baltensperger, U., and Worsnop, D. R.: Evolution of organic aerosols in the atmosphere, *Science*, 326, 1525-1529, 2009.

Juza, J.: The pendant drop method of surface tension measurement: Equation interpolating the shape factor tables for several selected planes, *Czechoslovak Journal of Physics*, 47, 351-357, 1997.

Kalberer, M., Paulsen, D., Sax, M., Steinbacher, M., Dommen, J., Prevot, A. S. H., Fisseha, R., Weingartner, E., Frankevich, V., Zenobi, R., and Baltensperger, U.: Identification of polymers as major components of atmospheric organic aerosols, *Science*, 303, 1659-1662, 2004.

Kanakidou, M., Seinfeld, J. H., Pandis, S. N., Barnes, I., Dentener, F. J., Facchini, M. C., Van Dingenen, R., Ervens, B., Nenes, A., Nielsen, C. J., Swietlicki, E., Putaud, J. P., Balkanski, Y., Fuzzi, S., Horth, J., Moortgat, G. K., Winterhalter, R., Myhre, C. E. L.,

Tsigaridis, K., Vignati, E., Stephanou, E. G., and Wilson, J.: Organic aerosol and global climate modelling: A review, *Atmos. Chem. Phys.*, 5, 1053-1123, 10.5194/acp-5-1053-2005, 2005.

Kawamura, K., Kasukabe, H., and Barrie, L. A.: Source and reaction pathways of dicarboxylic acids, ketoacids and dicarbonyls in arctic aerosols: One year of observations, *Atmos Environ*, 30, 1709-1722, 10.1016/1352-2310(95)00395-9, 1996.

Kawamura, K., and Yasui, O.: Diurnal changes in the distribution of dicarboxylic acids, ketocarboxylic acids and dicarbonyls in the urban Tokyo atmosphere, *Atmos Environ*, 39, 1945-1960, 10.1016/j.atmosenv.2004.12.014, 2005.

Keene, W. C., Pszenny, A. A. P., Maben, J. R., Stevenson, E., and Wall, A.: Closure evaluation of size-resolved aerosol pH in the New England coastal atmosphere during summer, *J Geophys Res-Atmos*, 109, D23202-doi:23210.21029/22004JD004801, 2004.

Kent, G. S., Yue, G. K., Farrukh, U. O., and Deepak, A.: Modeling atmospheric aerosol backscatter at CO₂ laser wavelengths. 1: Aerosol properties, modeling techniques, and associated problems, *Appl. Opt.*, 22, 1655-1665, 1983.

Kesselmeier, J., Kuhn, U., Rottenberger, S., Biesenthal, T., Wolf, A., Schebeske, G., Andreae, M. O., Ciccioli, P., Brancaleoni, E., Frattoni, M., Oliva, S. T., Botelho, M. L., Silva, C. M. A., and Tavares, T. M.: Concentrations and species composition of atmospheric volatile organic compounds (VOCs) as observed during the wet and dry season in Rondônia (Amazonia), *J. Geophys. Res.*, 107, 8053, 10.1029/2000jd000267, 2002.

King, S. M., Rosenoern, T., Shilling, J. E., Chen, Q., and Martin, S. T.: Cloud condensation nucleus activity of secondary organic aerosol particles mixed with sulfate, *Geophys.Res.Lett.*, 34, L24806, 2007.

King, S. M., Rosenoern, T., Shilling, J. E., Chen, Q., and Martin, S. T.: Increased cloud activation potential of secondary organic aerosol for atmospheric mass loadings, *Atmos.Chem.Phys.*, 9, 2959-2971, 2009.

Kirchstetter, T. W., Novakov, T., and Hobbs, P. V.: Evidence that the spectral dependence of light absorption by aerosols is affected by organic carbon, *J Geophys Res-Atmos*, 109, 2004.

Kiss, G., Tombacz, E., and Hansson, H. C.: Surface tension effects of humic-like substances in the aqueous extract of tropospheric fine aerosol, *J Atmos Chem*, 50, 279-294, 2005.

Köhler, H.: The nucleus in and the growth of hygroscopic droplets, *Transactions of the Faraday Society*, 32, 1936.

Krizner, H. E., De Haan, D. O., and Kua, J.: Thermodynamics and kinetics of methylglyoxal dimer formation: A computational study, *The Journal of Physical Chemistry A*, 113, 6994-7001, 10.1021/jp903213k, 2009.

Kroll, J. H., Ng, N. L., Murphy, S. M., Varutbangkul, V., Flagan, R. C., and Seinfeld, J. H.: Chamber studies of secondary organic aerosol growth by reactive uptake of simple carbonyl compounds, *J. Geophys. Res.*, 110, D23207, 2005.

Kundu, S., Kawamura, K., Andreae, T. W., Hoffer, A., and Andreae, M. O.: Molecular distributions of dicarboxylic acids, ketocarboxylic acids and α -dicarbonyls in biomass burning aerosols: Implications for photochemical production and degradation in smoke layers, *Atmos. Chem. Phys.*, 10, 2209-2225, 10.5194/acp-10-2209-2010, 2010.

Lajohn, L. A., Christiansen, P. A., Ross, R. B., Atashroo, T., and Ermler, W. C.: Abinitio relativistic effective potentials with spin orbit operators .III. Rb through Xe, *Journal of Chemical Physics*, 87, 2812-2824, 1987.

Lance, S., Medina, J., Smith, J. N., and Nenes, A.: Mapping the operation of the DMT continuous flow CCN counter, *Aerosol Science and Technology*, 40, 242-254, 2006.

Lee, A. K. Y., Herckes, P., Leaitch, W. R., Macdonald, A. M., and Abbatt, J. P. D.: Aqueous OH oxidation of ambient organic aerosol and cloud water organics: Formation of highly oxidized products, *Geophys. Res. Lett.*, 38, L11805, 10.1029/2011gl047439, 2011.

Li, Z., Schwier, A. N., Sareen, N., and McNeill, V. F.: Reactive processing of formaldehyde and acetaldehyde in aqueous aerosol mimics: Surface tension depression and secondary organic products, *Atmos. Chem. Phys.*, 11, 11617-11629, 10.5194/acp-11-11617-2011, 2011.

Li, Z. D., Williams, A. L., and Rood, M. J.: Influence of soluble surfactant properties on the activation of aerosol particles containing inorganic solute, *J Atmos Sci*, 55, 1859-1866, 1998.

Liao, H., and Seinfeld, J. H.: Global impacts of gas-phase chemistry-aerosol interactions on direct radiative forcing by anthropogenic aerosols and ozone, *J Geophys Res-Atmos*, 110, Artn D18208 Doi 10.1029/2005jd005907, 2005.

Liggio, J., Li, S. M., and McLaren, R.: Reactive uptake of glyoxal by particulate matter, *J Geophys Res-Atmos*, 110, D10304-doi:10310.11029/12004JD005113, 2005.

Lim, Y. B., Tan, Y., Perri, M. J., Seitzinger, S. P., and Turpin, B. J.: Aqueous chemistry and its role in secondary organic aerosol (SOA) formation, *Atmos. Chem. Phys.*, 10, 10521-10539, 10.5194/acp-10-10521-2010, 2010.

Lin, M., Walker, J., Geron, C., and Khlystov, A.: Organic nitrogen in PM_{2.5} aerosol at a forest site in the Southeast US, *Atmos. Chem. Phys.*, 10, 2145-2157, 10.5194/acp-10-2145-2010, 2010.

Liu, P. S. K., Leaitch, W. R., Banic, C. M., Li, S. M., Ngo, D., and Megaw, W. J.: Aerosol observations at Chebogue point during the 1993 North Atlantic Regional Experiment: Relationships among cloud condensation nuclei, size distribution, and chemistry, *J. Geophys. Res.*, 101, 28971-28990, 10.1029/96jd00445, 1996.

Loeffler, K. W., Koehler, C. A., Paul, N. M., and De Haan, D. O.: Oligomer formation in evaporating aqueous glyoxal and methyl glyoxal solutions, *Environ Sci Technol*, 40, 6318-6323, 2006.

Lukács, H., Gelencser, A., Hoffer, A., Kiss, G., Horvath, K., and Hartyani, Z.: Quantitative assessment of organosulfates in size-segregated rural fine aerosol, *Atmos.Chem.Phys.*, 9 231-238, 2009.

Lund Myhre, C. E., and Nielsen, C. J.: Optical properties in the UV and visible spectral region of organic acids relevant to tropospheric aerosols, *Atmos. Chem. Phys.*, 4, 1759-1769, 10.5194/acp-4-1759-2004, 2004.

Matijevic, E., and Pethica, B. A.: The properties of ionized monolayers, part 1. Sodium dodecyl sulfate at the air/water interface, *Trans.Faraday Soc.*, 54 1383-1389, 1958.

McMurry, P. H.: A review of atmospheric aerosol measurements, *Atmos Environ*, 34, 1959-1999, 2000.

McNeill, V. F., Patterson, J., Wolfe, G. M., and Thornton, J. A.: The effect of varying levels of surfactant on the reactive uptake of N_2O_5 to aqueous aerosol, *Atmos. Chem. Phys.*, 6, 1635-1644, 10.5194/acp-6-1635-2006, 2006.

McNeill, V. F., Wolfe, G. M., and Thornton, J. A.: The oxidation of oleate in submicron aqueous salt aerosols: Evidence of a surface process, *The Journal of Physical Chemistry A*, 111, 1073-1083, 10.1021/jp066233f, 2007.

McNeill, V. F., Yatavelli, R. L. N., Thornton, J. A., Stipe, C. B., and Landgrebe, O.: Heterogeneous OH oxidation of palmitic acid in single component and internally mixed aerosol particles: Vaporization and the role of particle phase, *Atmos. Chem. Phys.*, 8, 5465-5476, 10.5194/acp-8-5465-2008, 2008.

McNeill, V. F., Sareen, N., and Schwier, A. N.: Surface-active organics in atmospheric aerosols, submitted, 2012.

Meller, R., Raber, W., Crowley, J. N., Jenkin, M. E., and Moortgat, G. K.: The UV-visible absorption spectrum of methylglyoxal, *Journal of Photochemistry and Photobiology A: Chemistry*, 62, 163-171, 10.1016/1010-6030(91)87017-p, 1991.

Meskhidze, N., Nenes, A., Conant, W. C., and Seinfeld, J. H.: Evaluation of a new cloud droplet activation parameterization with in situ data from CRYSTAL-FACE and CSTRIFE, *J. Geophys. Res.*, 110, D16202, 10.1029/2004jd005703, 2005.

Michaud, V., El Haddad, I., Yao, L., Sellegri, K., Laj, P., Villani, P., Picard, D., Marchand, N., and Monod, A.: In-cloud processes of methacrolein under simulated conditions - part 3: Hygroscopic and volatility properties of the formed secondary organic aerosol, *Atmos. Chem. Phys.*, 9, 5119-5130, 10.5194/acp-9-5119-2009, 2009.

Molina, M. J., Ivanov, A. V., Trakhtenberg, S., and Molina, L. T.: Atmospheric evolution of organic aerosol, *Geophys. Res. Lett.*, 31, L22104, 10.1029/2004gl020910, 2004.

Moore, R. H., Ingall, E. D., Sorooshian, A., and Nenes, A.: Molar mass, surface tension, and droplet growth kinetics of marine organics from measurements of CCN activity, *Geophys. Res. Lett.*, 35, L07801, 10.1029/2008gl033350, 2008.

Moore, R. H., Nenes, A., and Medina, J.: Scanning mobility CCN analysis - a method for fast measurements of size-resolved CCN distributions and activation kinetics, *Aerosol Science and Technology*, 44, 861-871, 2010.

Müller, B., and Heal, M. R.: The mass accommodation coefficient of ozone on an aqueous surface, *Physical Chemistry Chemical Physics*, 4, 2002.

Muller, P.: Glossary of terms used in physical organic chemistry (IUPAC recommendations 1994), *Pure Appl. Chem.*, 66, 1077-1184, 1994.

Nemet, I., Vikić-Topić, D., and Varga-Defterdarović, L.: Spectroscopic studies of methylglyoxal in water and dimethylsulfoxide, *Bioorganic Chemistry*, 32, 560-570, 2004.

Nenes, A., and Seinfeld, J. H.: Parameterization of cloud droplet formation in global climate models, *J. Geophys. Res.*, 108, 4415, 2003.

Nozière, B., and Esteve, W.: Organic reactions increasing the absorption index of atmospheric sulfuric acid aerosols, *Geophys. Res. Lett.*, 32, L03812, 10.1029/2004gl021942, 2005.

Nozière, B., Dziedzic, P., and Cordova, A.: Formation of secondary light-absorbing "fulvic-like" oligomers: A common process in aqueous and ionic atmospheric particles?, *Geophys Res Lett*, 34, L21812, 10.1029/2007GL031300, 2007.

Nozière, B., and Esteve, W.: Light-absorbing aldol condensation products in acidic aerosols: Spectra, kinetics, and contribution to the absorption index, *Atmos Environ*, 41, 1150-1163, 2007.

Nozière, B., Dziedzic, P., and Cordova, A.: Common inorganic ions are efficient catalysts for organic reactions in atmospheric aerosols and other natural environments, *Atmos. Chem. Phys. Discuss.*, 9 1-21, 2009a.

Nozière, B., Dziedzic, P., and Cordova, A.: Products and kinetics of the liquid-phase reaction of glyoxal catalyzed by ammonium ions (NH_4^+), *J Phys Chem A*, 113, 231-237, 2009b.

Park, S. C., Burden, D. K., and Nathanson, G. M.: The inhibition of N_2O_5 hydrolysis in sulfuric acid by 1-butanol and 1-hexanol surfactant coatings, *J Phys Chem A*, 111, 2921-2929, 2007.

Paulot, F., Wunch, D., Crouse, J. D., Toon, G. C., Millet, D. B., DeCarlo, P. F., Vigouroux, C., Deutscher, N. M., González Abad, G., Notholt, J., Warneke, T., Hannigan, J. W., Warneke, C., de Gouw, J. A., Dunlea, E. J., De Mazière, M., Griffith, D. W. T., Bernath, P., Jimenez, J. L., and Wennberg, P. O.: Importance of secondary sources in the atmospheric budgets of formic and acetic acids, *Atmos. Chem. Phys.*, 11, 1989-2013, 10.5194/acp-11-1989-2011, 2011.

Paulsen, D., Dommen, J., Kalberer, M., Prevot, A. S. H., Richter, R., Sax, M., Steinbacher, M., Weingartner, E., and Baltensperger, U.: Secondary organic aerosol formation by irradiation of 1,3,5-trimethylbenzene- NO_x - H_2O in a new reaction chamber for atmospheric chemistry and physics, *Environ Sci Technol*, 39, 2668-2678, 2005.

Petters, M. D., and Kreidenweis, S. M.: A single parameter representation of hygroscopic growth and cloud condensation nucleus activity, *Atmos.Chem.Phys.*, 7, 1961-1971, 2007.

Pósfai, M., Gelencsér, A., Simonics, R., Arató, K., Li, J., Hobbs, P. V., and Buseck, P. R.: Atmospheric tar balls: Particles from biomass and biofuel burning, *J. Geophys. Res.*, 109, D06213, 10.1029/2003jd004169, 2004.

Possanzini, M., Di Palo, V., Petricca, M., Fratarcangeli, R., and Brocco, D.: Measurements of lower carbonyls in Rome ambient air, *Atmos Environ*, 30, 3757-3764, 10.1016/1352-2310(96)00110-0, 1996.

Prenni, A. J., DeMott, P. J., Kreidenweis, S. M., Sherman, D. E., Russell, L. M., and Ming, Y.: The effects of low molecular weight dicarboxylic acids on cloud formation, *The Journal of Physical Chemistry A*, 105, 11240-11248, 10.1021/jp012427d, 2001.

Prenni, A. J., Petters, M. D., Kreidenweis, S. M., DeMott, P. J., and Ziemann, P. J.: Cloud droplet activation of secondary organic aerosol, *J. Geophys. Res.*, 112, D10223, 2007.

Ravishankara, A. R.: Heterogeneous and multiphase chemistry in the troposphere, *Science*, 276, 1058-1065, 1997.

Raymond, T. M., and Pandis, S. N.: Cloud activation of single-component organic aerosol particles, *J. Geophys. Res.*, 107, 4787, 10.1029/2002jd002159, 2002.

Raymond, T. M., and Pandis, S. N.: Formation of cloud droplets by multicomponent organic particles, *J. Geophys. Res.*, 108, 4469, 10.1029/2003jd003503, 2003.

Roberts, G. C., Nenes, A., Seinfeld, J. H., and Andreae, M. O.: Impact of biomass burning on cloud properties in the Amazon basin, *J. Geophys. Res.*, 108, 4062, 2003.

Romakkaniemi, S., Kokkola, H., Smith, J. N., Prisle, N. L., Schwier, A. N., McNeill, V. F., and Laaksonen, A.: Partitioning of semivolatile surface-active compounds between bulk, surface and gas phase, *Geophys. Res. Lett.*, 38, L03807, 10.1029/2010gl046147, 2011.

Rosano, H. L., and La Mer, V. K.: The rate of evaporation of water through monolayers of esters, acids, and alcohols, *Journal of Physical Chemistry*, 60, 348-353, 1956.

Rudich, Y.: Laboratory perspectives on the chemical transformations of organic matter in atmospheric particles, *Chemical Reviews*, 103, 5097-5124, 2003.

Rudich, Y., Donahue, N. M., and Mentel, T. F.: Aging of organic aerosol: Bridging the gap between laboratory and field studies, *Annual Review of Physical Chemistry*, 58, 321-352, doi:10.1146/annurev.physchem.58.032806.104432, 2007.

Ruehl, C. R., Chuang, P. Y., and Nenes, A.: Distinct CCN activation kinetics above the marine boundary layer along the California coast, *Geophys. Res. Lett.*, 36, L15814, 10.1029/2009gl038839, 2009.

Ruehl, C. R., Chuang, P. Y., and Nenes, A.: Aerosol hygroscopicity at high (99 to 100%) relative humidities, *Atmos.Chem.Phys.*, 10, 1329-1344, 2010.

Russell, L. M., Takahama, S., Liu, S., Hawkins, L. N., Covert, D. S., Quinn, P. K., and Bates, T. S.: Oxygenated fraction and mass of organic aerosol from direct emission and atmospheric processing measured on the R/V Ronald Brown during TEXAQS/GoMACCS 2006, *J Geophys Res-Atmos*, 114, doi:10.1029/2008JD011275, 2009.

Salma, I., Ocskay, R., Varga, I., and Maenhaut, W.: Surface tension of atmospheric humic-like substances in connection with relaxation, dilution, and solution pH, *J Geophys Res-Atmos*, 111, D23205-doi:23210.21029/22005JD007015, 2006.

Sareen, N., Schwier, A. N., Shapiro, E. L., Mitroo, D., and McNeill, V. F.: Secondary organic material formed by methylglyoxal in aqueous aerosol mimics, *Atmos. Chem. Phys.*, 10, 997-1016, 2010.

Saxena, P., and Hildemann, L. M.: Water-soluble organics in atmospheric particles: A critical review of the literature and application of thermodynamics to identify candidate compounds, *J Atmos Chem*, 24, 57-109, 1996.

Schwier, A. N., Sareen, N., Mitroo, D., Shapiro, E. L., and McNeill, V. F.: Glyoxal-methylglyoxal cross-reactions in secondary organic aerosol formation, *Environ Sci Technol*, 44, 6174-6182, 10.1021/es101225q, 2010.

Seinfeld, J. H., and Pandis, S. N.: Atmospheric chemistry and physics from air pollution to climate change, xxvii, 1326 p, Wiley, New York, 1998.

Seinfeld, J. H., and Pankow, J. F.: Organic atmospheric particulate material, Annual Review of Physical Chemistry, 54, 121-140, Doi 10.1146/Annurev.Physchem.54.011002.103756, 2003.

Sempère, R., and Kawamura, K.: Comparative distributions of dicarboxylic acids and related polar compounds in snow, rain and aerosols from urban atmosphere, Atmos Environ, 28, 449-459, 10.1016/1352-2310(94)90123-6, 1994.

Setschenow, J. Z.: Über die konstitution der salzungen auf grund auf ihres verhaltens zu kohlen-säure, Z.Physik.Chem., 4, 117-125, 1889.

Shapiro, E. L., Szprengiel, J., Sareen, N., Jen, C. N., Giordano, M. R., and McNeill, V. F.: Light-absorbing secondary organic material formed by glyoxal in aqueous aerosol mimics, Atmospheric Chemistry and Physics, 9, 2289-2300, 2009.

Shulman, M. L., Jacobson, M. C., Carlson, R. J., Synovec, R. E., and Young, T. E.: Dissolution behavior and surface tension effects of organic compounds in nucleating cloud droplets, Geophys Res Lett, 23, 277-280, 1996.

Sin, D. W. M., Wong, Y.-C., and Louie, P. K. K.: Trends of ambient carbonyl compounds in the urban environment of Hong Kong, Atmos Environ, 35, 5961-5969, 10.1016/s1352-2310(01)00359-4, 2001.

Skoog, D. A., Holler, F. J., and Nieman, T. A.: Principles of instrumental analysis, Saunders College Publishing, New York, 1997.

Smith, D. F., Kleindienst, T. E., and McIver, C. D.: Primary product distributions from the reaction of OH with m-, p-xylene, 1,2,4- and 1,3,5-trimethylbenzene, J Atmos Chem, 34, 339-364, 1999.

Sorjamaa, R., Svenningsson, B., Raatikainen, T., Henning, S., Bilde, M., and Laaksonen, A.: The role of surfactants in Köhler theory reconsidered, *Atmos Chem Phys*, 4, 2107-2117, 2004.

Stemmler, K., Vlasenko, A., Guimbaud, C., and Ammann, M.: The effect of fatty acid surfactants on the uptake of nitric acid to deliquesced NaCl aerosol, *Atmos Chem Phys*, 8, 5127-5141, 2008.

Surratt, J. D., Kroll, J. H., Kleindienst, T. E., Edney, E. O., Claeys, M., Sorooshian, A., Ng, N. L., Offenberg, J. H., Lewandowski, M., Jaoui, M., Flagan, R. C., and Seinfeld, J. H.: Evidence for organosulfates in secondary organic aerosol, *Environ Sci Technol*, 41, 517-527, 2007.

Surratt, J. D., Gomez-Gonzalez, Y., Chan, A. W. H., Vermeylen, R., Shahgholi, M., Kleindienst, T. E., Edney, E. O., Offenberg, J. H., Lewandowski, M., Jaoui, M., Maenhaut, W., Claeys, M., Flagan, R. C., and Seinfeld, J. H.: Organosulfate formation in biogenic secondary organic aerosol, *J Phys Chem A*, 112, 8345-8378, 2008.

Tabazadeh, A.: Organic aggregate formation in aerosols and its impact on the physicochemical properties of atmospheric particles., *Atmos Environ*, 39, 5472-5480, Doi 10.1016/J.Atmosenv.2005.05.045, 2005.

Tan, Y., Carlton, A. G., Seitzinger, S. P., and Turpin, B. J.: SOA from methylglyoxal in clouds and wet aerosols: Measurement and prediction of key products, *Atmospheric Environment*, 44, 5218-5226, 10.1016/j.atmosenv.2010.08.045, 2010.

Tang, I. N., and Munkelwitz, H. R.: Water activities, densities, and refractive-indexes of aqueous sulfates and sodium-nitrate droplets of atmospheric importance, *J Geophys Res-Atmos*, 99, 18801-18808, 1994.

Tang, I. N.: Thermodynamic and optical properties of mixed-salt aerosols of atmospheric importance, *J Geophys Res-Atmos*, 102, 1883-1893, 1997.

Tang, I. N., Tridico, A. C., and Fung, K. H.: Thermodynamic and optical properties of sea salt aerosols, *J Geophys Res-Atmos*, 102, 23269-23275, 1997.

Taraniuk, I., Graber, E. R., Kostinski, A., and Rudich, Y.: Surfactant properties of atmospheric and model humic-like substances (HULIS), *Geophys Res Lett*, 34, L16807-
doi:16810.11029/12007GL029576, 2007.

Thornberry, T., Murphy, D. M., Thomson, D. S., de Gouw, J. A., Warneke, C., Bates, T. S., Quinn, P. K., and Coffman, D.: Measurement of aerosol organic compounds using a novel collection/thermal-desorption PTR-ITMS instrument, *Aerosol Science and Technology*, 43, 486-501, 2009.

Thornton, J. A., and Abbatt, J. P. D.: N_2O_5 reaction on submicron sea salt aerosol: Kinetics, products, and the effect of surface active organics, *J Phys Chem A*, 109, 10004-10012, Doi 10.1021/Jp054183t, 2005.

Tuazon, E. C., Atkinson, R., MacLeod, H., Biermann, H. W., Winer, A. M., Carter, W. P. L., and Pitts, J. N.: Yields of glyoxal and methylglyoxal from the nitrogen oxide(NO_x)-air photooxidations of toluene and m- and p-xylene, *Environ Sci Technol*, 18, 981-984, 10.1021/es00130a017, 1984.

Tuazon, E. C., MacLeod, H., Atkinson, R., and Carter, W. P. L.: α -dicarbonyl yields from the NO_x -air photooxidations of a series of aromatic hydrocarbons in air, *Environ Sci Technol*, 20, 383-387, 10.1021/es00146a010, 1986.

Tuazon, E. C., Aschmann, S. M., Nishino, N., Arey, J., and Atkinson, R.: Kinetics and products of the OH radical-initiated reaction of 3-methyl-2-butenal, *Phys Chem Chem Phys*, 7, 2298-2304, 2005.

VanReken, T. M., Ng, N. L., Flagan, R. C., and Seinfeld, J. H.: Cloud condensation nucleus activation properties of biogenic secondary organic aerosol, *J. Geophys. Res.*, 110, D07206, 2005.

Virtanen, A., Joutsensaari, J., Koop, T., Kannosto, J., Yli-Pirila, P., Leskinen, J., Makela, J. M., Holopainen, J. K., Poschl, U., Kulmala, M., Worsnop, D. R., and Laaksonen, A.: An amorphous solid state of biogenic secondary organic aerosol particles, *Nature*, 467, 824-827, 2010.

Volkamer, R., Platt, U., and Wirtz, K.: Primary and secondary glyoxal formation from aromatics: Experimental evidence for the bicycloalkyl-radical pathway from benzene, toluene, and p-xylene, *The Journal of Physical Chemistry A*, 105, 7865-7874, 10.1021/jp010152w, 2001.

Volkamer, R., Molina, L. T., Molina, M. J., Shirley, T., and Brune, W. H.: Doas measurement of glyoxal as an indicator for fast VOC chemistry in urban air, *Geophys. Res. Lett.*, 32, L08806, 10.1029/2005gl022616, 2005.

Volkamer, R., Jimenez, J. L., San Martini, F., Dzepina, K., Zhang, Q., Salcedo, D., Molina, L. T., Worsnop, D. R., and Molina, M. J.: Secondary organic aerosol formation from anthropogenic air pollution: Rapid and higher than expected, *Geophys. Res. Lett.*, 33, L17811, 10.1029/2006gl026899, 2006.

Volkamer, R., Martini, F. S., Molina, L. T., Salcedo, D., Jimenez, J. L., and Molina, M. J.: A missing sink for gas-phase glyoxal in Mexico City: Formation of secondary organic aerosol, *Geophys Res Lett*, 34, 10.1029/2007gl030752, 2007.

Volkamer, R., Ziemann, P. J., and Molina, M. J.: Secondary organic aerosol formation from acetylene (C₂H₂): Seed effect on SOA yields due to organic photochemistry in the aerosol aqueous phase, *Atmos. Chem. Phys.*, 9, 1907-1928, 10.5194/acp-9-1907-2009, 2009.

Whitby, K. T.: The physical characteristics of sulfur aerosols, *Atmospheric Environment*, 12, 135-159, 1978.

Yu, G., Bayer, A. R., Galloway, M. M., Korshavn, K. J., Fry, C. G., and Keutsch, F. N.: Glyoxal in aqueous ammonium sulfate solutions: Products, kinetics and hydration effects, *Environmental Science & Technology*, 45, 6336-6342, 10.1021/es200989n, 2011.

Zhang, Q., Jimenez, J. L., Canagaratna, M. R., Allan, J. D., Coe, H., Ulbrich, I., Alfarra, M. R., Takami, A., Middlebrook, A. M., Sun, Y. L., Dzepina, K., Dunlea, E., Docherty, K., DeCarlo, P. F., Salcedo, D., Onasch, T., Jayne, J. T., Miyoshi, T., Shimojo, A., Hatakeyama, S., Takegawa, N., Kondo, Y., Schneider, J., Drewnick, F., Borrmann, S.,

Weimer, S., Demerjian, K., Williams, P., Bower, K., Bahreini, R., Cottrell, L., Griffin, R. J., Rautiainen, J., Sun, J. Y., Zhang, Y. M., and Worsnop, D. R.: Ubiquity and dominance of oxygenated species in organic aerosols in anthropogenically-influenced Northern Hemisphere midlatitudes, *Geophys. Res. Lett.*, 34, L13801, 10.1029/2007gl029979, 2007a.

Zhang, Q., Jimenez, J. L., Worsnop, D. R., and Canagaratna, M.: A case study of urban particle acidity and its influence on secondary organic aerosol, *Environ Sci Technol*, 41, 3213-3219, 2007b.

Zhao, J., Levitt, N. P., Zhang, R. Y., and Chen, J. M.: Heterogeneous reactions of methylglyoxal in acidic media: Implications for secondary organic aerosol formation, *Environ Sci Technol*, 40, 7682-7687, 2006.

Zhao, R., Lee, A. K. Y., and Abbatt, J. P. D.: Investigation of aqueous-phase photooxidation of glyoxal and methylglyoxal by aerosol chemical ionization mass spectrometry: Observation of hydroxyhydroperoxide formation, *The Journal of Physical Chemistry A*, 10.1021/jp211528d, 2012.

Zhou, X. L., and Mopper, K.: Apparent partition-coefficients of 15 carbonyl-compounds between air and seawater and between air and fresh-water - implications for air sea exchange, *Environ Sci Technol*, 24, 1864-1869, 1990.